Understanding the Process-Response Mechanism of Hierarchical Nature in a Large Scale Braided River

Thesis submitted in partial fulfilment of the requirements for the award of the degree of

Doctor of Philosophy

in

Civil Engineering

by

CHEMBOLU VINAY

[Roll No. 156104034]

with the supervision of

Subashisa Dutta

Department of Civil Engineering
Indian Institute of Technology Guwahati
Guwahati – 781039, Assam, India

March, 2020

Understanding the Process-Response Mechanism of Hierarchical Nature in a Large Scale Braided River

CHEMBOLU VINAY

Indian Institute of Technology Guwahati

Department of Civil Engineering, Guwahati, Assam 781039

To

The People of Brahmaputra Valley

ACKNOWLEDGEMENTS

This phase was one of the beautiful and remarkable period of my life. It has taught me living a life. I am extremely thankful to my conscience for not letting me down in dark times and, when things were going turbulent. Thanks to my diary for hearing me so patiently and making me realize I can make any good thing possible. Thanking every event that happened for transforming me into a better person. There are many people I travelled during this journey and, thanks to one and all for a happy friendship.

I thank my professor, Subashisa Dutta for not just introducing me to the field of hydraulics but also for being there as a second parent throughout. I have a full respect and affection towards him at every stage of my life. Anjaneyulu, these 6 years of togetherness with you made me to walk through different thoughts of life and, thanks to you for those gems and taking care of me as and when needed. Suresh, I am all thankful to your help in difficult times and, thanks for being there as an elder brother. Thanks to beloved brothers, Chandan and Reddick for having full confidence in me while handling their works. Thanks to the extended family Satish, Shreedevi, Suman, Bazal Da, Bhuvana, Amit Dubey, Ketan and Lasya for friendly cooperation and togetherness. Thanks to good friends Nama, Vinay, Viswanth, Venky and Kranthi for their nice friendship and unconditional affection towards me.

Special thanks to Yasin, Satish, Krishna, Bhatlu, Gandhi, Geetha and Madhu for your friendly love and care. Swamy, your wish was always a blessing to me. Thanks for your big wishes towards me. Thanks to Amma, Nanna, Nayu Baby, Akka and Bavagaru for love and more. Finally, due thanks to Doctoral Committee, Department of Civil Engineering and Indian Institute of Technology Guwahati for all help.

CHEMBOLU VINAY

DECLARATION

I, **Chembolu Vinay**, author of the Ph. D. thesis "**Understanding the Process-Response Mechanism of Hierarchical Nature in Large Scale Braided River**" would like to certify that

- The work presented in this thesis is original research work carried out by me.
- The research work has not been submitted for any degree or diploma or any other qualification either in this institute or in any other university.
- Whenever I have used resources [theory, concepts, texts, data, graphs, figures or any other similar nature] from other sources, a due credit by citing in the text of the thesis is clearly made.
- The work presented here is free from plagiarism to the best of my knowledge, and I take the responsibility for any issues.
- I also affirm that thesis supervisor is not responsible for any possible instance of plagiarism within this submitted work.

Date: CHEMBOLU VINAY

Place: [156104034]

Indian Institute of Technology Guwahati

Department of Civil Engineering, Guwahati, Assam 781039

Subashisa Dutta, Ph. D.

Professor and Former Head

(subashisa@iitg.ac.in)

CERTIFICATE

This is to certify that thesis entitled "**Understanding the Process-Response Mechanism of Hierarchical Nature in Large Scale Braided River**" submitted by **Chembolu Vinay**, in partial fulfilment of the requirements for the award of degree of Doctor of Philosophy, to Indian Institute of Technology Guwahati, Assam, India, is a record of the bonafide research work carried out by him under my guidance and supervision at the Department of Civil Engineering, Indian Institute of Technology Guwahati, Assam, India. To the best of my knowledge, no part of the work reported in this thesis has been presented for the ward of any degree at any other institution.

Date: Subashisa Dutta

Place:

ABSTRACT

Braided rivers are characterized by complex, unstable river network formed due to the interaction of high flow energy and intense sediment transport. They generate complex morphological adjustments over a braided corridor as a response to changes in flow and sediment supply. Understanding of river behavior and mechanics through field, laboratory, and modeling based studies can be beneficial in their management and also for effective river training. This thesis aims to work for understanding the river processes of the Brahmaputra River.

Morphology of the Brahmaputra River is complex and dynamic due to high variability in flow and sediment, wide sand-bed corridor and severe bank erosion. Understanding the long-term morphological dynamics and adjustments of the river provides the information on river response to seasonal changes in river flow conditions. To study the morphological condition of the river, the present work utilizes entropy theory to investigate the variability in the surface areas of sandbars. Two indices namely intensity disorder index and planform disorder index are computed to represent the variability in sand bar dynamics. The intensity entropy disorder index followed a decreasing trend in dry and post-monsoon seasons; tending towards lower deviation from a uniform distribution. The planform disorder index was computed to investigate the relation between annual planform disorder and, monsoonal, peak flood stream power. It was noted that except for extreme flood years the planform disorder index correlated well with monsoonal stream power. Distinctive trends in stream power and associated variability in morphological parameters are also observed.

Hierarchical channels of the braided rivers exhibit complex flow and morphological characteristics due to changes in discharge, width-to depth ratio and upstream channel changes. To investigate the flow structure and suspended sediment distribution at hierarchical channels detailed acoustic Doppler current profiler survey is carried out and analyzed in this study. Hierarchical

channels include cross-sections at main, secondary and tertiary channels with *w/d* ranging from 50 to 800. The results highlight the contribution of planform curvature in higher width-to-depth ratio channels for generation of secondary cells, overcoming the bedform interactions usually governing the secondary cells in large rivers. For the channels with low width-to-depth ratio, the flow structure processes are observed to be similar to smaller rivers. Short-term morphological adjustments are very prominent in the Brahmaputra River. In higher width-to-depth ratio channels, the influence of upstream morphological changes coupled with local flow structure alters the changes in planform and cross-section morphology. With reduction in width-to depth ratio, the upstream morphological changes are observed to influence the channel morphology irrespective of the flow structure. The study reveal the process-response mechanism in the Brahmaputra River are observed to be interdependent and highly complex in nature.

In natural riverine environments, vegetation occurs as patches of reeds, grasses and other heterogeneous plant forms. Few locations of the Brahmaputra River corridor are covered with flexible grasses and heterogeneous plant patches. Considering the importance of vegetation for planform stability and ecological aspects, an experimental investigation on the flow and turbulent characteristics in heterogeneous vegetation patches is carried out. Experiments are conducted using different forms (grass, leafy and cylindrical) of natural vegetation planted, alternatively and also as a mixed variety of patches in a staggered pattern. The results show that the presence of other vegetation forms in mixed heterogeneous patch increases the velocity reduction compared to flexible grass forms. The additional drag due to mixed vegetation reduce the shear generated turbulence at the canopy top. The heterogeneous patches are observed to provide spatial heterogeneity in velocity fields and, varying zones of increased and diminished turbulence. Specifically, patch form and its alignment significantly control the velocity reduction and, momentum transfer between canopy and overflow regions.

The understanding of flow-vegetation interaction is extended to study the morphological response of the braided loop subjected to vegetation cover over the sand bar. Vegetation cover as a roughness coefficient is incorporated in the model, and hydrodynamic and morphological simulations are carried out for one year period to monitor the river response. The results reveal the presence of vegetation roughness stabilizes the sand bar and decrease the braiding intensity. Moreover, increase in vegetation roughness over the sand bar favored the deepening of the secondary channel, and improved the discharge sharing between the channels. The vegetation-river response can be extended further by monitoring the process at field scale for river corridor management and its

stabilization. The present thesis work provides the comprehensive understanding of the process-response mechanism of hierarchical nature in the Brahmaputra River.

End of the abstract

CONTENTS

LIST OF FIGURES

LIST OF TABLES

LIST OF SYMBOLS

Symbol	Description
Ω	Stream power
ω	Specific stream power
φ	Energy Dissipation
γ	Specific weight of water
D_{50}	Representative diameter
E	Specific Energy
h_d	Deflected plant height
h_f	Total head loss
h_t	Thickness of active momentum exchange
n	Manning's roughness coefficient
Q	Discharge
R	Hydraulic Radius
S	Slope
τ_b	Bed shear stress
U, V, W	Time averaged velocity in streamwise, spanwise and vertical directions
u', v', w'	Fluctuating velocity in streamwise, spanwise and vertical directions
-u'w' or $RS_{u'w'}$	Reynold stress in vertical direction
-u'v' or $RS_{u'v'}$	Reynold stress in spanwise direction
-v'w' or $RS_{v'w'}$	Reynold stress in streamwise direction
u_{rms}, w_{rms}	Turbulence intensity in streamwise and vertical directions
V_p	Primary Velocity Component
V_s	Secondary Velocity Component
R	Hydraulic Radius
w/d	Width-to-depth ratio

LIST OF ABBREVIATIONS

Terms	Description
ADCP	Acoustic Doppler Current Profiler
ADV	Acoustic Doppler Velocimeter
BI	Braiding Intensity
CCHE	Center for Computational Hydroscience and Engineering
ETM	Enhanced Thematic Mapper
FCB	Fluid Corrected Backscatter
GPS	Global Positioning System
HEC-RAS	Hydrologic Engineering Center- River Analysis System
IDI	Intensity Disorder Index
IE	Intensity Entropy
MSP	Monsoonal Stream Power
PDI	Planform Disorder Index
SSC	Suspended Sediment Concentration
TKE	Turbulent Kinetic Energy
TM	Thematic Mapper
USGS	United States of Geological Survey

1

INTRODUCTION

Braided rivers are characterized by complex, unstable river network formed due to the interaction of high flow energy and intense sediment transport [Smith, 1971]. They generate complex morphological adjustments over a braided corridor as a response to changes in flow and sediment supply [Bridge, 1993; Ashworth *et al.*, 2000]. Understanding of river behavior and mechanics through the field, laboratory, and modeling based studies can be beneficial in their management and also for effective river training [Bristow and Best, 1993; Paola, 2001]. This thesis aims to work for understanding the river processes of the Brahmaputra River.

1.1 THE BRAHMAPUTRA RIVER SYSTEM

Many researchers consider the Brahmaputra River as one of the classic example of the large and dynamic braided river system for understanding hydrodynamics and morphological features [Coleman, 1969; Goswami, 1985; Thorne *et al.*, 1993; Sarma, 2005; Karmaker and Dutta, 2011]. The Brahmaputra River is one of the largest rivers in the world, carries enormous discharge and sediment load during monsoon season. Unlike other river basins, the basin experiences high-intensity long duration rainfall events which generate flood peaks of long- duration along with regular monsoon flood waves. These rainfall events also trigger landslides, soil erosion, and other soil erodible sources and produce large sediment waves passing through in the river. The water and sediment waves

cause large scale floods, bank erosion, and changing river planforms annually; controlling the status of socio-economic condition in the river valley.

The impact of water and sediment waves on short and long term morphological responses in the braided river is one of the challenging tasks for the hydrologist and the geomorphologists with limited *in-situ* hydraulic and morphological observation dataset. The limited data collection is due to its large width (1.2 to 18 km) and discharge variation (3,000 to 40,000 m^3/s) in 1000 km long braided river system [Karmaker *et al.*, 2011]. During a low flow season, the braided nature of the river divides the flow into multiple numbers of channels and creates a problem for conducting *in-situ* measurements using survey vessels. The river remains distinctive due to high flow and sediment variability, severely erodible banks and wider braided belt resulting in dynamic morphological changes [Goswami, 1985]. Large scale turbulence, sediment mixing, bank erosion, vertical vortex formation and secondary current formation are commonly observed during the monsoon flow. Advanced river surveying equipment like acoustic Doppler current profiler, sub-surface sonar helps to investigate the river hydrodynamic and morphological characteristics in the critical sections. With recent advancement in geo-spatial technologies, such as satellite altimetry in monitoring the river water level and micro-wave imagery for large-scale sediment mixing and mapping the turbulence patterns during monsoon period have proven to be successful [Dubey, 2016]. This can overcome the many challenges with the traditional field measurements. To protect from large scale floods and severe bank erosion, many of the river training works are in practice for site-specific issues along the river. Embankments, gabion revetment, geo-tube piled embankment, land spurs and low-cost permeable spurs are the common river training structures having their own merits and demerits in protecting from floods and bank erosion. Therefore, to plan, design and maintain the river-training-works and short and long-term mitigation for floods and bank-erosion issue, detailed understanding of river behavior and hydrodynamic characteristics is highly necessary.

The present thesis aims to work for this challenge. This study aims for an integrated approach to understanding the hydrodynamic and morphological condition of the Brahmaputra River through field, modeling and satellite imagery-based analysis. In this study, optical satellite imagery for mapping morphological features, advanced river surveying equipment for field data measurements and, river mathematical models are used for achieving the objectives. For this work, the middle Brahmaputra River reach between

Tezpur to Guwahati is considered for analysis [Figure 1.1]. This reach comprises of different zones of flow and morphological variability due to changes in braided belt width and, suits best for studying the river behavior. This understanding can be contribution to the management of the large fluvial river system.

1.2 AIMS AND SCOPE OF THE THESIS

Considering the research needs with emphasis to river morphology, mechanics, and management, the following objectives are outlined for the present research study.

- To study the yearly island morphodynamics of the Brahmaputra River using entropy analysis and multi-date satellite imagery.
- To analyze the flow structure and associated morphological changes at hierarchical channels of the Brahmaputra River using acoustic Doppler current profiler (ADCP) data and satellite imagery.
- To study experimentally the effect of heterogeneous natural vegetation on hydrodynamics characteristics under submerged flow conditions.
- To investigate the predictions of two-dimensional hydrodynamic and morphological model in simulating the morphological changes of the Brahmaputra River and study the morphological response of a braided loop subjected to varying vegetative cover.

1.3 STUDY AREA

The Brahmaputra River in Assam, between Tezpur and Guwahati [Figure 1.1] is chosen as a study area. The reach is 140 km long, and its braided belt width varies between 1.2 km to 15 km, giving a wide accommodation space for morphological activity. The river exhibits severe braiding and makes its path tortuous, but at Tezpur and Guwahati, the river is geologically confined to a single channel [Lahiri and Sinha, 2014; Karmaker *et al.*, 2017]. The daily discharge hydrograph of the river is highly fluctuating [Goswami, 1985]. The mean daily discharge at Guwahati varies from 4,420 m^3/s in the dry season to 51,156 m^3/s during the flood [Singh *et al.*, 2013]. The bed and bank material of the river is a composite of fine sand and silt, falling under highly erodible zone [Karmaker and Dutta, 2011]. Morphological changes such as thalweg shifting, severe bank erosion and migrating sandbars are most common in this river [Coleman, 1969; Thorne *et al.*, 1993]. The majority of sandbars in the reach are un-vegetated and highly dynamic, *i.e.*, any change in the fluvial

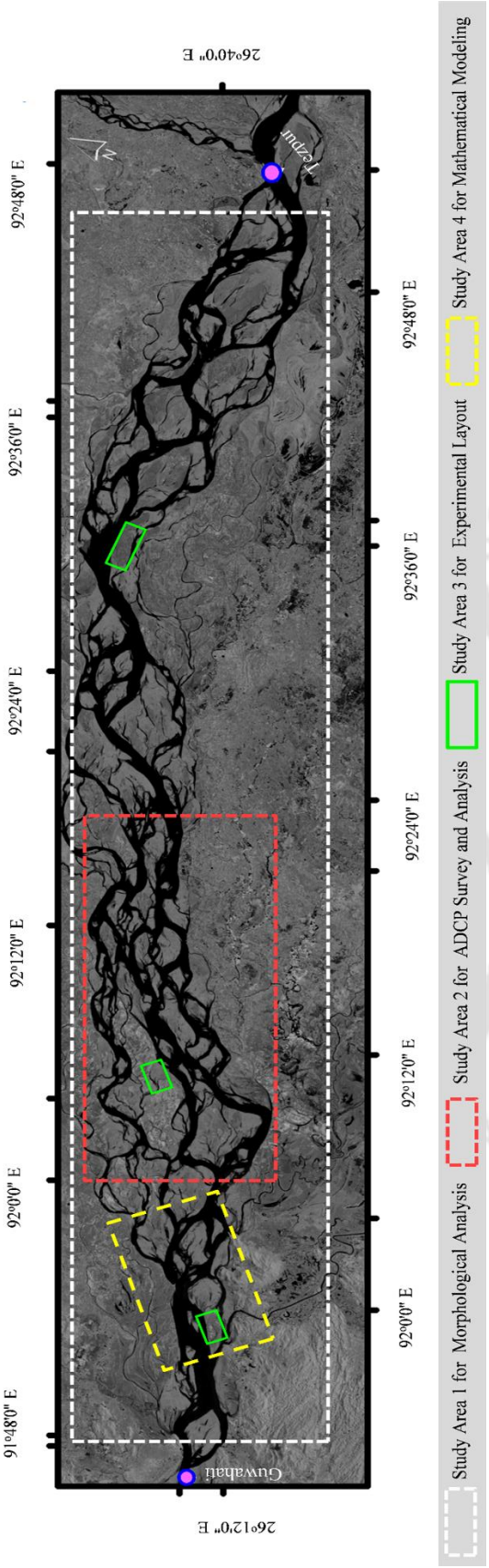

Figure 1.1 Study area showing the Brahmaputra River between Tezpur to Guwahati, Assam India

system variables reflects in sandbar characteristics. Flow and sediment variability, wider braided belt width and highly volatile banks make the river vulnerable to frequent morphodynamics. Figure 1.1 show the study area for different objectives planned for the research work.

1.4 ORGANISATION OF THESIS

The research work in this thesis is presented in seven chapters. The thesis focuses on understanding the process-response mechanisms in the Brahmaputra River through field, lab and modeling based techniques. The thesis is divided in to chapters based on objectives of the present study. Initially, morphological condition of the river is studied through entropy based analysis. This is followed by understanding the river hydrodynamic and morphological processes through field techniques and satellite imagery. The later chapter investigates the flow-vegetation interaction through lab-based experimental study. Finally, numerical modeling is carried out to evaluate the performance evaluation of the river models and application of river model to predict morphological changes due to presence of riparian vegetation cover. The chapter-wise description of the thesis is

- *Chapter 1* discussed the overview of the Brahmaputra River system and morphological dynamics followed by aims and scope of the thesis.
- *Chapter 2* reports the review of literature carried on theory of braided river, morphological dynamics and flow-vegetation-sediment interaction necessary for the present research.
- *Chapter 3* deals with entropy-based morphological analysis of the sandbar dynamics in the Brahmaputra River.
- *Chapter 4* deals with general characteristics of the Brahmaputra River system, flow, suspended sediment distribution and morphological changes in hierarchical channels of the complex braided river network.
- *Chapter 5* deals with the experimental study on flow characteristics through heterogeneous natural vegetation patches under submerged flow conditions.
- *Chapter 6* studies the evaluation of morphological predictions of the river mathematical models and discusses the morphological response of a braided loop subjected to percentages of vegetation cover.
- *Chapter 7* summarizes the present research and suggests the future scope of the present work.

2

REVIEW OF LITERATURE

Braided rivers are characterized by complex, unstable river network formed due to the interaction of high flow energy and intense sediment transport [Smith, 1971]. They generate complex morphological adjustments over a braided corridor as a response to changes in flow and sediment supply [Bridge, 1993; Ashworth *et al.*, 2000]. Understanding of river behavior and mechanics through the field, lab, and modeling based studies can be beneficial in their management and also for effective river training [Bristow and Best, 1993; Paola, 2001]. In this chapter review of works on braiding, processes and feedback mechanism, morphological changes and modeling techniques are highlighted. Vegetation has become an important implication in braided river management for improving the physical characteristics and ecological standards of the river systems [Nepf and Ghisalberti, 2008]. A synoptic understanding of flow-vegetation-sediment interactions is also discussed here.

2.1 BRAIDED RIVER MORPHODYNAMICS

Braiding refers to the network of river channels, exhibiting a complex pattern of dividing and rejoining around the bars. They appear over different river scales from smaller gravel-bed streams to larger sand-bed rivers experiencing rapid channel adjustments and high rates of morphological activity. The dynamics of braided river network include shifting of channels, migration of braided loops, and significant variations in erosion and deposition pattern varying seasonally with river stage. These changes are complex,

interdependent, and modified over different time scales. Various conditions favor the braiding phenomenon, this include

- *Abundancy of bedload.* The supply of bedload from upstream and contributions from local morphological processes such as bank erosion favor braiding formation. Sediment supply in excess of transport capacity may lead to braiding initiation.
- *High stream power*. The presence of steeper slopes and availability of high discharge favors braiding.
- *Bank instability*. Easily erodible banks coupled with relatively higher stream power results in excess of sediment source favoring braiding. This process accelerates over wider river corridors producing complex river networks.
- *Discharge variability:* Seasonal changes in river discharge leads to rapid changes in bed load movement and deposition influencing the braided bar development. Laboratory studies [Leopold and Wolman, 1957; Ashmore, 1991] report the development of braiding at constant discharge, suggesting discharge variability is often not important for braiding.
- *Absence of vegetation:* The presence of vegetation over a river corridor influences the planform pattern through sediment deposition and arresting the multiple channel network [Tal and Paola, 2007].

Thus, the nature of braiding and the multi-channel network is governed by many interdependent processes working over a braided corridor. The following sub-sections discuss the review of the previous works on braided rivers for understanding morphology and behavior of braided channels.

2.1.1 Flow Structure in Braided Channels

Many researchers consider the Brahmaputra River as one of the classic examples of the large and dynamic braided river system for understanding hydrodynamics and morphological features [Coleman, 1969; Thorne *et al.*, 1993; Klaassen *et al.*, 1993; Best *et al.*, 2007]. The river remains distinctive due to high flow and sediment variability, severely erodible banks and wider braided belt resulting in dynamic morphological changes [Goswami, 1985]. Coleman [1969] for the first time, characterized the Brahmaputra River bedforms and their influence on macro-turbulent structures through *in-situ* measurements. Richardson and Thorne [1998] performed a field-based study to demonstrate the presence of large scale secondary currents in multi-thread flows and, developed an energy-based

threshold expression for prediction of channel bifurcation [Richardson and Thorne, 2000]. McLelland *et al.* [1999] carried investigation on detailed flow structure and sediment distribution around a developing braided bar at different stages of the monitoring period. This study highlights the absence of secondary flow helical cells in large sections of the width-to-depth ratio much greater than 100. Ashworth *et al.* [2000] described the process of braid bar initiation, growth, and development by continuous monitoring with bathymetric and ADCP surveys at different river stages. These studies have provided a good process-response based understanding of flow-planform interactions, however, limited their work to flow surrounding a braided bar.

2.1.2 Bifurcation and Confluences

Channel bifurcation and confluence units are considered as fundamental units of the braided river network. They control the channel bed morphology, movement of water and sediment and, eventually influence the stability of confluence-diffluence units [Hackney *et al.*, 2018]. Federici and Paola [2003] carried out an experimental investigation to study the stability of channel bifurcations in non-cohesive sediments. The study highlights the presence of lower Shields stress and non-uniformity in the incoming flow towards the formation of unstable bifurcations. Numerical modeling of bifurcations by Bolla Pittaluga *et al.* [2003] reports the nodal point control for water and sediment flux partition into the downstream branches. This work is experimentally evaluated by Bertoldi and Tubino [2007] confirming the local flow and bed structure at nodal location governing bifurcation dynamics. A recent study by Hackney *et al.* [2018] highlights the issues of the existing theory of bifurcation stability to large river systems governed by fine-grained sediment. Current models emphasize the importance of the secondary flow field in governing the bifurcation instability, which is contrary to those observed in large rivers of higher width-to-depth ratio. For example, McLelland *et a*l. [1999] report the absence of secondary flow in cross-sections of the Brahmaputra River of aspect ratio much greater than 100. A similar observation is reported for other river systems such as Rio Parana [Parsons *et al.*, 2007]. Thus, the challenge exists in understanding the bifurcation dynamics of large rivers and the development of numerical models.

Channel confluence is the critical component of braided river network exhibiting complex flow structure and rapid morphological changes. In natural river environments, confluences can be observed as symmetrical, asymmetrical, and confluent meander bed

[Riley and Rhoads, 2012] with variability in three-dimensional flow structure and bed morphology. This variability is associated with junction angle, momentum flux ratio, and planform symmetry at confluent zones. Major flow structure at confluence zones include (a) flow stagnation zone at upstream junction corner; (b) shear and mixing layer zones at confluence flow; (c) flow separation at downstream junction corner; (d) accelerated zone and (e) recovery zone. The morphological changes include (a) scour hole at the accelerated velocity of converging zone; (b) sediment deposition at stagnation flow region; (c) bar formation at flow separation regions. Most of the previous research defining the confluence flow structure and morphology is aimed at laboratory scale [Mosley, 1976; Best, 1988; Biron *et al.,* 1993], smaller-scale natural river confluences [Best, 1988; McLelland *et al.*, 1996; Rhoads and Sukhodolov, 2001] and numerical models development through existing theories [Bradbrook *et al.,* 2001]. In recent decades, researchers aimed at studying the large river confluences by understanding the importance of difference in morphology and behavior of the smaller and large rivers. Parson *et al*. [2007] highlight the influence of channel scale or width-to-depth ratio of smaller and large confluence in flow structure and confluence-diffluence dynamics. Szupiany *et al.* [2009] reports the flow structure, morphological changes and suspended sediment distribution in a width-to-depth ratio approaching 100 and, emphasizes the position of secondary flow cells in confluences of varying scale. However, the understanding of multi-thread river channel confluence and the influence of bank erosion dominated confluence on morphological adjustments is challenging and yet to be studied.

2.1.3 Bank Erosion

Riverbank erosion is the dominant process in large fluvial river systems subjected to dynamic morphological changes. For example, the Brahmaputra river banks are composed of fine sand and silt, which are severely eroded and contribute to intense bedload transport. The mechanisms of bank erosion process are thoroughly investigated by evaluating the erodibility parameters of composite river banks [Karmaker and Dutta, 2011]. Their results conclude river banks are severely erodible and least resistant. This work is further progressed to model seepage erosion through lysimeter experiments which revealed seepage gradient is dominant for development of undercuts [Karmaker and Dutta, 2013]. This phenomenon is highly particular in river banks unaffected due to fluvial erosion and mass cantilever failure. The extension of work for the development of stochastic bank

erosion prediction model improved the knowledge of process-response feedback mechanism in river [Karmaker and Dutta, 2015].

2.1.4 Morphology and Behavior of Braided Channels

The short-term and long-term morphodynamics of Brahmaputra River remained challenging till date to hydrologist and morphologist. The river morphology and behavior is characterized by high flow and sediment transport, erodible banks, and large width resulting in seasonal-scale morphological changes [Goswami, 1985]. Extreme floods and geo-dynamically sensitive catchment govern the complex morphological river processes. Sarma [2005] describes the fluvial morphology of the Brahmaputra River as complex planform features, rapid rates of erosion and deposition. This work is extended further to quantify annual bank erosion and bank line migration [Sarma and Phukan, 2006] relating to seasonal floods. A newer approach through wavelet analysis [Karmaker *et al.*, 2017] is applied over the middle Brahmaputra to quantify river morphodynamics. This study argues no significant control of flood stream power to braiding indices. Although morphological indices exist for characterizing the braiding intensity, newer indices like planform index and flow geometry index [Akhtar *et al.*, 2004] found better to characterize the highly braided rivers. Many of other works also characterized the stability and morphological condition of the lower Brahmaputra River in Bangladesh [Takagi *et al.*, 2007].

2.1.5 Vegetation Interactions

Riparian vegetation development has a significant impact on river morphodynamics and plays an important role in the improvement of river ecosystem [Gurnell *et al.*, 2012]. The importance of riparian vegetation is recognized recently and is widely used for river management. A laboratory study by Gran and Paola [2001] shows vegetation cover reduced the number of active channels and migration rate of braided river network. With the addition of vegetation to a sidebar Rominger *et al.* [2010] observed reduction in longitudinal velocity over the bar and increased velocity in open channel. This behavior helps for the simultaneous development of the open channel and bar stabilization. Tal and Paola [2010] through laboratory experiments observed a shift of multi-thread network to single thread stable channel due to vegetation over the braided network. A similar study by Van dijk *et al.* [2013] observes channel deepening, stable banks with tighter bends with the increase in vegetation densities. Bertoldi *et al.* [2015] investigated the combined effect of vegetation and wood dispersal on braided morphology subjected to cycles of flooding.

Their study reports riparian vegetation increased channel stability, reduced braiding intensity, and lateral erosion.

2.1.6 Modeling of Braided Rivers

The applicability of numerical models is increased in recent years to understand the flow and morphological characteristics. However, the necessity of reliable field measurements and full-scale model development with hierarchical braided river processes is a major challenge to understand river behavior. Development of two-dimensional and three-dimensional river models for morphological predictions with changing flow-sediment regimes can be extremely helpful for dynamic braided rivers. Thomas and Nicholas [2002] developed a two-dimensional model using cellular routing scheme to simulate the bedload transport and associated morphological changes. Nicholas [2003] extends the previous work by simulating a two-dimensional model to braided river reach and highlights the issues and potential of models for real-time river applications. This includes *in-situ* measurement errors, variability in model grid-scale, and river processes bringing the difference in simulated and observed flow parameters. The complexities in modeling arise due to nonlinearities, unsteadiness, time scale, secondary flows and finite-length effects [Repetto, 2000]. Other simplified models were also developed to understand the river morphological characteristics [Murray and Paola, 2003; Coulthard *et al.*, 2006]. Recent advancement in computational techniques helped for development of two-dimensional and three-dimensional models for qualitative predictions of planform characteristics of braided rivers [Kleinhans, 2010; Lotsari *et al.*, 2013; Schuurman *et al.*, 2013; Schuurman and Kleinhans, 2015]. However, there is a challenge for the development of numerical models applicable to simulate hierarchical processes in large and dynamic rivers.

2.2 FLOW-VEGETATION-SEDIMENT INTERACTIONS

In-channel vegetation is considered as a nuisance [Lopez and Gracia, 2001] for many years due to the reduction in conveyance capacity [Wu *et al.*, 1999] and increased resistance for smooth movement of high flows. Vegetation has become an important implication in river restoration schemes for improving the physical characteristics and ecological standards of the river systems [Nepf and Ghisalberti, 2008]. Aquatic or riparian vegetation significantly alters the flow and turbulent structure and, influences the habitat life, water quality, pollutant and nutrient dispersal, and sediment transport. Moreover, in

braided rivers, the vegetation has shown positive feedback in controlling the braiding intensity [Tal and Paola, 2007] and, promoting bar and bank accretion processes [Bertoldi *et al.*, 2011].

2.2.1 Flow Vegetation Interactions

Earlier research on flow through vegetation mainly focused on determining roughness coefficients in vegetated channels [Ree 1958; Chen, 1976]. Growing recognition of vegetation in improving the river health and restoration has attracted many researchers to understand the physical processes in flow vegetation interactions at different scales [Nepf, 2012]. Jarvella [2002] and Wilson [2007] experimentally investigated the flow resistance offered by the natural plants by varying density, pattern and hydraulic parameters. Their results showed roughness coefficient is highly dependent on vegetation height and decreases with increase in submergence. Wilson *et al.* [2003] have conducted detailed laboratory experiments to study the flow structure of submerged flexible vegetation with and without frond foliage. The presence of fronds absorbed the flow momentum and decreased the momentum exchange activity over the canopy top. Jarvela [2005] identified the logarithmic velocity profile in natural vegetation under deeply submerged flow conditions. Shucksmith *et al.* [2010] conducted a laboratory study to understand the mixing processes in vegetated open-channel flows. The presence of shear layer at the canopy top increased the longitudinal mixing in submerged condition and reduced mixing in emergent flow condition. Ortiz *et al.* [2013] examined the effects of turbulence structure on suspended sediment depositions in patchy vegetation. The study reports two-dimensional flow structure in emergent case and three-dimensional flow structure in submerged condition. Devi and Kumar [2015] investigated the effect of seepage on the turbulence structure. Researchers also contributed towards developing numerical models to determine mean flow and turbulence structure in vegetated channels [Lopez and Gracia, 1998; Lopez and Gracia, 2001; Dijikstra and Uittenbogaard, 2010; Kim *et al.*, 2015; Marjoribanks *et al.*, 2015].

2.2.2 Sediment Vegetation Interactions

This section of the literature review discusses research works carried out on the effect of vegetation in trapping the sediment. The studies discussed here are laboratory-based investigation of transport and deposition of sediment near vegetation patches. Jordanova and James [2003] conducted experiments to study the effect of emergent

vegetation on bedload transport. Their results showed that the presence of vegetation reduced the shear stress acting on the bed through momentum absorption by stem drag, which in turn promoted sediment deposition and reduced bedload transport. Sharp and James [2006] experimentally investigated distribution of suspended sediment deposition in emergent vegetation for varying grain size, flow depths and stem densities. Zong and Nepf [2009] identified the flow and deposition patterns around the patch of emergent vegetation located at the wall of channel. Three distinct zones i.e. the diverging zone of increased velocity reduction and sediment deposition, fully developed zone and shear layer zone of increased turbulence levels and decreased deposition were observed along the patch. Kothyari *et al.* [2010] experimentally studied the effectiveness of tall vegetation for controlling sediment transport under varying vegetation densities, channel slopes and sediment sizes. Follet and Nepf [2012] observed the scour in circular sparse and dense vegetation patches due to the increase in turbulence levels. The difference in deposition patterns was observed due to the difference in flow diversion and wake structure. Kim *et al.* [2014] performed laboratory analysis to investigate bed morphological changes around a fine patch of vegetation for different flow blockage, submergence ratio and bed entrainment conditions. Their results showed that sediment deposition inside the patch was highly dependent on flow blockage and obstruction. Shi *et al.* [2016] conducted a series of experiments to study the effect of grain size and channel velocity on sediment deposition patterns of emergent circular patches. A similar study by Liu and Nepf [2016] investigated the effect of channel velocity and stem generated turbulence on sediment deposition patterns. The authors conclude deposition inside the patch was due to absence of stem scale turbulence.

2.3 CHAPTER SUMMARY

The literature review on braided river morphodynamics reveals that while investigating the flow structure, previous studies limited to understand the processes surrounding the braided bar. However, the river behavior and response at hierarchical channels of varying width-to-depth ratio is different and yet to be understood. Previous works on morphological studies focused to investigate river morphological change detection and quantification. These studies could not provide detailed observations on temporal dynamics of river morphological condition. The literature review on flow-vegetation interactions reveal the necessity of understanding the flow structure in heterogeneous vegetation forms which are frequently observed over the riverine corridor.

3

ENTROPY BASED MORPHOLOGICAL ANALYSIS

The Brahmaputra River system is strongly disturbed by high magnitude earthquake called, Medog earthquake in 1950. The huge source of sediment combined with large scale floods generated complex morphodynamic responses for nearly half a century. This makes important to understand present morphological condition of the river. This chapter addresses following question through entropy based analysis.

- It has been greater than 50 years that great Assam earthquake disturbed the river planform. How is the planform stability of the river in the recent decade?
- Previous studies argue flood stream power control the river morphodynamics. How is this theory applicable to the Brahmaputra River?
- There are many dominant, inter-dependent processes happening in the large fluvial systems. How do different morphological variables respond during seasonal morphological changes?

3.1 INTRODUCTION

Braided rivers are often characterized by an irregular planform due to high stream power and associated morphological processes; such as erosion, deposition and channel migration [Bridge, 1993a; Ferguson, 1993; Klaassen *et al.,* 1993]. They produce complex and distinctive forms over the river corridor in response to fluctuating flow and sediment supply [Smith, 1977; Ashworth *et al.,* 2000; Piegay *et al.,* 2009; Zolezzi *et al.,* 2009].

Understanding their dynamic behavior helps effective river management and also for planning and maintenance of river training works [Bristow and Best, 1993; Gilvear, 1993; Paola, 1996; Nicholas *et al.*, 2006; Piegay *et al.*, 2009; Bawa *et al.*, 2014; Sarker *et al.*, 2014].

Among many braided rivers in the world, the Brahmaputra River is one of the best examples of a large sand-bed braided river system [Coleman, 1969; Thorne *et al.*, 1993; Mosselman *et al.*, 1995]. The river is characterized by high flow and sediment transport variability, very erodible banks and, high width resulting in seasonal-scale morphological changes [Goswami, 1985; Karmaker and Dutta, 2011; Karmaker and Dutta, 2013; Karmaker and Dutta, 2015]. The river has also been disturbed by earthquakes and high magnitude and duration floods [Valdiya, 1999; Goswami, 1985] which generate complex morpho-dynamic responses [Sarker *et al.*, 2014]. Millions of people are affected by river's morphodynamics. Enhanced knowledge of the morphological understanding of the river is needed for effective mitigation strategies and also for planning and designing sustainable engineering interventions [Sarker *et al.*, 2014]. Many of the previous morphological change studies of the Brahmaputra River focused on bank line migration and its erosion rate [Klaassen *et al.*, 1993; Thorne *et al.*, 1993; Gilfellon *et al.*, 2003; Khan and Islam, 2003; Sarma, 2005; Sarma and Phukan, 2006; Alam *et al.*, 2007; Baki and Gan, 2012; Sarker *et al.*, 2014] and some other studies on braiding parameters [Gilfellon *et al.*, 2003;Takagi *et al.*, 2007] and their relation with stream power [Akhtar *et al.*, 2011; Karmaker *et al.*, 2017]. Yet, knowledge of the morphological behavior of the river is limited and remain challenging for engineers and geomorphologist due to its dynamic nature. This chapterr uses entropy to contribute to this challenge.

The concept of entropy has been used in morphological studies at different scales. Leopold and Langbein [1962] made use of the entropy concept for the first time to understand stream network behavior. Their study employed thermodynamics theory relating heat energy and temperature to potential energy and elevation in streams. A similar principle was adopted by Teuling *et al.* [2006] to derive an expression for entropy production in a meandering river. Bandyopadhyay [2014] also utilized a thermodynamic approach to evaluate the landscape stability in Kanur river basin. Likewise, alternative forms of entropy, derived from information theory [Shannon, 1948] have been used to study morphological patterns in streams. Fiorentino *et al.* [1993] and Claps *et al.* [1994] utilized information entropy for fractal river networks and also derived relations with mean

drainage basin elevation and for river profiles. Tejedor *et al.* [2017] using information entropy studied the optimality principle in self-organized deltas in relation to the transport of water and sediment fluxes. Other studies have utilized entropy concepts for predicting equilibrium morphologies [Nield, 2006], river bed changes [Guo-bin and Ted, 2012], analyzing fluvial processes [Guo-bin and Lina, 2013], modeling stream bank erosion [Pitchford *et al.*, 2014], bridge-pier scour [Pizarro *et al.*, 2017] and, velocity entropy for laboratory braided rivers [Mirauda *et al.*, 2017]. This makes entropy an important concept in geomorphic studies, reflecting its relevance to precipitation and stream flow characteristics [Singh, 1997; Mayurama *et al.*, 2005; Chen *et al.*, 2008; Mishra *et al.*, 2009, Brunsell, 2010; Liu *et al.*, 2013; Salas and Poveda, 2015] as important drivers of drainage networks. However entropy has been less widely used in relation to river morphodynamics, and this is the focus of this paper.

Sandbars are the key morphological features which are highly uncertain in large braided rivers [Ashworth and Lewin, 2012]. In the Brahmaputra River, due to high flow and sediment variability, sandbars are highly dynamic and frequently subjected to morphological changes at varying flow stages. Most of the studies on the Brahmaputra River focused on change detection. The variability in terms of sandbar adjustment over a time period has not been investigated. In this context, informational entropy a measure of uncertainty or variability or dispersion [Mishra *et al.*, 2009] is used here to quantify sandbar dynamics in the Brahmaputra River. Specifically, the variability is quantified in terms of disorder index using entropy methods applied over seasonal and annual time-scales.

3.2 STUDY AREA AND DATA SETS

3.2.1 Study Area

The Brahmaputra River in Assam, between Tezpur and Guwahati [Figure 3.1] is considered here. The reach is 140 km long, and its braided belt width varies between 1.2 km to 15 km, giving a wide accommodation space for morphological activity. The river exhibits severe braiding and makes its path tortuous, but at Tezpur and Guwahati, the river is geologically confined to a single channel [Goswami, 1985; Sarma, 2005; Lahiri and Sinha, 2014; Karmaker *et al.*, 2017]. The daily discharge hydrograph of the river is highly fluctuating [Goswami, 1985]. The mean daily discharge at Guwahati varies from 4,420 m^3s^{-1} in the dry season to 51,156 m^3s^{-1} during the flood [Singh *et al.*, 2013]. The bed and bank material of the river is a composite of fine sand and silt, falling under highly erodible

zone [Karmaker and Dutta, 2011]. Morphological changes such as thalweg shifting, severe bank erosion and migrating sandbars are most common in this river [Coleman, 1969; Thorne *et al.*, 1993]. The majority of sandbars in the reach are un-vegetated and highly dynamic, *i.e.*, any change in the fluvial system variables reflects in sandbar characteristics. Flow and sediment variability, wider braided belt width and highly volatile banks make the river vulnerable to frequent morphodynamics.

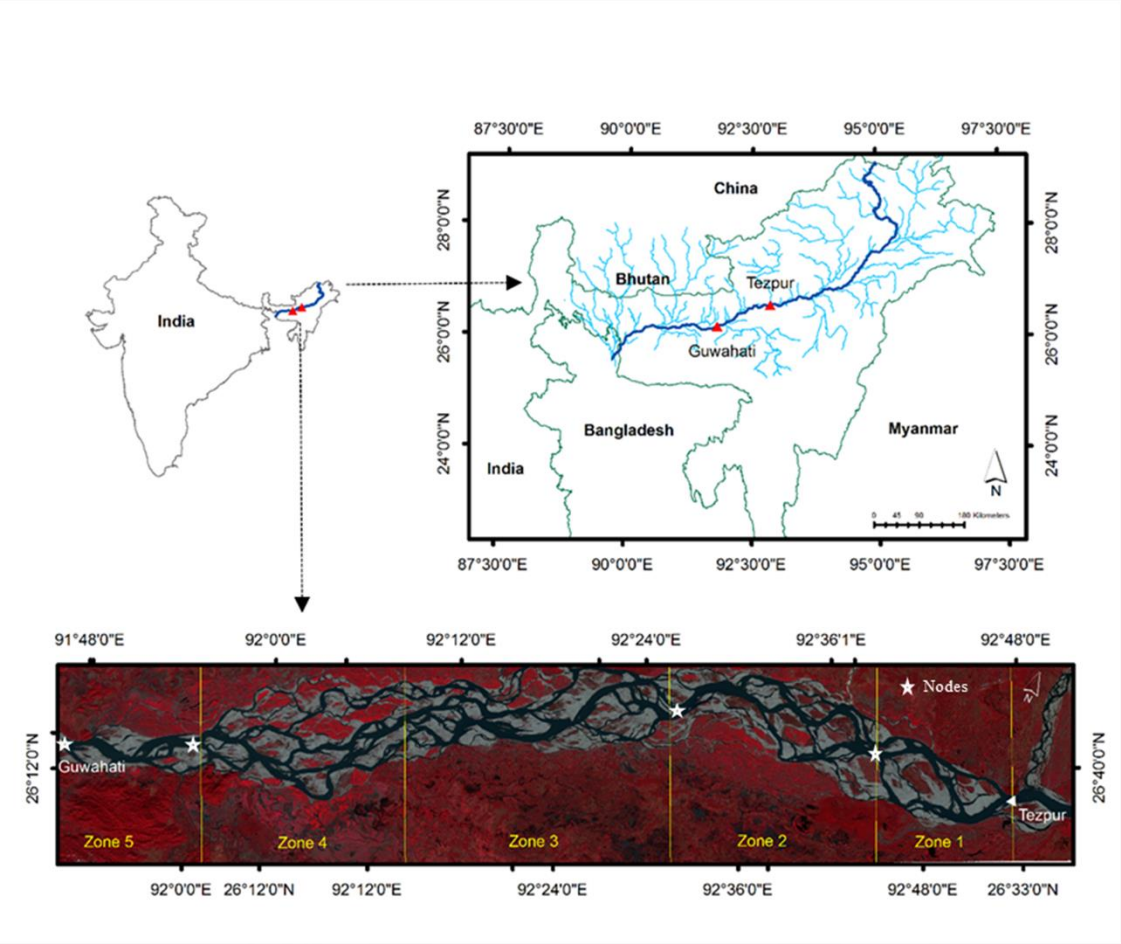

Figure3.1 Map of the Brahmaputra River showing its catchment and the study reach

3.2.2 Data Sets

Optical Data

To investigate the yearly morphological variability of sandbar distributions, optical satellite images were collected from the USGS Landsat Archive. Cloud-free optical images derived from Landsat 4-5 TM, Landsat 7 ETM^{+} and Landsat 8 were selected for both dry (February) and post-monsoon (November) season. In total, 32 images were chosen covering a period from 2000 to 2015 with one in February and other in November. During the rising stage, the river activates all its secondary and tertiary channels, and other leftover

traces and, forms new sandbars between these channels. In the low flow season, the river deactivates its farther paths and flows mainly through first-order channels. Thus, optical images collected during both the seasons may provide distinctive information on sandbar characteristics.

Hydrological and Bathymetry Data

The hydrological data used in the study comprises discharge and water level data, obtained from Central Water Commission of India. The data were available for Tezpur and Guwahati gauging stations for the period 2000-2013. Also, peak flood data from 1970 to 2013 were available at Guwahati gauging station. The river cross sections in the study reach were collected from Brahmaputra Board, Water Resources Ministry. There are 14 cross sections covering the entire braided belt width at 10 km interval between Tezpur and Guwahati. These data were used to set up a one-dimensional model for evaluating the mean specific stream power (**ω**) to correlate with morphological variability.

3.3 METHODOLOGY

3.3.1 Geomorphological Mapping

All the satellite images were digitized in ArcGIS 10.2 to map the sandbars, thalweg line, bank line and their dimensions were analyzed. It was observed that dry season (January through March) was dominated by the medium to large sized bars, and in rising and falling season (April to June and October to December) the same bars were dissected into multiple small bars, resulted in increased bar density. During the peak monsoon season (July to September), most of the bars were submerged, and the river flows through a single channel. Very few sandbars in the study reach were vegetated, and rest were bare and readily exposed to morphological activity. A simple figurative example to illustrate braided planform response for different water levels is shown in Figure 3.2.

The size of the sandbars in the study area varied from as small $\leq 5 \times 10^5$ m^2 to very large ($>5 \times 10^6$ m^2). In general, smaller bars are highly unstable and are frequently subjected to morphological changes (they even disappear); whereas larger bars are more stable, according to their size, shape and location [Baki and Gan, 2012]. From the frequency analysis, the number of smaller sandbars was observed to be higher as compared to medium and large sized bars. Typical sandbar distribution identified over the study reach is shown in Figure 3.3. To carry out further analysis, the river reach was divided into five zones

[Figure 3.1] based on node points (Zone 1, 2, 4, 5) and abrupt braided belt width change (Zone 3). The node points in Zone 1, 2, 4 and 5 were observed to be consistent over the study and the braided belt is fairly uniform within each zone. Table 3.1 lists the details of each zone and the significant morphological characteristics observed.

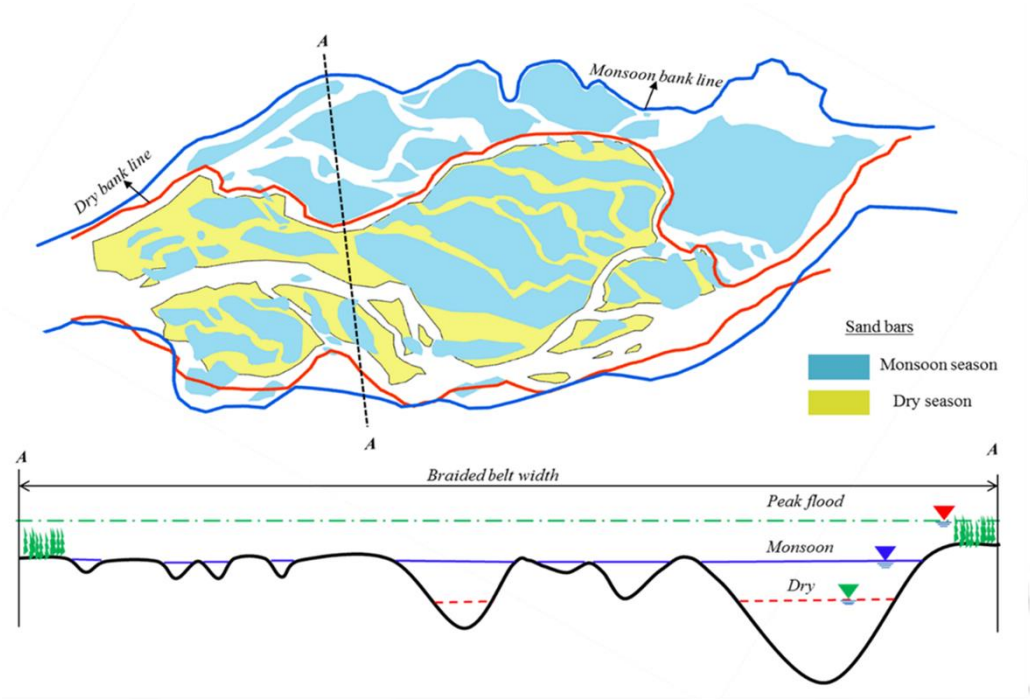

Figure 3.2 Response of the braided planform at different water levels

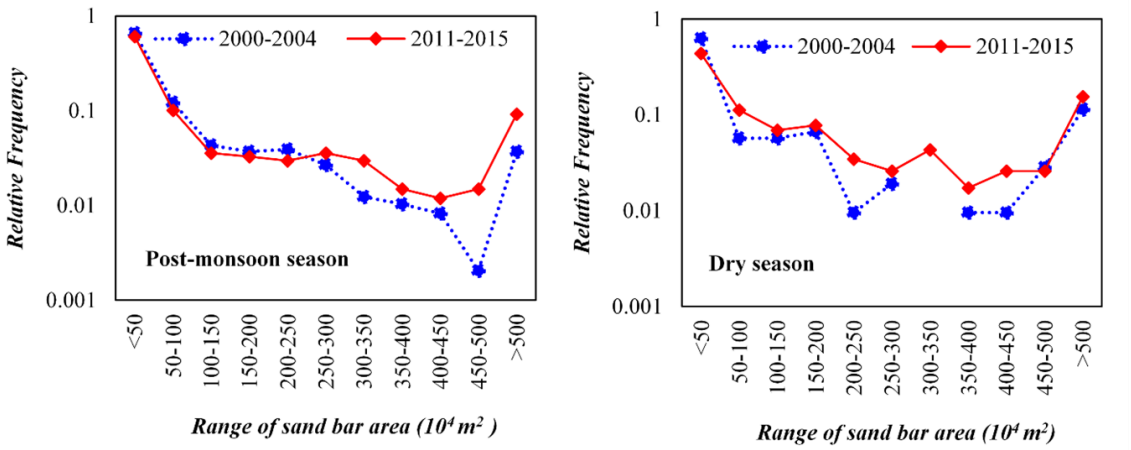

Figure 3.3 Typical sandbar distribution identified over the study reach in Post-monsoon and dry season

Table 3.1: Details of the zones in study area

Zone	Length (km)	Braided Belt Width			Average Slope (m/km)	Average Specific Stream Power (W/m^2)	Morphological Characteristics
		Average (km)	Range (km)	Std. Dev. (km)			
1	15	6.7	6.3-7.4	0.29	0.134	3.54	Moderately braided
2	25	9.0	8.7-9.2	0.21	0.121	2.30	Moderately braided
3	30	9.6	9.3-9.9	0.17	0.114	2.06	Intensely braided
4	25	11.7	11.3-12.6	0.33	0.112	1.74	Intensely braided
5	15	4.2	3.9-5.2	0.34	0.105	4.50	Straight reach and less braided

3.3.2 Intensity Entropy

The concept of entropy used in the study was Shannon's information entropy, which is a measure of uncertainty or variability or disorder associated with the random variable *X* (=$x_1, x_2, x_3 \ldots\ldots\ldots x_n$). Shannon [1948] defined uncertainty of occurrence of an event x_i out of possible events in *X* as entropy *H(X)*, which is given by

$$H(X) = -\sum_{i=1}^{n} p_i \log_2 p_i \qquad (3.1)$$

Where, p_i is the probability of x_i, which is based on empirical frequency of *X* values. The present study uses the concept of intensity entropy (*IE*) to investigate the seasonal variability associated with the area wise distribution of sandbars in the Brahmaputra River. The *IE* can be evaluated as follows

1. The areas of the sandbars were determined for dry and post-monsoon season for all the years. Then, for each season frequency of sandbars were segregated into *n* number of classes [Baki and Gan, 2012] based on their area [Figure 3.3].
2. Considering the number of sandbars (f_i) in a particular class (*n*) of a season to the total number of sandbars in that season (*N*), the relative frequency was calculated as f_i/N (=p_i).
3. Probabilities were calculated for the individual season for all the years by taking into account all the number of sandbars formed in that season. Then, the intensity entropy was calculated as

$$IE = -\sum_{i=1}^{n} \left(\frac{f_i}{N}\right) \log_2 \left(\frac{f_i}{N}\right) \qquad (3.2)$$

The value of *IE* ranges as $0 \leq IE < \infty$ and is expressed in bits.

The intensity entropy evaluated here provides the measure of uncertainty in the distribution of sandbar surface areas. Its value reaches maximum when the sandbars are equally distributed between all classes and, is minimum (=0) only if all sandbars fall into a particular class. It is to be noted that in the Brahmaputra River, the distribution of sandbars depends on the flow regime and varies with time. To assess the entropy-based variability in each season, the intensity disorder index (*IDI*) proposed by the Mishra *et al.*, [2009] was used. This is defined as the difference between maximum possible entropy (IE_{max}) and the entropy for individual distribution (*IE*). Its value is higher for highly variable series.

Moreover, by using *IDI* computed seasonally another indicator was proposed to evaluate the annual disorder occurred on the braided planform, which is termed as annual planform disorder index (*PDI*). It is defined by differencing the *IDI* computed in post-monsoon and *IDI* in successive dry season. Mathematically, this is

$$IDI_{Nov.} = IE_{max} - IE_{Nov.} \quad (3.3)$$

$$IDI_{Feb.} = IE_{max} - IE_{Feb.} \quad (3.4)$$

$$PDI_{(i)} = IDI_{Nov.(i)} - IDI_{Feb.(i+1)} \quad (3.5)$$

Where, $IDI_{Nov.}$ and $IDI_{Feb.}$ are intensity disorder index computed for post-monsoon and dry seasons; IE_{max} is the maximum possible intensity entropy for uniform distribution; $IE_{Nov.}$ and $IE_{Feb.}$ are the November and February intensity entropies for individual distribution.

3.3.2 Stream Power Analysis

Stream power (**Ω**) is defined by Bagnold [1966] as the rate of liberation of kinetic energy from potential energy during the downward movement of the flow. The variability in stream power often governs the morphological activity of the river [Bizzi and Lerner, 2012; Bawa *et al.*, 2014; Akhtar *et al.*, 2011; Karmaker *et al.*, 2017]. Therefore, in this study stream power analysis was carried to investigate whether any link can be found between *PDI* and stream power. To evaluate the stream power, a one-dimensional model, HEC-RAS [Brunner, 1995] was set up and simulated with daily discharge hydrographs to compute monsoonal and peak flood stream power. The model computes specific stream power (**ω**, Wm^{-2}), which is represented mathematically as

$$\boldsymbol{\omega} = V\tau_b = V\gamma RS \quad (3.6)$$

Where, V is average velocity of the flow; τ_b is bed shear stress; γ is specific weight of water; R is hydraulic radius and S is dimensionless energy gradient.

3.4 RESULTS AND DISCUSSION

3.4.1 Variability in Total Intensity Disorder Index

Figure 3.4 shows the plot of the yearly variation of *IDI* in dry and post-monsoon season. It is observed that post-monsoon season has a higher deviation than the dry season. During the post-monsoon period, due to high flow conditions, the majority of the large dimension bars were dissected into small bars; resulting in increased concentration of the

density of small bars. In the dry season, the low river flow causes the multiple channels to dry up and restricts flow to first-order braided channels. This results in more uniform distribution of sandbars among all the classes relative to the post-monsoon season.

It is also observed that between the dry and the post-monsoon season, the variability decreased as a function of time. This is due to significant variation in sandbar distribution with time over a braided planform. Figure 3.3 shows the typical sandbar distribution for two different time periods (2000-2004 and 2011-2015). The distribution shows a clear increase in the frequency of medium to large sized sandbars in the dry and post-monsoon seasons. In the early period (2000-04) smaller and unstable bars are more dominant but in the later period (2011-15) the contribution from medium-larger sized bars is significant resulting in decreased variability with time. The variability in hydrologic regime [Nicholas *et al.*, 2013] and, also periodic disturbances (earthquakes) have a profound influence on river morphology. Any change in these controlling variables leads to a sequence of fluvial changes within the system at different scales. It is observed that peak floods [Figure 3.5] in the Brahmaputra river basin have decreasing with time over the last four decades. Moreover, dynamic morphological changes have occurred for nearly half a century due to a sediment wave generated by the 1950 Assam earthquake may also contribute to this temporal evolution [Sarker 2003; Sarker and Thorne, 2006]. Therefore, the decreased variability in sandbar areas over a braided planform may be due to decreased intensity of peak floods and continued response to the Assam earthquake.

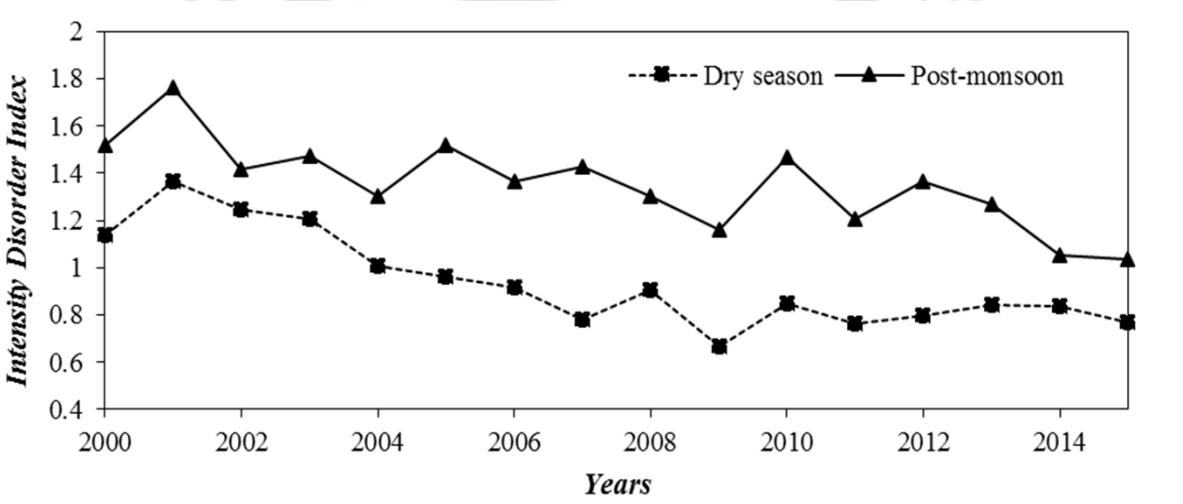

Figure 3.4 Yearly variation of intensity disorder index in dry and post-monsoon season

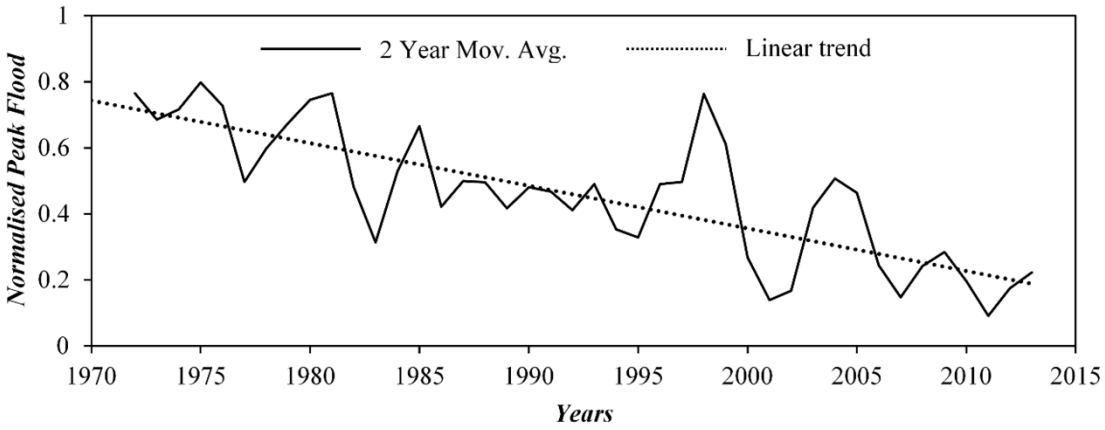

Figure 3.5 Temporal variation of peak floods in the Brahmaputra River at Guwahati

3.4.2 Variability in Zone Wise Intensity Disorder Index

Yearly variation of the zone wise intensity disorder index was studied by dividing the study reach into various zones (Zone 1: Tezpur to Zone 5: Guwahati) based on node points and braided belt width variability (discussed in section 3.1). The braided belt width in the study area varies as Zone 4>Zone3>Zone2>Zone1>Zone5. Usually, in braided rivers, braiding intensity increases with braided belt width and vice-versa and, due to multiple channels more sandbars are observed. The variability in sandbar areas formed in each zone and their distribution is a function of flow stage, discharge, bank erosion and the river capacity to carry sediment. Therefore, *IDI* was computed for sandbars distribution in each zone for dry and post-monsoon season to evaluate the uniformity. Figure 3.6 shows the spatiotemporal variability of *IDI* contours for post-monsoon and dry season. The plot shows *IDI* in dry season is more uniform than post-monsoon because of increased density of the medium-large bars as the flow is mainly through first-order channels. The deviation between zones also decreased with time. Figure 3.7 and 3.8 represent the zone wise variability of *IDI* for post-monsoon and dry season. It is observed that during dry season *IDI* is fluctuating for Zone 1 and 5. This is because, in the dry season there is lower flow and lower braided belt width (less braiding intensity) in Zone 1 and 5, the flow is diverted towards the single channel and resulted in no formation of sandbars. Post-monsoon, the other channels in these zones were activated and formed sandbars resulting in decreased variability. It can also be inferred from the plots that in both the seasons the variability in *IDI* followed a decreasing trend with time. To be more specific, Zone 2, 3 and 4 followed decreasing trends in deviation from uniform distribution.

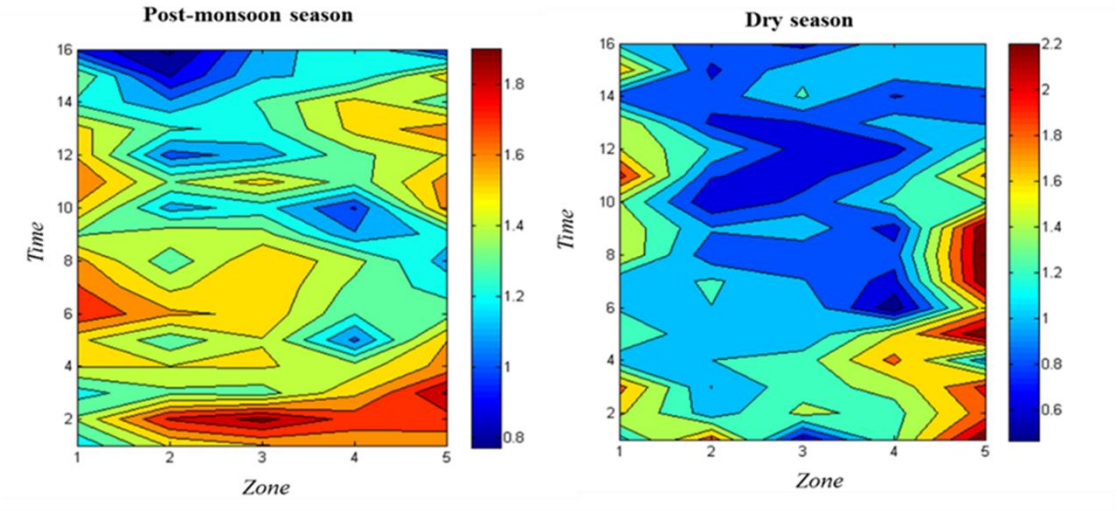

Figure 3.6 Spatio-temporal variability of *IDI* contours for post-monsoon and dry season

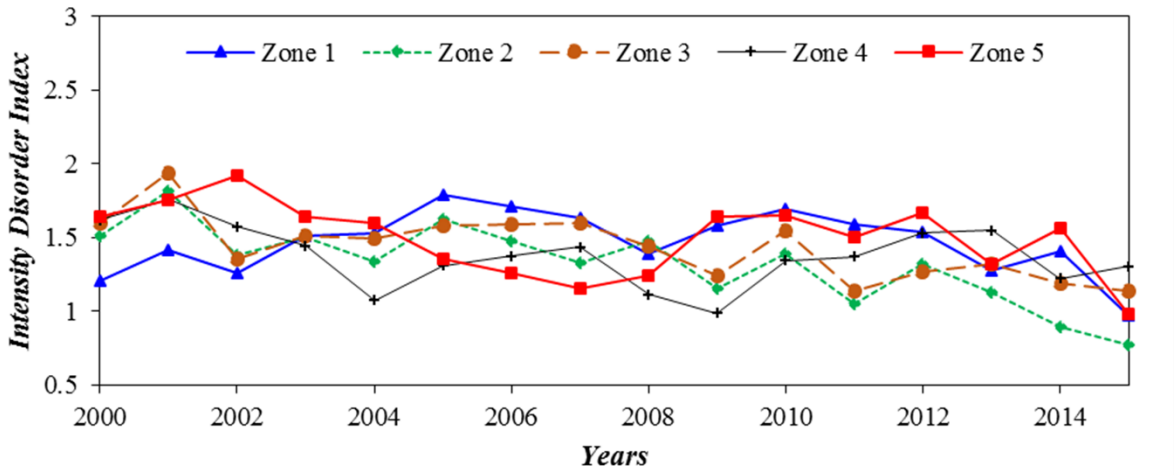

Figure 3.7 Yearly variation of zone wise intensity disorder index in Post-monsoon season

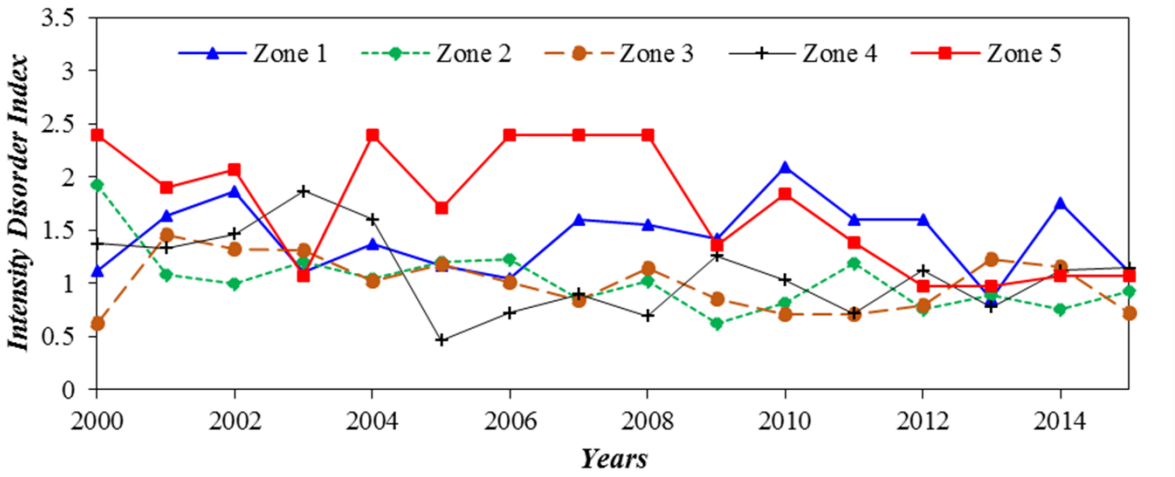

Figure 3.8 Yearly variation of zone wise intensity disorder index in dry season

3.4.3 Variability in Planform Disorder Index and Stream Power

The impact of the seasonal flood on the braided planform is reflected in morphological changes. These changes include shifting of the thalweg, development of new channels, bank erosion, and all this may reflect in sandbar formation and their variability. The disturbance caused by the seasonal flood increases the planform disorder in the post-monsoon season and eventually decreases in the dry season. Therefore, an index termed the planform disorder index (*PDI*) was computed by differencing the *IDI* in post-monsoon and dry season. Along with this, the driving force controlling the braided planform morphology *i.e.* specific stream power (**ω**) was also computed to investigate the link between *PDI* and **ω**. It has been reported that stream power does not directly control braided belt movement or the braiding indices in the Brahmaputra River [Karmaker *et al.*, 2017]. This is quite different from many other studies where flood stream power has been argued to control the morphodynamics [Jain *et al.*, 2006; Kale, 2008; Barker *et al.*, 2009; Akhtar *et al.*, 2011; Bizzi and Lerner, 2012; Bizzi and Lerner, 2015; Magilligan *et al.*, 2015]. Herein, both monsoonal and peak flood specific stream power was calculated and related to *PDI* to find the parameter responsible for planform disorder. Figure 3.9 shows the variability in *PDI* and normalized specific stream power for monsoon and peak flood. Interestingly, the results showed that specific stream power represent the *PDI* trend. Furthermore, for most of the years, monsoonal stream power followed the trend with *PDI* better than peak flood stream power. The Brahmaputra River usually experiences average 9 flood waves of different durations annually [Karmaker and Dutta, 2010]. Hence, the peak flood alone may not be responsible for planform change; other flood peaks and the response of the braided channels together can contribute to the change. Additionally, smaller floods occurring frequently may have a greater cumulative effect on geomorphic work than one or two major floods [Charlton, 2007].

Figure 3.9 also shows two distinct time periods divided on the basis of monsoonal stream power (*MSP*). In period 1 (2000-2004) *MSP* is increasing and in period 2 (2005-2014) *MSP* is decreasing, which shows an important observation regarding the *PDI* variability with *MSP*. *PDI* and *MSP* are inversely related to each other in period 1 and correlated in period 2. Perhaps, during the increased stream power period other fluvio-morphological processes become more important. To investigate the response of other morphological parameters during the increasing stream power period parameters such as thalweg shift and sinuosity, erosion, deposition were evaluated [Figure 3.10]. Table 3.2

shows variation in the intensity of different morphological variables along the increasing stream power period. In 2004 (high stream power), bank erosion and thalweg shift are highly dominant which is followed by *PDI* and sinuosity and, in 2001 (low stream power) *PDI*, deposition and thalweg sinuosity are highly dominant. Figure 3.10 also shows that morphological variables adjust among themselves during the high stream power period to spend the excess energy available. Overall, the analysis [Figure 3.10 and Table 3.2] showed that adjustments of other morphological parameters such as thalweg shift, bank erosion are dominant at higher stream power (increasing stream power period) rather than sand bar adjustments as seen in decreasing stream power period. This may reflect the differences between trends and styles of adjustment that are dominant in increasing and decreasing stream power periods.

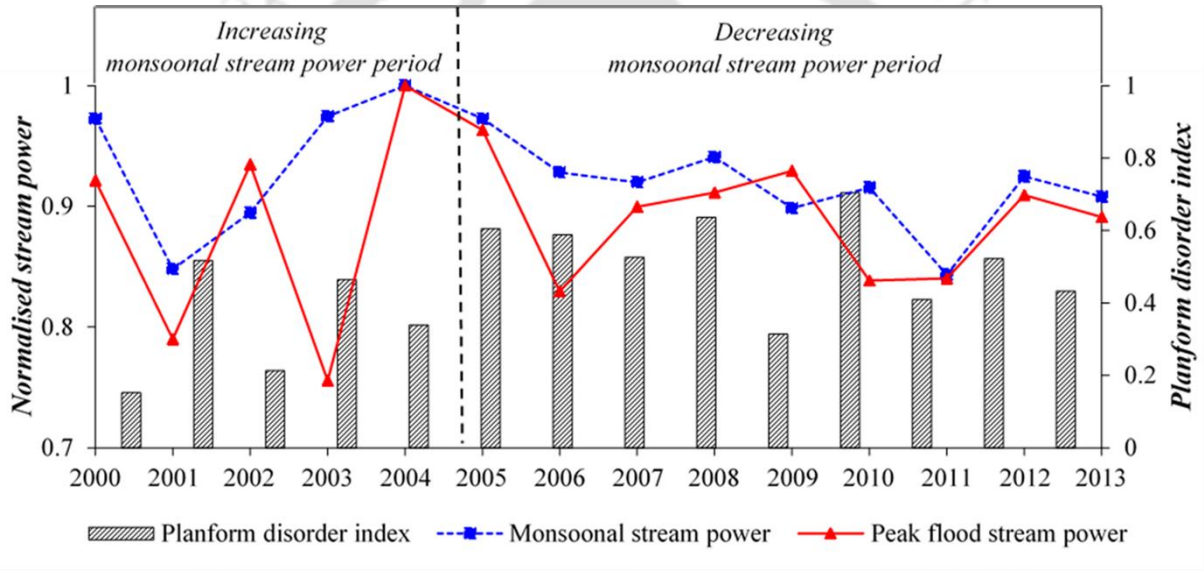

Figure 3.9 Annual variability in planform disorder index and specific stream power

In the years 2000 and 2004 the monsoonal and peak flood stream power are very high and the response is a lower *PDI*. In contrast, in the consecutive years 2001 and 2005 the low stream power contributed high *PDI*. It is clear that rising peak floods carry high erosion power (increased velocity and turbulence) which is responsible for changing shallower channels to deeper, eroding smaller and unstable bars and causing severe bank erosion. As the flood falls, sporadic patterns are observed in depositions of eroded material. The effect of such high magnitude floods takes time to absorb within the system before it moves towards a new planform [Charlton, 2007]. Possibly the *PDI* computed by differencing the post-monsoon and succeeding dry season could not reflect the intensity of the disorder caused by the flood. In turn, its effect may be seen in the next year where the

seasonal monsoon flood readily occupied the defined paths leftover or created by the peak flood, and increased the *PDI*. Other factors such as the number of flood peaks, their fluctuations, flood duration, critical thresholds and mostly river behavior show a profound influence on geomorphic response [Costa and O'Connor, 1995; Magilligan *et al.*, 2015].

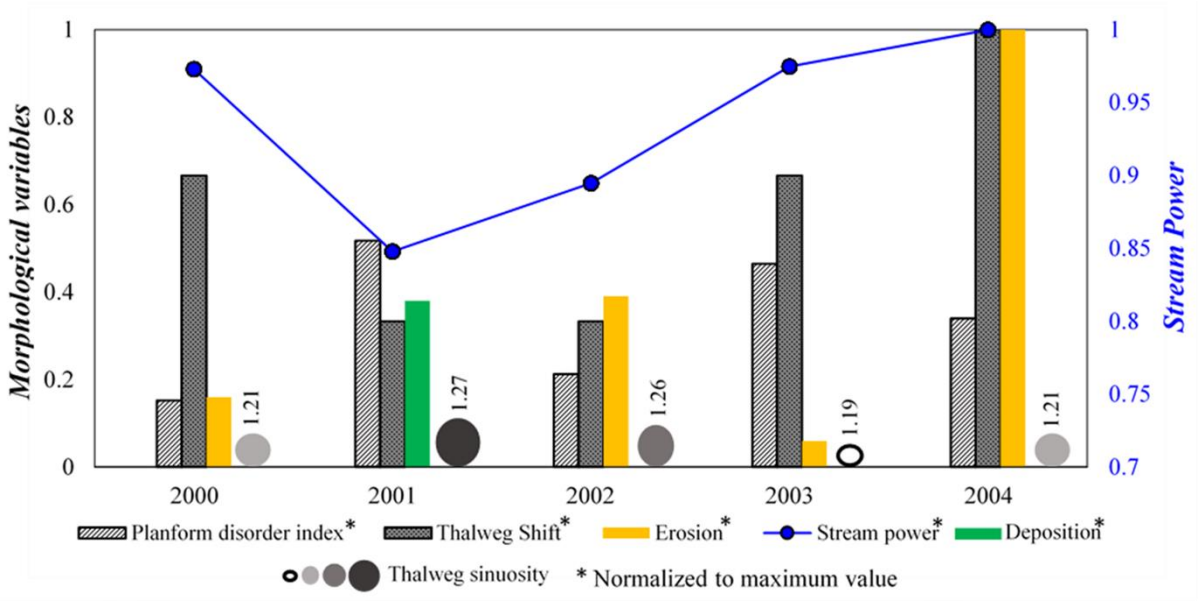

Figure 3.10 Response of the morphological variables in increasing stream power period

Table 3.2: Intensity variation of morphological variables in increasing stream power period

Morphological variables	2000	2001	2002	2003	2004
Stream power	○	◦	◌	●	●
Planform disorder index	◦	●	◌	●	○
Thalweg shift	○	◦	◌	●	●
Thalweg sinuosity	◌	●	●	◦	○
Erosion	●	-	○	◌	●
Deposition	-	●	-	-	-

● Dominant; ● Very High; ○ High; ◌ Moderate; ◦ Low

(1) Year 2005 also represented similar morphological variables response as 2001

(2) Thalweg shift is considered as number of times in a reach the main thalweg line migrated towards opposite bank

3.5 CHAPTER SUMMARY

In the present study, the concept of intensity entropy is used to assess the annual variability associated with the distribution of sandbars over the braided planform of the Brahmaputra River. Two indices namely intensity disorder index (*IDI*) and planform disorder index (*PDI*) relating to the variability in sandbars distribution are computed. Indices provided understanding of the time-dependent adjustment of sandbars in the Brahmaputra River. The results of the study lead to the following conclusions. First, the variability in sandbars arrangement for a braided reach tends to be decreasing. The contribution of medium to large sized bars is increasing with time resulting in less deviation from a uniform sandbar arrangement. For individual zones within the reach, the variability also decreased with time. The changing variability in peak flood magnitudes and the relaxed effect of 1950 Assam earthquake may have caused this change in sandbars adjustments. Second, for the Brahmaputra River, monsoonal stream power is found to be better related to the annual planform disorder index than the peak flood stream power. As the river usually experiences average 9 flood waves of different durations annually, the peak flood alone may not be responsible for planform change. Third, two distinctive trends in stream power variability are found; when decreasing, stream power is well correlated with the planform disorder index. When increasing, adjustments in other morphological parameters such as thalweg shift, bank erosion are dominant rather than sand bar changes. The study presented a new approach to represent planform disorder of a braided river system in terms of sandbars adjustments. The entropy theory can be further explored to study its applications in detail in geomorphic studies.

4

MORPHOLOGY AND BEHAVIOUR OF HIERARCHICAL CHANNELS

Braided network of the Brahmaputra River consist of hierarchical channels carrying varying discharge, geometry and location. The river is characterized by high flow and river energy making various morphological adjustments. Moreover, the presence of nodal and multi-thread locations generate complex morphodynamics processes making important to understand the river hydraulic characteristics. This influence the nature of bed deposits across the river and effects the movement of sediment transport. This chapter addresses the following questions through field and satellite data analysis.

- How is the river hydrodynamic and morphological characteristics in hierarchical channels of complex braided river network?
- Where the Brahmaputra River spends its energy in geomorphic work?
- How the hydraulic parameters are varied at nodal and multi-thread locations? How is the influence of cross-section morphology on flow parameters?
- What is the nature of bed deposits in the Brahmaputra River along the river course?
- What kind of turbulent structures are present in the river? How they influence the river behavior?
- Previous studies argue absence of secondary circulation cells in large rivers. Is it true for the Brahmaputra River?

4.1 INTRODUCTION

Sandbed braided rivers are characterized by complex, unstable river network formed due to the interaction of high flow energy and intense sediment transport [Smith, 1971; Graf, 1981; Ferguson *et al.,* 1992; Mosselman, 1995; Ashmore, 2013; Schuurman *et al.*, 2013]. They generate complex morphological adjustments over a braided corridor as a response to changes in flow and sediment supply (Smith, 1978; Bridge, 1993; Ashworth *et al.*, 2000; Bertoldi *et al.*, 2009; Zolezzi *et al.*, 2009]. Understanding of river behavior and mechanics thorough field, lab and modeling based studies can be extremely helpful in their management and also for effective river training [Davoren and Mosley, 1986; Bristow and Best, 1993; Paola, 2001; Ashworth *et al.*, 2000; Best *et al.*, 2003; Nicholas *et al.*, 2013; Sarker *et al.*, 2014].

Many researchers consider the Brahmaputra River as one of the classic example of large and dynamic braided river system for understanding hydrodynamics and morphological features [Coleman, 1969; Thorne *et al.*, 1993; Klaassen *et al.*, 1993; Best *et al.*, 2007]. The river remains distinctive due to high flow and sediment variability, severely erodible banks, and, wider braided belt resulting in dynamic morphological changes [Goswami, 1985; Singh *et al.*, 2004; Karmaker and Dutta, 2013, 2015]. The river catchment has also been disturbed by high magnitude seismic events and extreme floods that cause long-term morphodynamics response in the river system [Dhar and Nandargi, 2000; Sarker and Thorne, 2006; Karmaker and Dutta, 2010; Lahiri and Sinha, 2014]. Hundreds and thousands of people are annually affected by bank erosion and morphology change. Enhanced knowledge of flow structure, river response, and planform dynamics is needed for socio-economic management and, successful planning and implementation of river training works [Sarker *et al.*, 2014].

Previous works of the Brahmaputra River mainly focused on morphological change detection and/or quantification studies such as erosion and deposition, channel and bank migration, braiding indices and other related [Khan and Islam, 2003; Bhakal *et al.*, 2005; Sarma, 2005; Sarma and Phukan, 2006; Takagi *et al.*, 2007; Akhtar *et al.*, 2011; Sarker *et al.*, 2014; Karmaker *et al.*, 2017; Saikia *et al.*, 2018]. Although limited in number, but studies carried out by Coleman [1969], Richardson and Thorne [1998, 2000], McLelland *et al.* [1999] and Ashworth *et al.* [2000] made a significant contribution to river flow and sediment processes utilizing acoustic sounding equipment. Coleman [1969] for the first

time, characterized the Brahmaputra River bedforms and their influence on macro-turbulent features through vigorous in-situ measurements. Richardson and Thorne [1998] performed a field-based study to demonstrate the presence of large scale secondary currents in multi-thread flows and, developed an energy-based threshold expression for prediction of channel bifurcation [Richardson and Thorne, 2000]. McLelland *et al.* [1999] investigated detailed flow structure and sediment distribution around a developing braided bar at different stages of the monitoring period. This study highlight the absence of secondary flow helical cells in large sections of the width-to-depth ratio much higher than 100. Ashworth *et al.* [2000] described the process of braid bar initiation, growth, and its development by continuous monitoring with bathymetric and ADCP surveys at different river stages. Their study conceptually summarizes the key stages in bar development and, the influence of bedforms on bar growth and migration. These studies have provided a good process-response based understanding of flow-planform interactions, however, limited their work to flow surrounding a braided bar. The present work aims to focus on this challenge.

The braided network of the Brahmaputra River is composed of hierarchical (primary, secondary and tertiary category) channels adjusting over the braided corridor. For example, at larger braided belt width complex network of secondary and tertiary channel dominates and, decreasing braided belt results in more flow diversion towards the primary channels [Chembolu and Dutta, 2018]. This makes important to understand the different channels (hierarchical) response to changes in discharge, width-to-depth ratio, and their location. Also, flow structure coupled with bank erosion and, the influence of upstream morphological changes have shown complex morphodynamics response at different channels of the river network. Thus, in order to better understand the river behavior, the present objective focuses on reporting findings from flow structure and morphological changes at hierarchical channels of the Brahmaputra River, India.

The objectives of this work include: (a) investigate the flow structure and suspended sediment distribution at hierarchical channels where the width-to-depth ratio variation is very large and typically in the order of 50 to 800; (b) examine the influence of flow structure on morphological changes using satellite imagery analysis; and (c) study the concept of energy loss and its impact on river morphological adjustments.

4.2 STUDY AREA, SURVEY DETAILS AND METHODS

4.2.1 Study Area

The Brahmaputra is one of the largest and dynamic braided river systems in the world, with a catchment area of 5.8 x 10^5 sq.km that includes parts of China, India, and Bhutan [Datta and Singh, 2004]. In India, the river traverses 918 km, joining 32 major tributaries and acts as a single drainage system. The river planform varies its braided belt width between 18 km to 1.2 km at nodal points [Sarma, 2005] and, average slope is in the order of 10^{-4} [Goswami, 1985]. The daily discharge hydrograph is highly fluctuating with mean dry season flow of 4420 m^3/s and flood flow of 51156 m^3/s observed at Guwahati [Singh *et al.*, 2004]. The river bed and bank material are in the range of fine sand-silt, falling under severely erodible zone [Karmaker and Dutta, 2011]. Morphologically, the river is sensitive and, frequently subjected to channel migration, thalweg shift, and bank erosion. The flow and associated turbulent structures, bedforms, and migrating sand bars significantly control the river morphodynamics [Coleman, 1969]. The study reach considered here is one of the active morphological zone located between the nodal points Tezpur and Guwahati [Figure 4.1]. Table 4.1 shows the variability in morphological parameters of the study area. River survey was conducted in-between 15 June to 18 June at 8 typical cross-sections of hierarchical braid channels. These include primary, secondary, tertiary channels and large confluence-diffluence sections. On survey dates, the average discharge and corresponding water level at Guwahati was 16,000 m^3/s and 44 m.

Table 4.1: Morphological Parameters Variability in the Study Reach

S. No.	Parameter	Avg.	Range	Std. Dev.
1	[a] Braiding Intensity (BI)			
	• Dry season	5.04	3.5	1.18
	• Post-monsoon	10.9	6.2	1.63
2	Braided belt width (km)	8.5	0.38	0.10
3	[b] Bar density (number/10km)			
	• Dry season	10	8	2
	• Post-monsoon	44	49	12
4	[c] Thalweg shift (number)	~3	4	1.09
5	Thalweg sinuosity	1.22	0.092	0.025

Note: [a] Braiding Intensity = 2(length of all the bars in reach)/length of the midway reach (Brice, 1964); [b] Bar density corresponds to number of bars per 10 km; [c] Thalweg shift is no. of times in a reach the main thalweg line migrated towards the opposite bank.

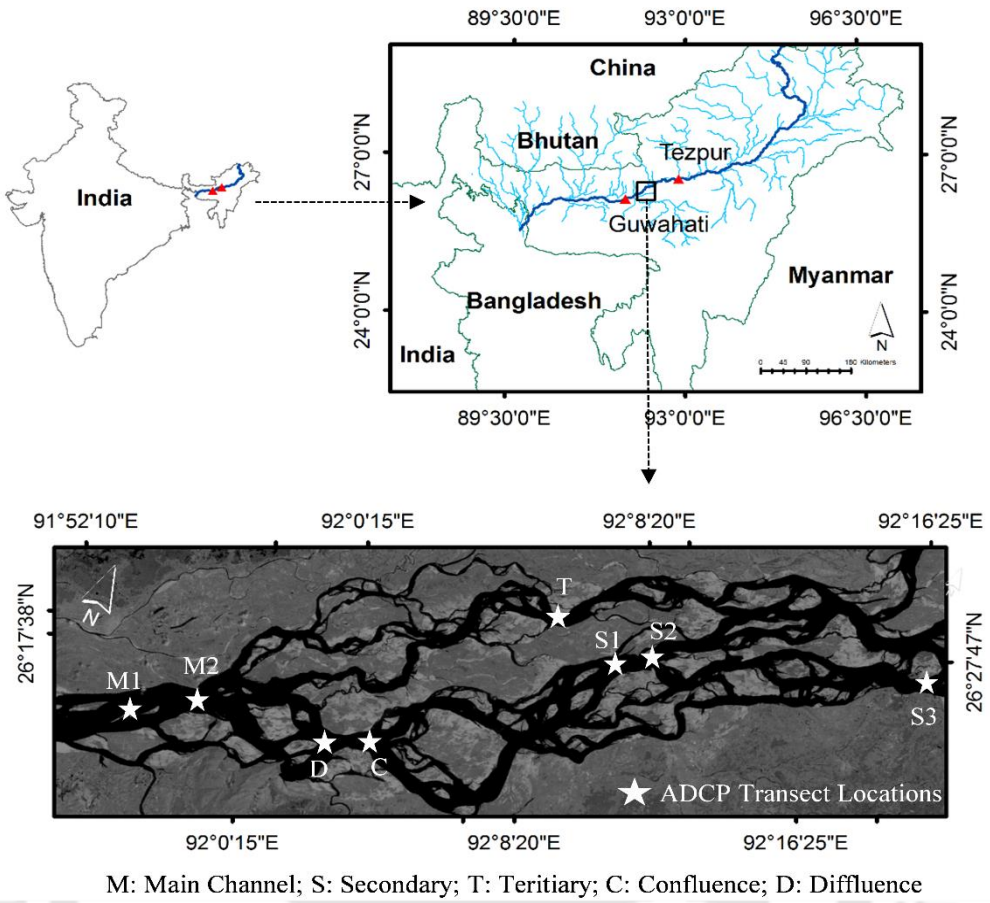

Figure 4.1: Map of the Brahmaputra River showing its catchment, study area and, location of the measured transects

4.2.2 Survey Particulars

Three-dimensional velocity components were measured with a 600 kHz (exact frequency 614.4 kHz) Workhorse Rio Grande acoustic Doppler current profiler (ADCP) operated from a moving survey vessel. ADCP was integrated with GPS and, configured for default parameters (Cell Size: 0.5 m, Water Mode 1, Bottom Mode 5, bottom track pulse length) recommended for large rivers by manufacturers [Teledyne RD Instruments, 2009] and, authors experience from previous data collection [Karmaker *et al.*, 2010; Chembolu *et al.*, 2016]. All the four transducers were immersed 0.30 m beneath the water surface depending on flow conditions. The data was not measured inside the ADCP depth (0.30 m), blanking distance (0.5 m) below transducers and, bottom ~6% of the measured flow depth due to side-lobe interference. Following recommendations from previous studies [Mueller *et al.*, 2009; Szupiany *et al.*, 2009, 2012], the vessel speed to water speed ratio was maintained lesser than 1 and, vessel track along the survey lines was held as constant

as possible. ADCP survey was conducted in monsoon season over four days (15 June to 18 June) at 8 different transects covering hierarchical channels of a braided river network. River stage was nearly steady during the survey period with a maximum water level difference of 0.6 m according to record from Guwahati gauging station. Surveys include 2 main channels (M), 3 secondary channels (S), 1 tertiary channel (T), a confluence (C), and diffluence (D) zone. A summary of the survey particulars and gross hydraulic conditions is shown in Table 4.2. All the survey transects chosen were different in terms of location, asymmetry in river cross-sections, discharge and largely varying width-to-depth ratios (*w/d*). For example, transects M1, C, D characterize multi-thread flow, M2 and S3 represent growth of submerged bar, D and T with *w/d* ratios 800 and 50.

Table 4.2: Survey Particulars and General Hydraulic Characteristics

S. No	Date of Survey	Transect ID	Velocity (ms^{-1})		Depth (m)		Width (m)	Discharge (m^3/s)
			Avg.	Max.	Avg.	Max.		
1	16 June	M1	1.204	2.08	5.6	7.9	2242	14457
2	16 June	M2	1.353	2.17	6.1	11.7	1660	12772
3	17 June	S1	1.486	2.01	8.4	10.8	635	6696
4	18 June	S2	1.405	1.82	7.4	8.9	613	5504
5	18 June	S3	1.068	1.64	5.2	6.5	1405	7069
6	17 June	T	1.12	1.53	6.0	7.5	330	2175
7	15 June	C	1.235	2.01	5.7	9.7	2234	11829
8	15 June	D	1.025	2.09	4.3	7.0	4393	14827

M: Main Channel; S: Secondary Channel; T: Tertiary Channel; C: Confluence; D: Diffluence location

4.2.3 Primary and Secondary Flow Velocity Components

In large rivers like the Brahmaputra, three-dimensional velocity field significantly influence the fluvial processes and associated morphological adjustments. Flow and sediment transport around a braid-bar, bifurcation, and confluence zones are affected by secondary currents at different river stages [Richardson and Thorne, 1998]. Therefore a reliable method must be chosen to define secondary currents from the velocity measurements for understanding the interactions between hydro-morphological processes [Lane *et al.,* 2000]. Secondary currents can be often defined as velocity components perpendicular to the main flow direction. In rivers, the primary direction of the flow is not always parallel to the banks or channel centerline and, can align any direction to the

longitudinal slope. Hence, it is necessary to reorient the velocity vectors such that primary and secondary components are obtained relative to mean direction vectors [Claude *et al.*, 2014]. To calculate secondary current vectors, Lane *et al*. 2000 stated different methods like (a) centerline; (b) Rozovskii (c) zero net cross-stream discharge; (d) discharge continuity method. In smaller streams, when lateral flow changes are not significant, methods like discharge continuity and zero net cross-stream discharge can easily be applied where one secondary plane across the width is considered. In the rivers like the Brahmaputra with larger widths, significant transverse flow changes, and dynamic bed form-flow interactions the direction of the velocity vector is often not same along the channel width. Thus, the present work utilizes Rozovskii method to derive primary and secondary velocity components, which defines flow direction for each vertical velocity profile rather than one derived for the whole cross-section. Rozovskii method was used for other rivers like Rio Parana [Parsons *et al.*, 2007; Szupiany *et al.*, 2009], Loire in France [Claude *et al.*, 2014] which exhibit significant transverse variations. Rozovskii method identifies important features of helical flows like consistent changes in the direction of primary velocity vector near the surface and the bed across the width [Szupiany *et al.*, 2009].

According to Rozovskii method, the primary velocity component (V_p) and secondary velocity component (V_s) of each point at any location is given as

$$V_p = V\cos(\theta-\varphi) \qquad (4.1)$$

$$V_s = V\sin(\theta-\varphi) \qquad (4.2)$$

$$V = \sqrt{V_N^2+V_E^2} \qquad (4.3)$$

Where V is the velocity vector at a point, **θ** is the orientation of vector V with respect to north, V_N and V_E are the north and east components of the velocity vector at a point, ***φ*** is the orientation of depth-averaged velocity vector on vertical with respect to north.

4.2.4 Suspended Sediment Concentration Mapping

Suspended sediment plays an important role in shaping the river planform, creating ecological zone and transporting micro nutrients [Vercruysse *et al.*, 2017]. In the river Brahmaputra, with finer bed material and severe bank erosion suspended sediment transport and distribution becomes highly important to understand morphological response

of the channels at varying flow conditions. The traditional point sampling procedures in the Brahmaputra is (a) tedious due to its large scale; (b) often dangerous to hold the survey boats stationary due to high currents; (c) data collected would be spatially limited and; (d) expensive and time consuming. Although ADCP is primarily designed for flow measurement, many researchers have used acoustic backscatter data as a measure for quantifying suspended sediment concentration in rivers and estuaries [Sassi *et al*., 2012]. This data is spatially rich and, provides detailed distribution of suspended sediment changes along the measured river transects. Furthermore, this information along with local hydrodynamic behavior can help us to understand and predict the possible morphological changes.

Suspended sediment in the water column backscatters the acoustic signals, but the intensity depends on instrument characteristics, sediment concentration and grain size distribution [Deines, 1999; Ozturk and Work, 2016]. Therefore estimation of suspended sediment requires corrections accounting for instrument specific factors, transmission losses, sound absorption losses due to fluid and sediment particles. The simplified sonar equation [Venditti *et al*., 2016] accounting corrections for these effects is

$$FCB = K_c * EI + 20 \log_{10} R + 2\alpha_f R - IC \qquad (4.4)$$

Where FCB is fluid corrected back scatter; K_c is an instrument-specific scale factor; EI is the echo intensity measured by the instrument in counts; R is the distance between transducers and the measured bin; α_f is water absorption coefficient; IC corresponds to several instrument specific constants. The main objective here is to link flow field and zones of increased sediment concentrations to morphological changes and, not specifically to distinguish silt-clay and sand concentration. Therefore, following the recommendation from Topping *et al.* [2007] and Wright *et al.* [2010] that FCB can be directly related to total sediment concentration, the present study has not accounted for corrections for transmission losses due to sediment characteristics. Also, instrument-specific constants (IC) were ignored, which only affect the signal magnitude but not the relative variability [Venditti *et al.*, 2016].

To develop a relationship between FCB and suspended sediment concentration (SSC), simultaneous measurements of ADCP and direct water sampling were carried out. Field samples at different locations and depths were collected to obtain a wide range of sediment concentrations for better estimation of SSC along the cross-section. The locations

include zones of low velocity, eroding banks, submerged sand bar and, sample depths ranging between 1 to 3 m. Stationary ADCP measurements were made at the same locations for a duration up to 3 to 5 minutes. The results of the laboratory analysis showed total suspended sediment concentration is varying between 115 mg/L to 1340 mg/L. FCB computed at each bin along the vertical was averaged accordingly to relate with field measured SSC at that point. The relationship established between $\log_{10}$ (SSC) and FCB is in good agreement with R^2 of 0.81 [Figure 4.2]. Using this relationship, SSC was evaluated along the cross-section at different transects in the study area. The maximum total suspended sediment concentration estimated in the present study was up to 1800 mg/L. This range was in agreement with other reported works on the Brahmaputra River nearby the study area [Dubey, 2017].

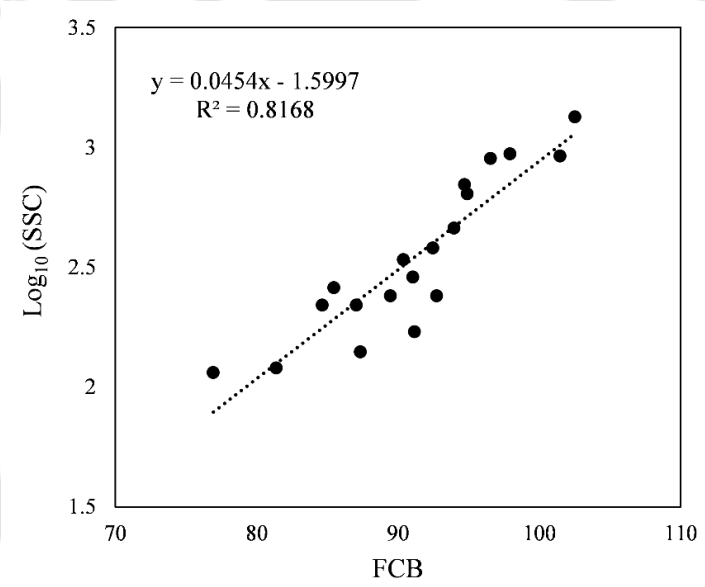

Figure 4.2: Relationship between fluid-corrected-backscattering (FCB) intensity and measured suspended sediment concentration (SSC)

4.2.5 Particle Size Distribution Analysis

Sediment characteristics, such as sediment type, particle size varies throughout the bed in lateral and vertical directions due to rapid changes in river stage and hydraulic parameters [Lick, 2008]. The variability in particle size and, cohesive and non-cohesive nature of sediment deposit often governs the sediment movement, suspension, and deposition patterns. To obtain the nature of bed deposits and bank material, different samples along the river were collected, oven-dried and analyzed in the laboratory. For coarser sediments (>75μm), mechanical sieving is done by passing the sediment through a series of sieves

ranging between 75 to 600μm. The finer and medium-size particles (<75μm) were analyzed by the hydrometer method because the smaller fractions cannot pass through the sieve individually.

4.2.6 Morphological Mapping

Optical satellite imagery was used to understand the link between flow structure and sediment distribution with morphological changes. Satellite images derived from Landsat 8 were collected from the USGS Landsat Archive. Two cloud-free images corresponding to same water level (44 m at Guwahati), one before the monsoon (May) and another post-monsoon (November) were chosen for the analysis. As the river survey was conducted in June month, selection of May and November months for morphological mapping is acceptable to study the changes pre and post-survey. Images were digitized in Arc-GIS 10.2 to map the changes in bank line, and other morphological features at the ADCP measured transects.

4.2.7 Energy Loss and Hydraulic Parameters Estimation

A river performs a series of adjustments to its flow and sediment transport such that the total energy loss is minimized [Simon, 1992]. Thus, the morphological behavior of the river greatly depends on energy availability and its dissipation rate. Therefore, in this study, to understand the gross characteristics of the river, energy loss estimation is carried between two nodal locations Tezpur (upstream) and Guwahati (downstream), distanced 150 km apart in a highly morphologically dynamic reach. More morphological details of this reach are discussed in the Chapter 3. To compute the energy dissipation, a one-dimensional model, HEC-RAS [Brunner, 1995] was set up and simulated with discharge hydrograph. The energy dissipation ($\boldsymbol{\varphi}$) for a river reach between two nodal sections can be expressed mathematically as

$$\boldsymbol{\varphi}_{\text{per unit length}} = \frac{\gamma Q h_f}{L} \text{ expressed in MW/km} \qquad (4.5)$$

$$h_f = \left[z_1 + y_1 + \frac{\alpha_1 V_1^2}{2g}\right] - \left[z_2 + y_2 + \frac{\alpha_2 V_2^2}{2g}\right] \qquad (4.6)$$

Where, γ is the unit weight of the water (Nm^{-3}), Q is the discharge (m^3/s), h_f is the total head loss (m) and L is the length of river reach between nodal locations (km). In the present work, model-simulated hydraulic parameters such as maximum channel depth and active

width were compared and analyzed at the nodal section and multi-thread cross-section for understanding the river response at varying flow stages.

4.3 RESULTS

4.3.1 General Characteristics of the River System

The Brahmaputra River is morphologically dynamic that adjusts to fluvial disturbances or changing channel geometry, hydraulics, and sediment load. The interactions between varying flow-sediment fluxes and braided channel forms make complex river-channel adjustments due to wide space for morphological activity and easily erodible banks. This section discusses the gross hydraulic and morphological characteristics of the Brahmaputra River to understand the river system response and behavior. Three important aspects discussed here include energy dissipation and morphological adjustments, hydraulic parameters at nodal and multi-thread cross-sections and, variability in bank and bed material deposits.

The seasonal variability in river-energy and the extent of geomorphic work carried is significantly high in the Brahmaputra River. In addition, geo-dynamically active zone and extreme floods induce additional disturbance to the fluvial system causing severe channel response adjusting with time. Figure 4.3a shows temporal trends in average energy dissipation and morphological adjustments for an active river reach between two nodal locations Tezpur and Guwahati. The average energy dissipated in low flow season (January to March and December), monsoon (June to October) and peak flood period (in August and September) was observed to be 5, 25 and 30 MW/km respectively. To dissipate the excess energy, the river performs a series of possible morphological adjustments such as erosion and deposition, thalweg shift, changes in sinuosity and sandbars variability across different seasons. Herein, two dominant, monthly changing morphological variables like sandbar density and thalweg sinuosity were considered [Figure 4.3a]. Morphological analysis revealed that sandbars count and thalweg sinuosity were trend-wise opposite over different seasons in a year. In the low flow season, where energy dissipation is less and flow is mainly confined to primary channels, the thalweg sinuosity is dominant with magnitude ~25% higher than the monsoon period. With increase in discharge, the river activates all its secondary and farthermost channels predominantly to dissipate the excess amount of energy. This was reflected in increase in sandbars count from ~100 in low flow season (5 MW/km) to ~400 in monsoon season (25 MW/km). Further in peak monsoon period with

energy dissipation >25 MW/km the sandbar count and thalweg sinuosity decreased considerably as the river flows more or less as a single channel. At this stage, the influence of macro turbulent structures, large scale bank erosion, and significant flow-sandbar vegetation interactions may be also dominant in dissipating the excess river-energy. Thus, the river adjusts different fluvio-morphological variables at different stages in response to flood events of varying intensity and duration.

The Brahmaputra River in its course is highly braided with width generally varies between 3 km to 18 km. At few locations such as Tezpur, Guwahati and Jogighopa, the river is geologically confined to a single channel of width nearly 1.5 km. These nodal reaches show significant influence on sediment distribution and, upstream and downstream channel morphology. To understand the variability in hydraulic parameters and their control on channel morphology, model simulated results at two different cross-sections one being a nodal section (~1.9 km) and another at widest part (~10 km) were analyzed [Figure 4.3b]. The maximum channel depth at nodal location varies as ~6 m in low flow season to ~ 16 m in monsoon, with the active channel width being slightly differed at 1.2 km and 1.6 km in low and monsoon period. However, at wider multi-thread cross-section the maximum channel depth was up to ~8 m in the main channel during the monsoon period and total active channel width of ~9.5 km, which is close to the braided belt width (~10 km). Moreover, in the peak monsoon period (July, August and September), the maximum channel depth in a high discharge carrying channel is nearly constant as the other channels were activated and receiving the excess flow. This is contrast to the nodal section where maximum channel depth was observed to be vertically increasing with flow. Reasons for the difference in hydraulic parameters is probably due to unstable banks not allowing the channel deepening and wider braided belt width allowing the planform adjustments by creating a multiple channels. Previous works [e.g., Karmaker *et al*., 2010; Karmaker and Dutta, 2011] have also shown that maximum stable bank height in the Brahmaputra River was close to ~9 m and, further channel deepening causes rapid bank erosion and consequent morphological adjustments. This implies that in the unstable river reaches, the main channel is severely prone to bank erosion and is not sustainable for a longer period.

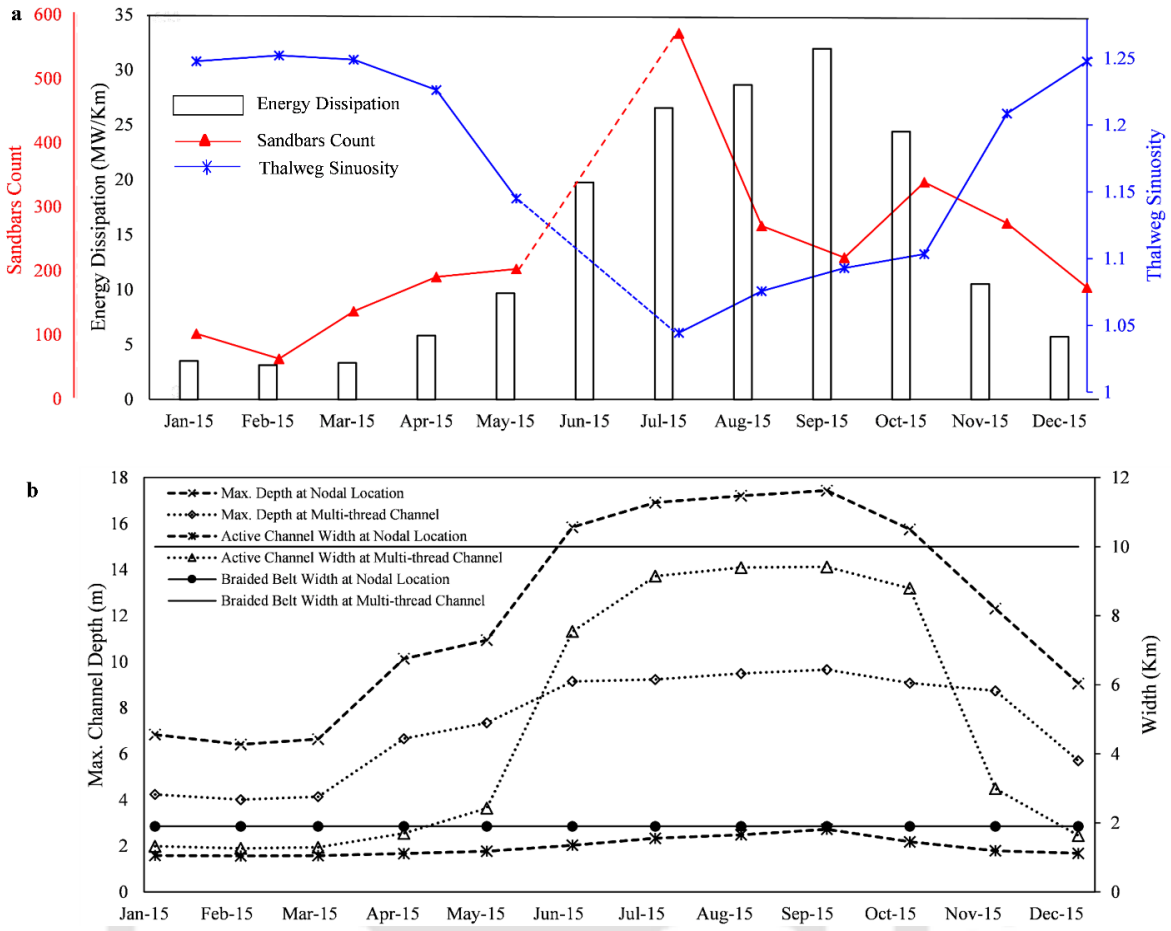

Figure 4.3: (a) Energy dissipation and morphological adjustments; (b) Hydraulic parameters variability at nodal and multi-thread cross-section of the Brahmaputra River

Bed and bank materials of the Brahmaputra River are composed of varying proportions of clay, silt and mostly of fine sand. The spatial and temporal variability of bed material deposits influences the flow structure, sediment movement, and morphological adjustments. An extensive field survey was carried in very low flow season to investigate the nature and type of bed deposits observed across the river reaches. Figure 4.4 shows the bed stratification and particle size analysis for various soil sample locations collected in the study reach. At site location 1, it was observed that top surface bed layer is composed of silt-fine sand composite (1) and a cohesive layer (3) sandwiched between fine sand deposits (2 and 4). Two relatively distinct top surface bed layers *i.e.*, clay and the silt-sand deposit was noticed at site location 3. The particle size analysis reveals that bed and bank is mostly composed of fine sand (0.125 to 0.25 mm); however, certain bed deposits are coarser to finer silt with cohesive in nature. In samples 1, 3 at least ~25% of the particles are finer than 0.004, indicating clay fraction in the sediment deposit. Over the sand bar top surface and banks, relatively coarser sediments with average D_{50} ~0.18 mm was observed.

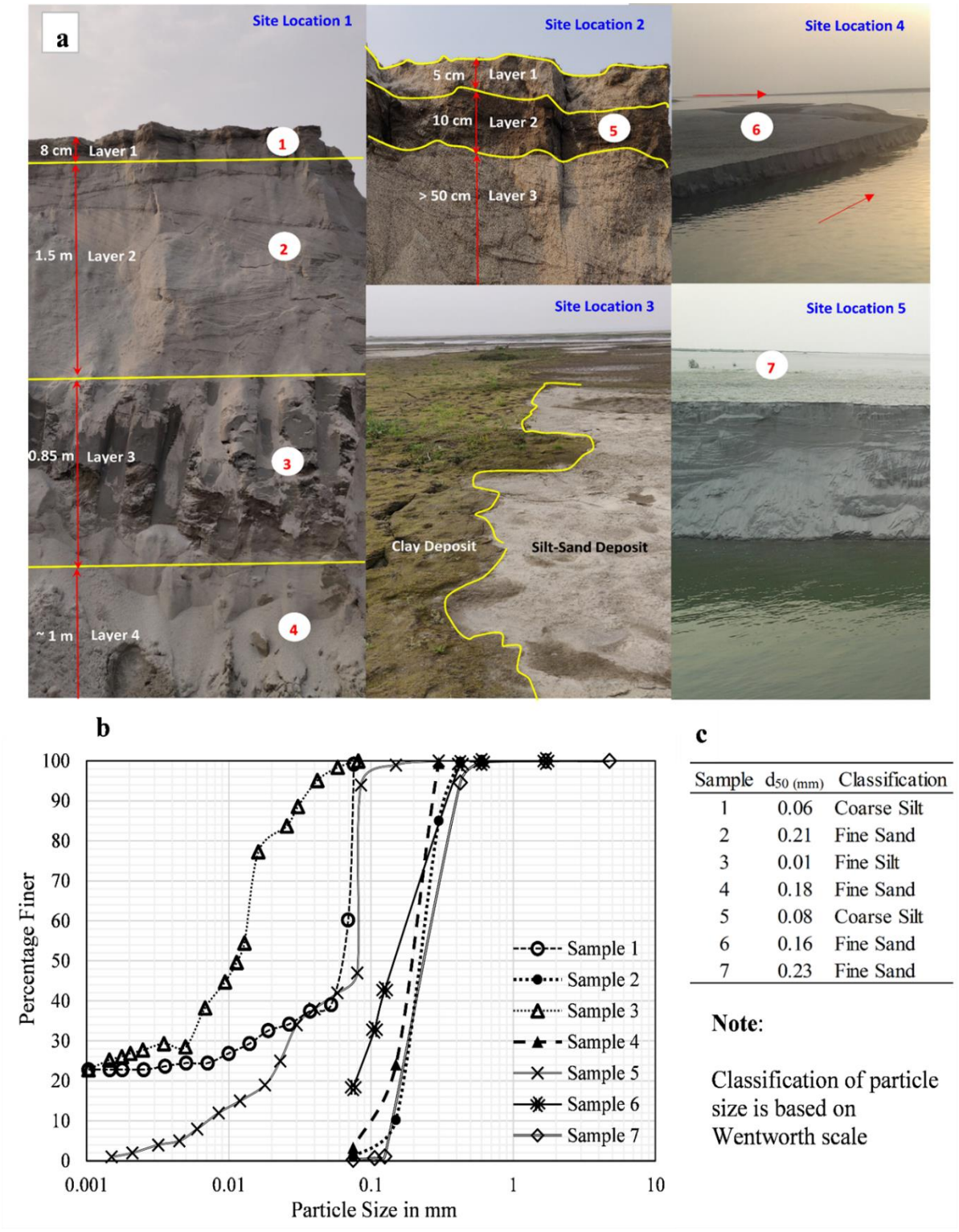

Figure 4.4 (a) Bed stratification and sample locations across the river reach, site location 1,2 and 3 is at river bed and location 4 and 5 is at braided bar and unstable bank; (b) Particle size distribution analysis; (c) Sample classification.

4.3.2 Velocity, Suspended Sediment Concentration and Morphological Changes

Primary, Secondary and Tertiary Channels

Figure 4.5 shows the primary and transverse velocity components at the cross-sections of primary channel M1 and M2, secondary channel S1 and S2, tertiary channel T. The first two sections, M1 and M2, were compound cross-sections positioned next to next in high discharge (~13000 m^3/s) carrying channel. Other sections S1, S2, and T were single-channel type located in lower discharge (~6000 m^3/s in S and ~2000 m^3/s in T) carrying channels of a braided network. The sections M1, M2 and S1, S2 were positioned on more or less straight reach and T on sharp meander bend [left side of Figure 4.8a-4.8c].

Within the main channel, the location of maximum velocity core remain distinct in two cross-sections M1 and M2, with a core on the left side (at ~1600 m) in M1 [Figure 4.5a] and relatively high-intensity core on the right (at ~300 m) in M2 [Figure 4.5b]. At section M1, the decrease in intensity of maximum velocity core and its shift is possible of two reasons, one, increase in channel widening to 2400 m resulting in uniform distribution of velocity across the transect and, two, channel transition from meandering (at M2) to straight (at M1) [refer Figure 4.8a, May month]. Across section M2, the dominant channel is between 0 to 550 m, followed by submerged deposition up to 1300 m and in-active channel till the end (1600 m). The growth of submerged bar or sedimentation at the mid-channel is interpreted as due to scoured material from the major confluence located ~300 m upstream of M2. There is a strip of slower velocity between 310 to 350 m, at M2 is probably the effect of stone outcrop in the channel immediate upstream. The secondary channels S1 and S2 were positioned ~3500 m apart on the same channel, with S1immediately followed by a lateral channel confluence and S2 located at reach center, far downstream of three-channel confluence [refer Figure 4.8b, May month]. Unlike M1 and M2, the sections S1, S2 were narrower (~600 m wide), definite in shape such that the maximum velocity core is at mid-section [Figure 4.5c, d]. The effect of lateral confluence at S1 is observed as a stagnation zone or low-velocity zone between 540 m to 640 m. Furthermore, a strip of velocity transition zone (480 m to 540 m in S1) sandwiched between stagnation zone, and maximum velocity zone (80 m to 480 m) was observed. However, at S2, the three-channel confluence discharge from upstream flows through constricted, smaller width channel resulting in accelerated flow and uniform distribution of maximum

velocity core across the transect. The tertiary channel section T was further narrower (approx. half the width of secondary channel section *i.e.*, ~350 m), located on sharp meander bend apex with different velocity distribution; one, maximum velocity core (150 m-350 m) in outer region of meander bend and two, distinct, relatively lower velocity core (0 m-150 m) in inner bend, representing true flow structure of a meander [Figure 4.5e].

Transverse components [Figure 4.5] and vertical velocity distribution [Figure 4.6] were observed to be significant, controlling the sediment transport and morphological changes. At T, a single secondary circulation cell possibly due to pressure gradients caused by centrifugal forces can be observed [Figure 4.5e]. In section S1, the effect of lateral channel confluence is shown as strong, counter-rotating, varying intensity secondary cell circulations in three-different regions across the transect [Figure 4.5c]. In region 1 (0 to 400 m) clock-wise circulations, the shear or mixing layer zone of region 2 (400 to 500 m) represents anti-clockwise circulations and region 3 of stagnant and recirculation zone were visible. While in section S2 [Figure 4.5d], no such strong circulation pattern was noticed although near-bed high magnitude transverse velocity components were present. In the main channel sections M1 and M2, the transverse components were observed to be significant at the dominant channel and velocity transition zones (e.g., see, 1280 to 1360 m in M2). The magnitude of the vertical velocity components are relatively same as transverse components and thus, showing patterns of upward and downward vertical currents across transects [Figure 4.6]. In almost, all the channel sections, series of narrower bands of upward (away from the bed) and downward (towards the bed) currents were observed.

Figure 4.7 shows suspended sediment concentration (SSC) distribution and transverse velocity fields at different sections of main, secondary and tertiary channel, while the morphological changes between pre (May) and post (Nov.) monsoon season at respective sections are shown in Figure 4.8. The SSC estimates at all sections vary in the order as low as 50 to 100 mg/L and higher up to 1800 mg/L. However, in the regions of maximum velocity core, the SSC across transect is more evenly distributed with magnitude in the order <500 mg/L. At the locations of banks, the influence of transverse and vertical velocity currents is significant in increasing the SSC due to sediment generated from unstable or very loose banks. The SSC magnitude at banks is predominantly higher (1000 to 1800 mg/L) than observed in the maximum velocity core regions. Further, in the main channel sections (M1 and M2; Figures 4.7a, 4.7b), the SSC is strongly influenced by irregular cross-section shape and short term morphological changes. For example, in M2

[Figure 4.7b], two different velocity and SSC distribution zones have shown the considerable effect on morphological changes [Figure 4.8a, Nov.] pre and post-monsoon season. First, the sediment concentrations of 1200 of 1800 mg/L show active sediment movement over a submerged deposition (500 to 1300 m) and eventually may result in downstream migration of the deposition observed as 1 in Figure 4.8a, Nov. Second, the confluence migration from upstream favored sediment deposition at inactive or low-velocity zone (1300 to 1600 m) resulting in constricted width and flow acceleration in other part of the channel. In the case of M1, higher velocities and increased sediment concentration at over and sloped surfaces of submerged deposits (100 to 300 m, 1680 to 2000 m) promoted degradation which is observed in morphological changes [Figure 4.8a, Nov.].

In the secondary and tertiary channel sections S1, S2, and T morphological changes [Figures 4.8b and 4.8c] were significant, showing unstable behavior of braided channels. SSC distribution at right banks of S1 and S2 shows increased sediment concentration levels, indicating the possibility of bank erosion. This observation reflects in morphological changes mapped post-monsoon season [Figure 4.8b, Nov], which is discussed in the next lines. The irregular depositions in the upstream and, migration of three-confluence scour deposition from the upstream may be the reason for the formation of sandbar in S2. The complete choking of channel section laterally eroded the banks (significantly on the right side) and formed a small-scale braided loop. This in turn shows downstream effect by forming a meander [white arrows, Figure 4.8b, Nov.] and allowing more flow diversion towards the right bank of section S1 causing bank erosion. Although SSC changes across T were not prominent, morphological changes pre and post-monsoon period were significant. In the pre-monsoon period (May) and when the section T was surveyed (June), the channel was on sharp meander bend (sinuosity ratio =1.65; radius of curvature =750 m; tightness ratio (radius to channel width) =1.75) which is generally unstable and indicates the formation of channel cutoff. This change was observed in post-monsoon period [Figure 4.8c, Nov.] where degradation on the outer bank, aggradation in the inner bank and channel chute cut-off forming a braided loop was noticed. This chute cutoff can be a short-term change and is probably caused to increase the energy loss during the high flow period. In the low flow period, the cutoff may be dried up and flow primarily moves through meander bend.

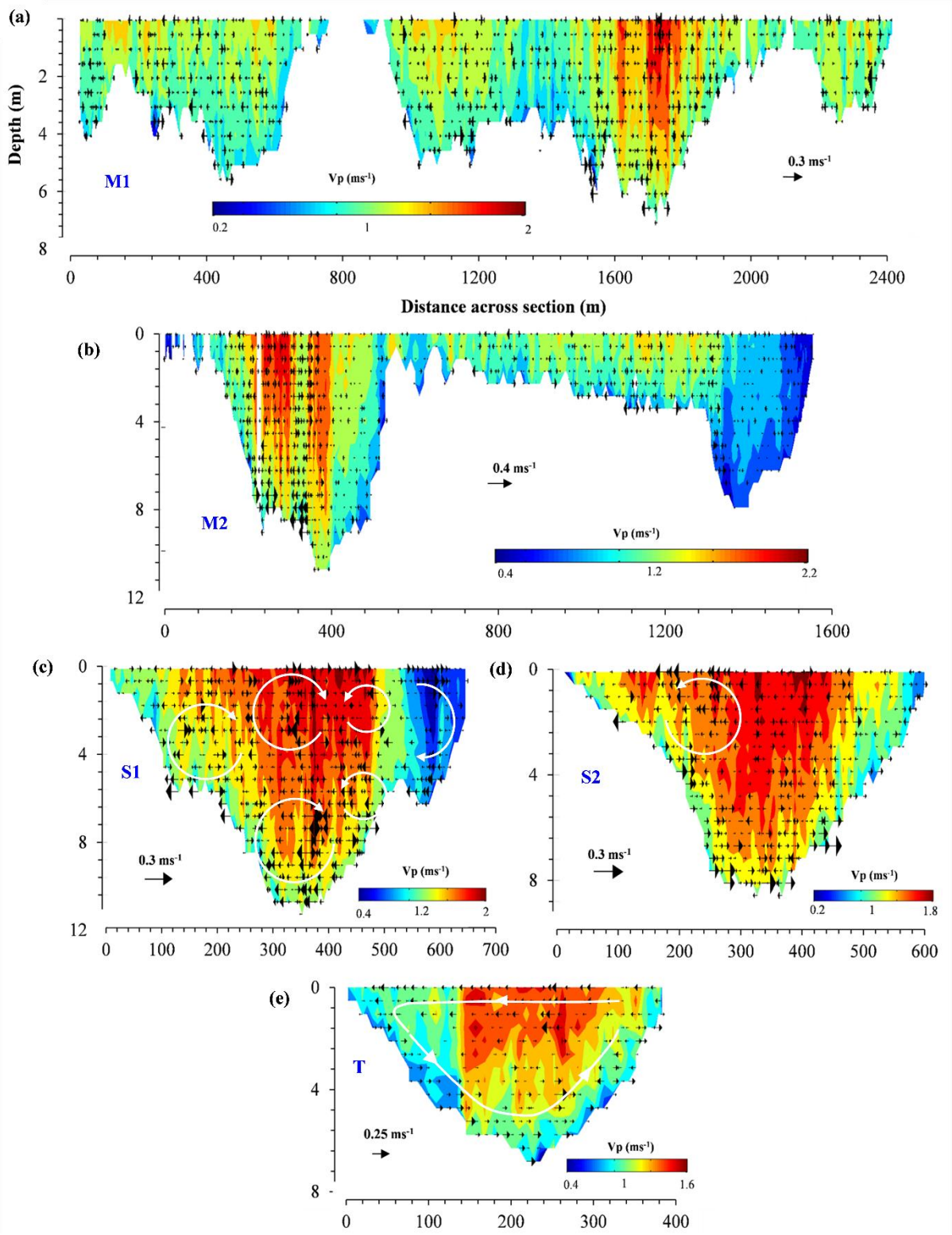

Figure 4.5 Primary and transverse velocity fields in the primary (M1, M2), secondary (S1, S2) and tertiary (T) channels. Flow direction is towards the observer.

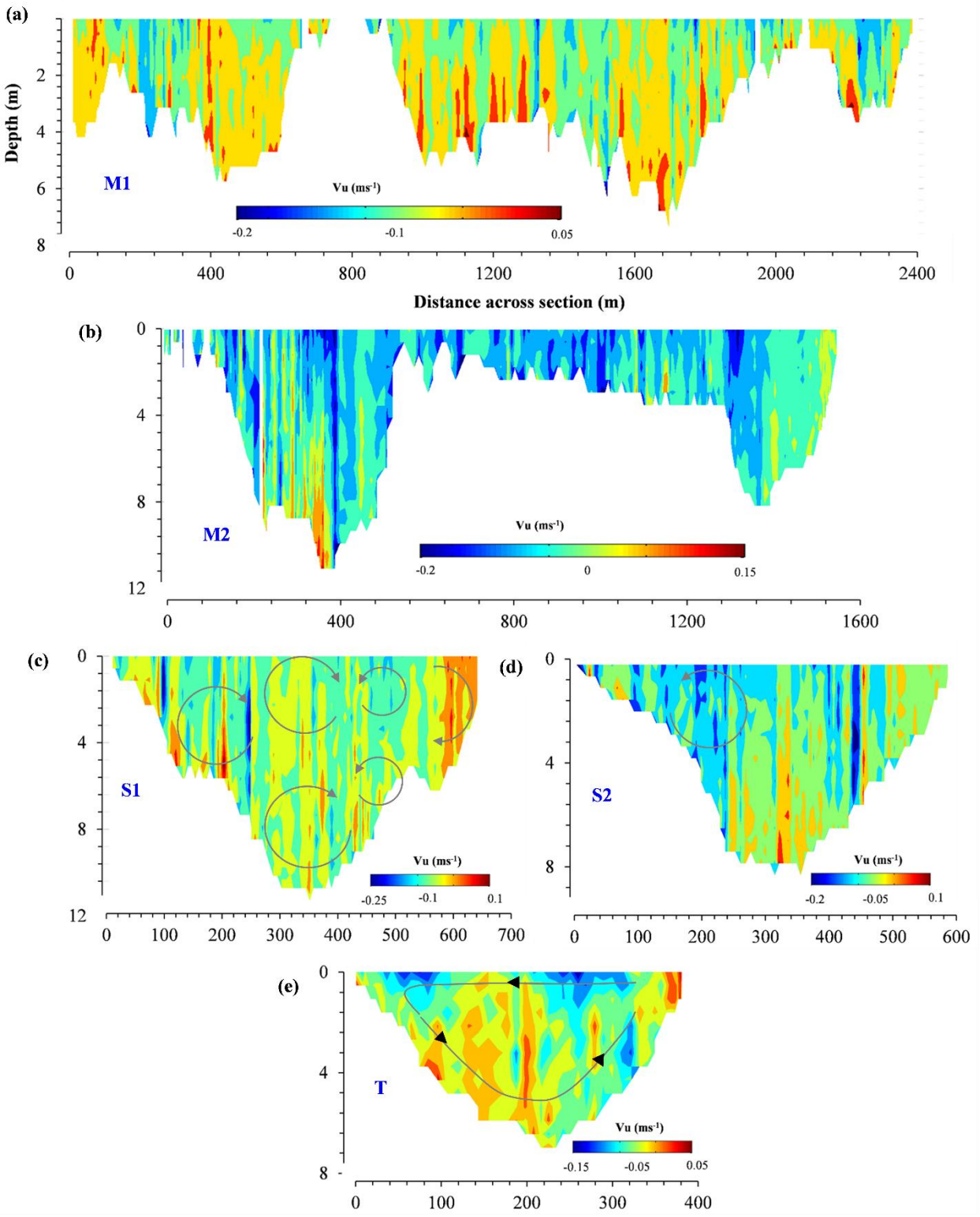

Figure 4.6 Vertical velocity fields in the primary (M1, M2), secondary (S1, S2) and tertiary (T) channels. Flow direction is towards the observer.

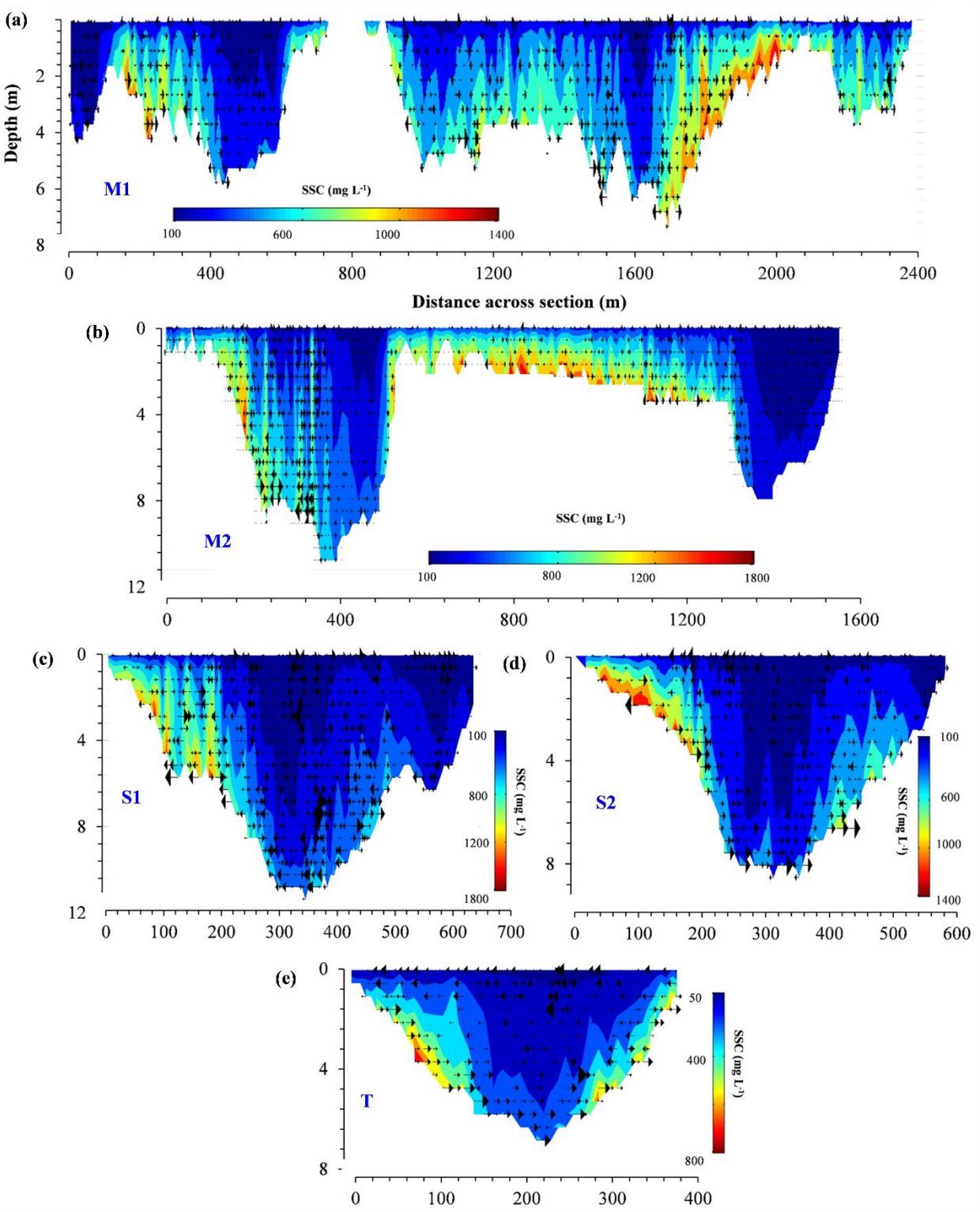

Figure 4.7 Suspended sediment concentration and transverse velocity fields in the primary (M1, M2), secondary (S1, S2) and tertiary (T) channels. Flow direction is towards the observer.

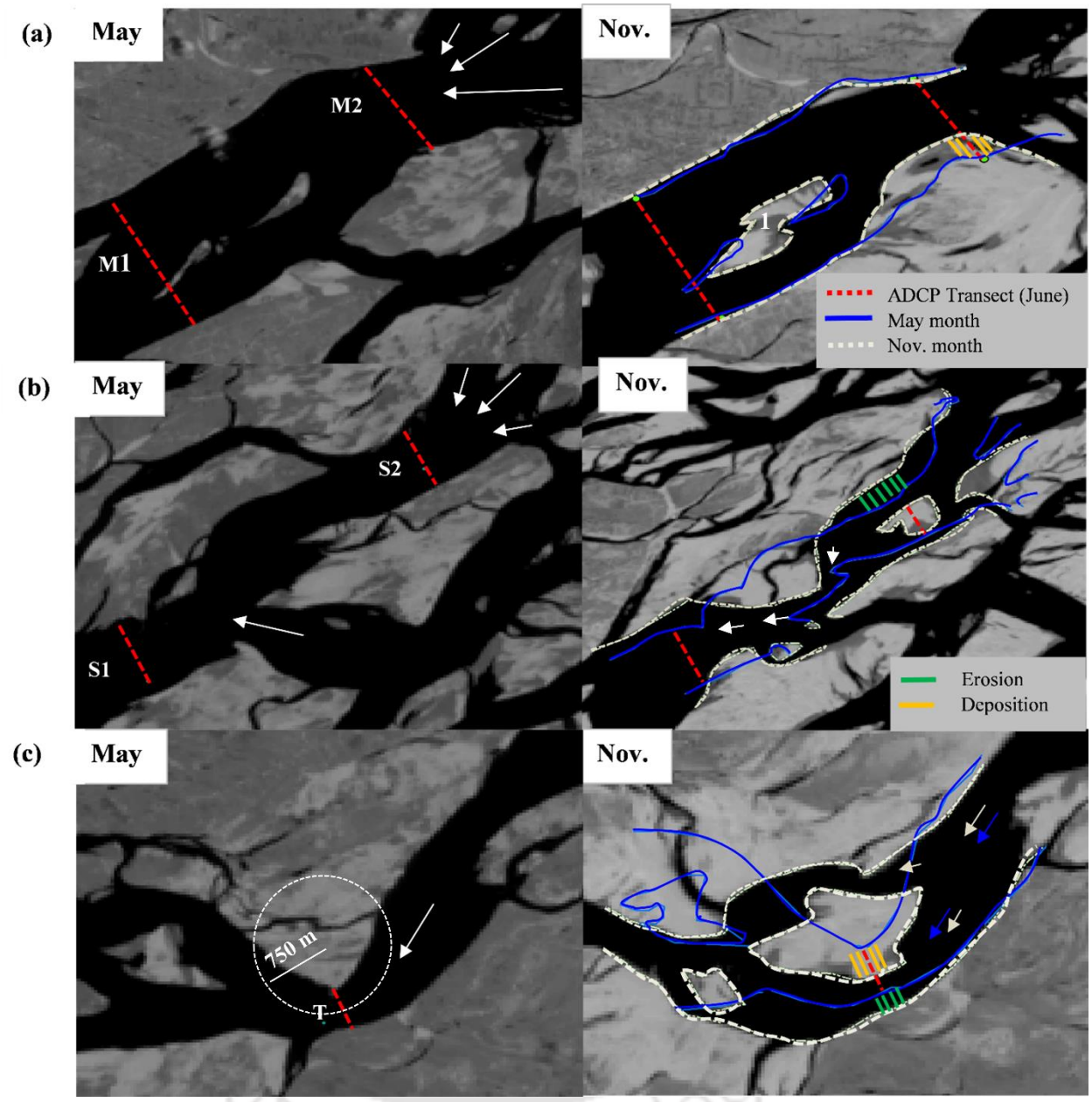

Figure 4.8 Pre and post monsoon (survey) morphological changes at (a) primary channels; (b) secondary channel and (c) tertiary channel.

Confluence-Diffluence Zones

This section discusses flow structure, SSC and morphological changes at large confluence and diffluence transects of highly morphologically active reach. In both the transects, the widths are wider with confluence zone of 2 km and diffluence of 4 km wide showing significant influence on velocity fields and sedimentation across the transect. The confluence section (C) is viewed as three-channel multi-thread cross-section located few

meters downstream of asymmetric braided loop confluence, tertiary channel and main channel, while the bifurcation section is a four-channel multi-thread cross-section with one channel being lateral tributary [Details on Figure 4.9, 4.10]. In the confluence zone [Figure 4.9a, 4.9b], three varying channel sections can be defined, *i.e.*, dominant mid-channel, active leftward channel, and in-active rightward channel. Within the mid-channel, the maximum velocity core (V_{avg}: 1.5 m/s) is concentrated, which is surrounded by the zones of lower velocities (V_{avg}: 0.4 m/s) on either side. Although the leftward channel relatively carries lower velocities (V_{avg}: 1 m/s), the velocity distribution across the channel is more uniform. This is probably due to location of upstream main channel [width: ~1200 m, see 3 on Figure 4.10, May] on the leftward side. There can be seen a strip of low-velocity zone between 320 to 400 m, which may interpreted as due to the effect of lateral channel confluence (4) to the main channel (3) [refer to Figure 4.10, May]. The rightward section resulting from a braided loop [Figure 4.10, May] within secondary channel is deeper and maintains a lower velocity (V_{avg}: 0.2 m/s) zone throughout. In the bifurcation zone [Figure 4.9c, 4.9d], a cross-over section (0 to 500 m) on left side, the central section covers a deeper main channel (2400 to 3700 m) and the developing channel (600 to 2400 m), in-active tributary section (3800 to 4100 m) on right side can be observed. In both confluence and diffluence sections, the extent of transverse currents and secondary circulations were limited to certain locations such as banks, mixing regions in confluence or, dominant main channel as observed at the bifurcation. Also, it is observed that there is no consistent magnitude and direction of transverse velocity vectors across transect except for the dominant main channel. Within the main channel, the secondary cell and transverse currents were limited to one-third of the channel section where maximum velocity core is present.

Figure 4.9b and 4.9d show the SSC distribution at the bifurcation and confluence sections, while Figure 4.10 shows morphological changes recorded pre and post-monsoon period. In both sections, the influence of velocity components on SSC distribution varies differently across transect. For example, at confluence section, in dominant mid-channel, the variability of SSC is high at secondary cell zone and unvarying at other locations, including maximum velocity core. But, the presence of secondary cells at banks of rightward in-active or leftward active channel has not shown remarkable influence on increasing the sediment concentration. In the bifurcation section, sediment concentration appear linked to the near-bed transverse currents, showing increase in

variability in developing and main channel (1000 to 3000 m). At other locations, despite the higher primary velocity, the effect on SSC variability is observed to be negligible due to lower transverse currents. As can be seen in Figure 4.10, the pre and post-monsoon morphological mapping reveal complex erosion-deposition pattern in the Confluence-Diffluence zone. This is mainly due to favorable flow structure and the channels response to upstream morphological changes. Lateral growth of mid-channel bar [5 km to 7 km, see Figure 4.10, Nov.] accompanied by an increase in curvature and migration of both the braided channels were significant changes. This may result in channel incision and bank erosion due to forcible pushing of the flow in the braided channels. At confluence section, the in-active or low-velocity rightward channel favored deposition and, this constriction diverts more accelerated flow towards the bifurcation section. The upstream in-channel deposition [6, see Figure 4.10] in the right braided channel allowed the evolution of new anabranch (7) joining downstream of the confluence section. The combined effect of accelerated flow and anabranch confluence probably lead to bed scour and, subsequent large scale deposition in the lower velocities and suspended sediment zones of bifurcation section. Thus, the influence of upstream morphological changes is observed to be significant in changes in confluence-diffluence zone.

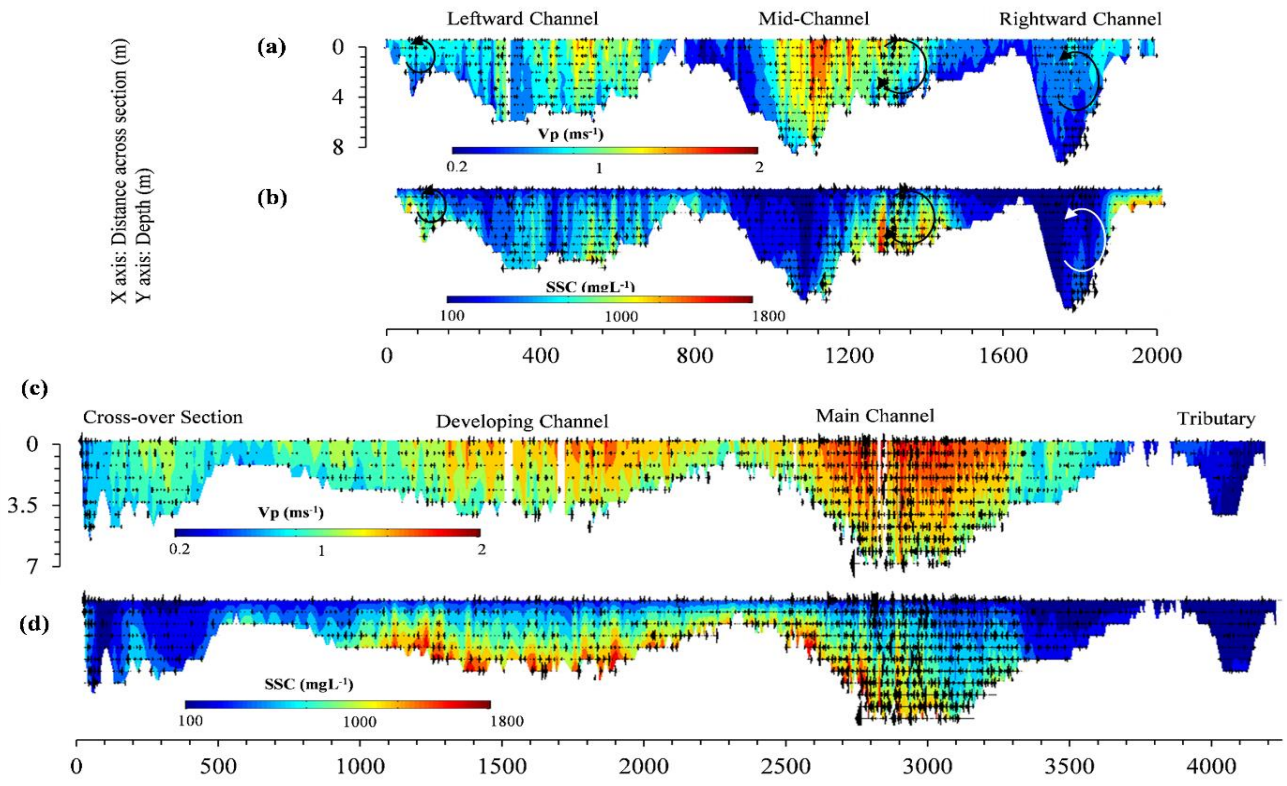

Figure 4.9 Primary velocity with transverse currents and suspended sediment distribution in (a, b) confluence and (c, d) bifurcation zones

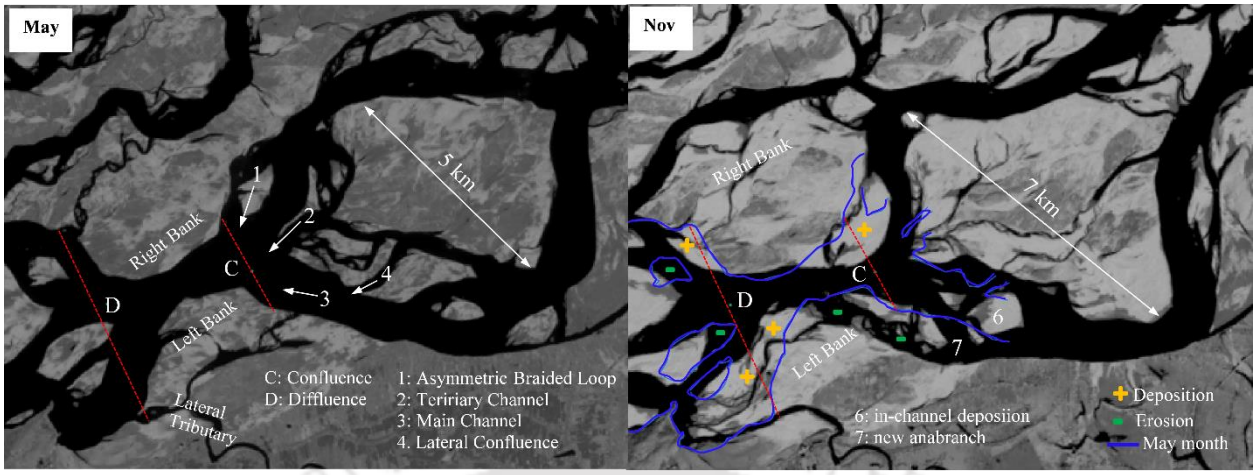

Figure 4.10 Pre and post-monsoon (survey) morphological changes at confluence-diffluence zone

Submerged Bar

Figure 4.11 shows the velocity components and suspended sediment distribution in two-channel cross-section with a submerged bar, while Figure 4.12 maps the morphological changes between pre and post-monsoon (survey) period. As can be seen in Figure 4.12a, the planform view of the transect S3 is observed as a single channel; however, the curvature on either side of the channel may be an indicator for the growth of submerged bar. ADCP survey reveals that two discrete maximum velocity cores were present in the cross-section, one at 120 m, towards the outer bank and another at the inner bank, 1320 m. The cross-section bathymetry shows asymmetric morphology with wider left anabranch (0 to 500 m) and narrower right anabranch (1200 to 1500 m). There is a growing mid-channel bar between 500 to 1200 m with maximum deposit height of ~5 m, close to the right anabranch. As a result, more flow is diverted towards the left anabranch, and higher velocities are prevailed throughout the section, whereas in the right anabranch except the maximum velocity core, the velocities surrounding are significantly low. Over the bar, velocities were higher with mostly uniform near the bed and surface. Figure 4.11a reveals, the transverse velocity components were limited to specific locations such as banks and bar top, and are not consistent throughout the section. Within the anabranches, the transverse components are nearly absent in the mid-channel and, at banks, helical secondary cells were observed across the depth. The development of opposite near-bed and surface transverse currents over the bar is probably due to the lateral exchange of flow between the bar and

the anabranches. This pattern over the bar is also shown in vertical velocity distribution, where alternative regions of upward and downward currents were observed.

Morphological mapping analysis [Figure 4.12] revealed that post-monsoon, the submerged bar is grown as an asymmetric mid-channel bar and exposed to the surface. The planform morphology shows the exposed bar looks elongated and narrow (width ~250 m), in contrast to ADCP data revealing a wider bar (~700). This cannot be concluded of any lateral bar erosion and, the bar may further emerge out with decrease in water level. In the left anabranch, the location of maximum velocity core at outer bank significantly eroded (~275 m) the leftward bank and becomes a dominant channel with an increase in channel width. This progressive bank erosion along the left bank is observed to aggrade immediate downstream in mid-channel and exposed out as bars. The right anabranch remains unaffected due to the presence of lower velocities at the bankside and, expected to further narrow down with the growth of mid-channel bar. In the post-monsoon period, the bank lines of both the anabranches appear to be straight, which may be due to lateral channel incision resulting from evolution and growth of mid-channel bars.

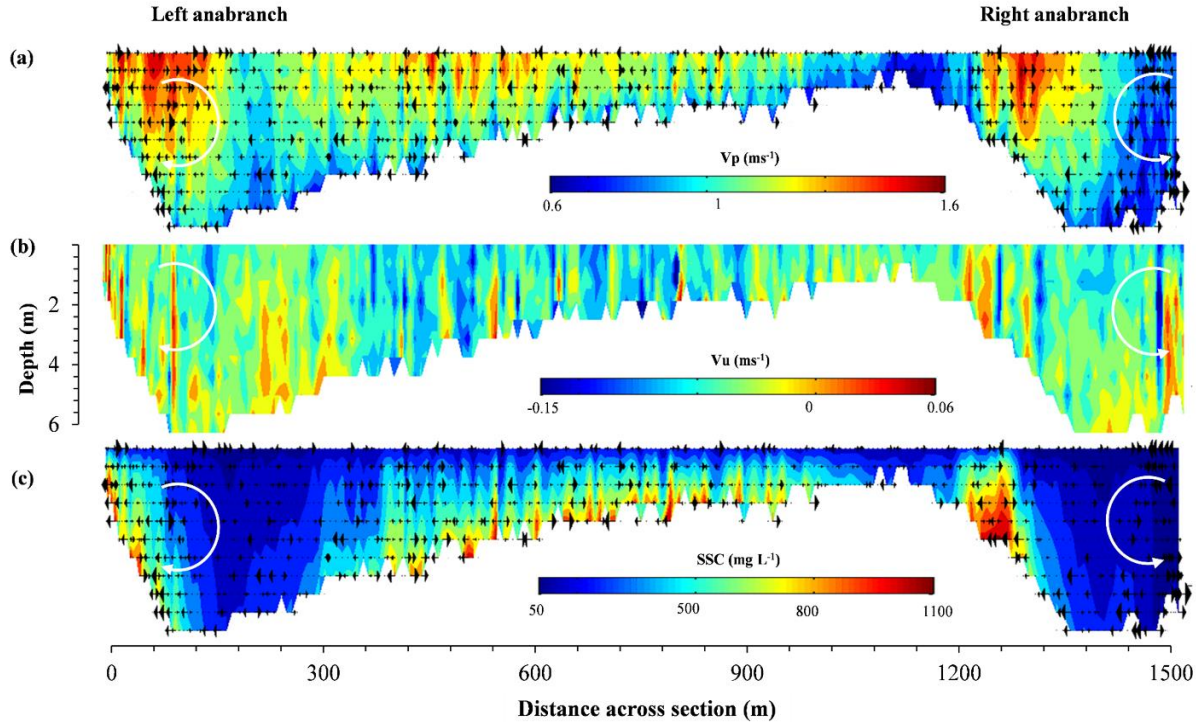

Figure 4.11 (a) Primary and transverse velocity fields; (b) vertical velocity fields; (c) suspended sediment distribution in a secondary channel cross-section with submerged bar

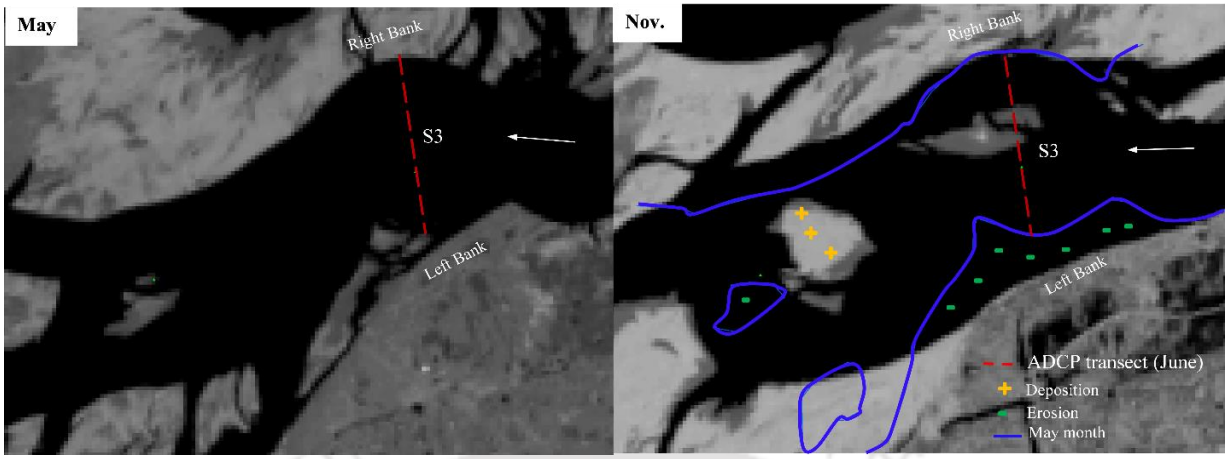

Figure 4.12 Pre and post monsoon (survey) morphological changes in a secondary channel cross-section with submerged bar

4.4 DISCUSSION

4.4.1 Threshold Expression and Channel Distinction

The results in the present work discuss the influence of flow structure on morphological changes at hierarchical channels with varying width-to-depth ratios, in a large sand-bed braided river. The morphology of selected channel cross-sections can be roughly divided into single channel form with one or two velocity threads and multi-channel form with two or more velocity threads. Although previous studies have established channel pattern thresholds [Leopold and Wolman, 1957; Parker 1976], it has been argued that these relations (e.g., Parker's diagram) could not be used to predict instability in cross-section to form a bifurcation [Richardson and Thorne, 2000]. Using the threshold expression $E=46.6(d/w)^{0.39}$, developed by Richardson and Thorne [2000] for channel distinction as single or multi-thread in Brahmaputra River, the present cross-section data is tested and the results are represented in Table 4.3. The analysis reveals that the relation holds good closer to the cross-sections with $\sim w/d$ >100 and, underperforms for $\sim w/d$ < 100. Additionally, it is noted that the cross-sectional data sets for the development of threshold expression were mostly composed of larger width-to-depth ratios (>100) and hence, this may be one reason for not applicability. Also, the cross-sections S2 and T (where threshold relation fails) are in complex braided network (braided belt width~10 km) covered with multiple sinuous channels and severely prone to channel migration. In this case, any upstream morphological changes may likely influence the channels and braided

network morphology due to flow deceleration (braided belt width~10 km) coupled with easily erodible banks. This is probably another reason for threshold expression to underperform. However, more detailed data sets of ~w/d < 100 at different locations would be helpful for proper justification of this observation or to build up a revised threshold expression.

Table 4.3 Prediction of channel-bifurcation using threshold expression, and outcome

Transect ID	~ (w/d)	$E_{theoretical} - E_{threshold}$	Prediction	Outcome	Remark
M1	400	Positive	Multi-thread	Multi-thread	√
M2	250	Positive	Multi-thread	Multi-thread	√
S1	75	Negative	Single	Single	√
S2	85	Negative	Single	Multi-thread	×
S3	270	Positive	Multi-thread	Multi-thread	√
T	50	Negative	Single	Multi-thread	×
C	345	Positive	Multi-thread	NA	NA
D	800	Positive	Multi-thread	Multi-thread	√

Note:

1. $E_{theoretical} = d + (v^2/2g)$; $E_{threshold} = 46.6\ (d/w)^{0.39}$ where E is specific energy, d is average depth of water, w is cross-section width, v is average velocity.
2. $E_{theoretical} > E_{threshold}$, prediction is multi-thread or else single thread. Outcome is evaluated by lean season satellite image.
3. √ corresponds to prediction and outcome are similar, × to not similar, and NA represents difficult to interpret from satellite image.

4.4.2 Flow Structure and Short-term Morphological Changes

Previous studies on the Brahmaputra River has been undertaken in understanding the morphological behavior and has shown that braided planform works in response to fluctuating flow energy, mobile bed sediments, and severely erodible banks. In general, multi-thread rivers associated with complex, interlinked channel network (e.g., confluence-diffluence units) develops three-dimensional flow structures which control sediment movement and morphological changes. Additionally, braid bar initiation, growth, and its morphological response during rising, high flow, and falling river stages alter the skewed flow structure in anabranches [Ashworth *et al.*, 2000]. At all the survey transects in this study, which covers primary, secondary, tertiary channels and the confluence-diffluence unit, different nature and behavior of three-dimensional flow structure and morphological adjustments were recorded due to considerable changes in channel w/d ratios. For example,

it is stated [Yalin, 1992; McLelland *et al*., 1999] that occurrence of helical secondary flow is difficult for channels with *w/d* >100 and however, suggests that factors such as planform curvature, channel-overbank flow interaction and bedforms do influence secondary flow generation. Herein, analysis of flow structure in transects M1, M2 and S3 with *w/d* >100 highlights the importance of planform curvature and supports the findings of Richardson and Thorne [1998] in secondary cell generation in anabranches. At three-channel transect M1, the absence of secondary flow cells is probably due to its location on the straight reach and no significant flow interaction at channel-bedform interface. However, at transects M2 and S3 with a mid-channel deposition, the planform curvature on one side in M2 and both sides in S3 generates secondary flow cells close to the outer banks.

Three transects in confluence influenced zones were analyzed in this study, one with *w/d* >>100, a multi-channel confluence section (*C*) located 0.25 km away from confluence and, another two transects with *w/d* <100, S1 being ~0.6 km away from single lateral channel confluence and S2, 1 km away from three-channels confluence. At transect C, which is close to the confluence, recirculation and flow separation in the rightward channel, accelerated velocity and flow mixing in the mid-channel were observed. The leftward channel is not significantly influenced by confluence, which may be due to its location along the main channel side, incoming flow orientation or effect of *w/d* ratio. Additionally, findings by Parsons *et al*. [2007] from a large confluence with *w/d*~200, reports the absence of secondary cells due to the interaction of bedforms and suggest a future investigation of river processes in large channel dimensions. At transect S1, recirculation zone, shear layer, fully developed counter-rotating secondary cells were observed, and in S2, which is far distant from the confluence, flow recovery was noticed. This implies that difference in generation and development of flow features might be position-dependent within the confluence influenced zone. Although confluence flow features observed here resemble well with those found in laboratory investigations and other field research studies, the influence of *w/d* ratio could be well documented only with detailed measurements.

Previous works on channel instability in the Brahmaputra River highlights the fluctuating flow energy environment and unstable banks in the continuous reshaping of the braided planform and cross-section morphology. Analysis of suspended sediment concentration in surveyed transects reveals mostly uniform distribution range (100 to 400 mg/L) irrespective of the channel discharge capacity. However, increased sediment

concentration (up to 1800 mg/L) in all the hierarchical channels is due to the effect of local flow features such as incoming flow orientation, secondary flow cells, and flow bedform interactions. In some cases, especially during falling river stage, celerity of bedform migration, excess of sediment supply in secondary and tertiary channels (which carry lower discharge) and in-channel sporadic depositions alter the cross-section morphology. Thus, in the Brahmaputra River, it is expected that the river bed and planform is adjusted for efficient balance between flow discharge, local sediment supply and upstream morphological changes [Coleman, 1969]. The significant short-term morphological changes observed in pre and post-monsoon period at survey transects were one, deposition at low-velocity zones, flow diversion and channel reorientation (M2, C, and D); two, initiation and development of mid-channel bar (S2, S3); three, neck cut-off and braided loop formation (T) and four, lateral migration of confluence-diffluence unit. These changes in turn rework flow structure and consequent sediment erosion, deposition and interdependent planform morphological changes.

4.4.3 Energy Expenditure, Macro-turbulence and Morphological Adjustments

The analysis of energy loss of a river between the nodal locations [Tezpur to Guwahati, distanced 150 km] reveals average energy dissipation of 5, 25 and 30 MW/km in low, monsoon and peak flood season respectively. With the increase in seasonal discharge (flow energy), the river may perform series of morphological adjustments such as erosion, deposition, changes in thalweg, bedforms and sand bars variability to balance the energy loss. Also, entropy-based morphological analysis [Chembolu and Dutta, 2018] reveal river system response was not local or site-specific and, suggests morphological adjustments may occur between nodal (control) points. This may imply (or raise a question) that gross changes in braided network morphology (between nodal points) are due to multiple morphological features working together as a system to achieve energy loss. The similar type of observation (in a different way) is also supported by Ashworth *et al.* [2000], where it is highlighted that gross morphological changes are significant contributors to sediment balance than local-scale, short-term changes. Earlier studies of the Brahmaputra River focused on local-scale flow and morphodynamics (e.g., around a braid bar) and presented a detailed investigation on site-specific river behavior and mechanics. The extension of such site-specific studies to node-node control reaches may improve the existing knowledge and, give insights on energy loss and reach morphological behavior.

In Figure 4.3a, changes in morphological features with energy dissipation shows at flooding stage (river flowing as a single channel) when river energy and energy dissipation is high, the response from thalweg sinuosity and sand bars density is relatively lower. At this stage, two more important factors may contribute to energy loss in addition to erosional processes. One, expansion and contraction losses resulting from changes in braided belt width [Figure 4.14] and another, macro-turbulent structures. Coleman [1969], reports the influence of bedform features on water surface turbulence patterns in the Brahmaputra River. It is highlighted that ripples and mega-ripples induce small eddies and vortices, larger bedforms such as dunes and sand waves induce surface boils and plane bed induces turbulence features controlled by scour holes that exist on the bed. The dimensions of the surface boils reache maximum up to 75 m (over dunes) and 240 m (over sand wave) and stays maximum up to 30 sec. A few images of the field-collected surface turbulent patterns is shown in Figure 4.13. Thus, bed form induced macro-turbulent structures may also significantly contribute to the energy loss of the river. Although, this observation may be preliminary, detailed studies on macro-turbulent structure and their influence are however necessary. Other rivers like Rio Grande [Harms and Fehnestock, 1965] and Mississippi [Matthes, 1947] are also prone to macro-turbulence.

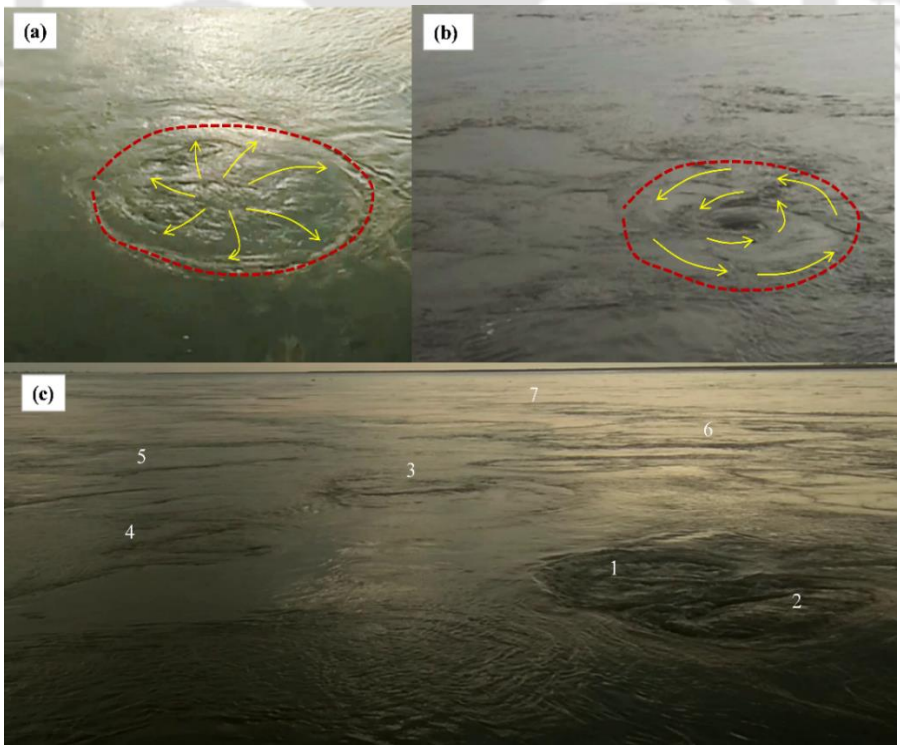

Figure 4.13 Plan view sketch of surface turbulence patterns in the Brahmaputra River; (a) Boil; (b) vortex type structure; (c) multiple turbulent features

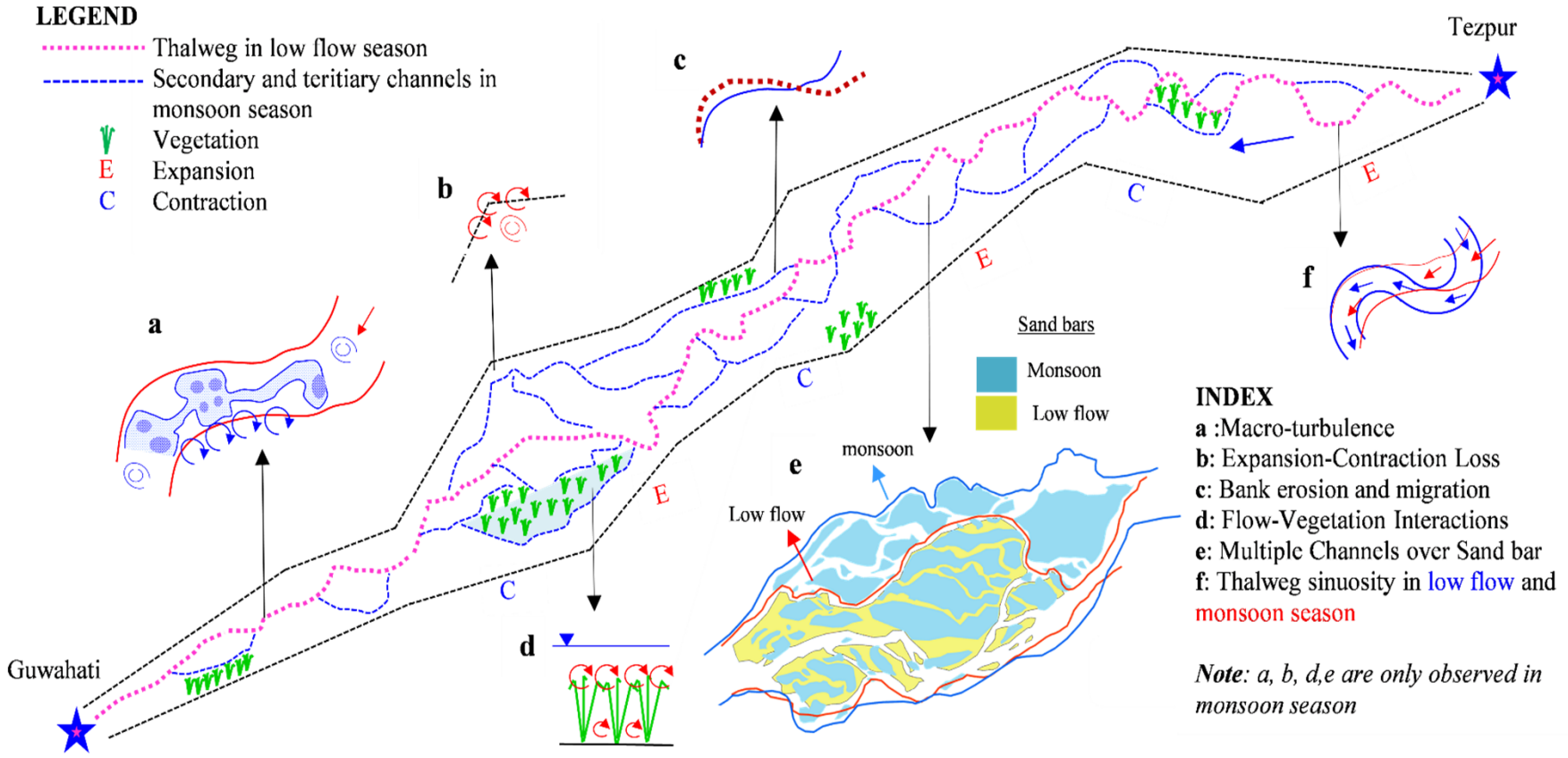

Figure 4.14 Conceptual sketch of various contributions to energy loss in the Brahmaputra River

4.5 CHAPTER SUMMARY

This objective presents a detailed investigation of flow structure and short-term morphological changes at hierarchical channels with varying width-to-depth ratios in the middle Brahmaputra River, India. Measurements of flow, suspended sediment transport combined with satellite imagery-based analysis were carried to understand the morphological response of a large sand bed braided river. The results of the study lead to the following conclusions.

1. Morphological variables tend to adjust in response to seasonal variability in energy dissipation. In the low flow season, thalweg sinuosity is observed to be dominant with magnitude ~25% higher than monsoon, while sand bars count increased from ~100 in low flow season to ~400 in monsoon season. Neither of the variables dominates in peak flooding period showing the contribution of other morphological parameters to energy dissipation.
2. The cross-section morphology of large channel with high width-to-depth ratios is observed as multi-thread with velocity core position depending on channel geometry. Planform curvature in these channels is significant in generating secondary helical cells overcoming the effect of bedforms.
3. In channels with width-to-depth ratio <100, the cross-section is a single thread with maximum velocity core at mid-section. The generation of secondary helical cells at meander and confluence sections are similar to those observed in other smaller rivers.
4. Short-term morphological changes are very prominent in the Brahmaputra River. The influence of upstream morphological changes coupled with local flow structure favored a significant change in planform and cross-section morphology. Further, at channels of $w/d < 100$, the order of upstream changes is much higher to influence the cross-section morphology irrespective of flow structure.
5. Higher concentrations of suspended sediment are noticed at specific locations influenced by local flow features such as the angle of attack, helical cells, and active sediment transport zones. Other sections are closely prone to lower sediment concentration ranging between 100 to 400 mg/L.

5

FLOW IN HETEROGENEOUS VEGETATION PATCHES

The Brahmaputra River riparian zones *i.e*., few of the sand bars and flood-plain, are covered with different vegetation elements. Long and flexible grasses are most widely seen over the sand bars, and heterogeneous vegetation patches are observed in the flood-plain zones. The river flood plains are very wide (in the range of 4 km to 10 km) and fully submerged during the monsoon season. At this stage, the nature of sediment deposits or nutrient dispersal across the river are highly different due to variability in hydraulic conditions. This allows the growth of heterogeneous vegetation patches in the river flood plain corridor. This chapter addresses following questions through experimental study.

- What kind of the flow structure is observed in flexible grasses and heterogeneous vegetation patches? How do they differ?
- How vegetation zones can be beneficial for river and ecology management?

5.1 INTRODUCTION

Vegetation have an important role in river restoration schemes for improving the physical characteristics and ecological standards of the river systems [Wilson *et al*., 2003; Bennett and Simon, 2004; Nepf and Ghisalberti, 2008; Kondolf *et al*., 2013; Brachet *et al*., 2015; Gurbisz *et al*., 2016, 2017; Vargas-Luna *et al*., 2018; Lera *et al*., 2019]. Aquatic or riparian vegetation significantly alters the flow and turbulent structure and, influences the riverine habitat [Bornette and Puijalon, 2011], water quality [Dosskey *et al*., 2010],

pollutant and nutrient dispersal [Perucca *et al*., 2009; Shucksmith *et al*., 2010], and sediment transport [Lopez and Gracia, 1998; Jordanova and Jame, 2003; Baptist, 2003; Kothyari *et al*., 2009]. Moreover, in braided rivers, the vegetation has shown positive feedback in controlling the braiding intensity [Gran and Paola, 2001; Tal and Paola, 2007] and, promoting bar and bank accretion processes [Bertoldi *et al*., 2011; Gurnell, 2014].

Earlier research on flow through vegetation mainly focused on determining roughness coefficients in vegetated channels [Ree, 1958; Chen, 1976]. Growing recognition of vegetation in improving the river health and restoration has attracted many researchers to understand the physical processes in flow vegetation interactions at different scales [Nepf, 2012; Curran and Hession, 2013]. Most of the research has been conducted in laboratory flumes using artificial, rigid [e.g., Bennett *et al*., 2002; Liu *et al*., 2008; King *et al*., 2012] or flexible type [e.g., Velasco *et al*., 2008; Chen *et al*., 2011] cylindrical vegetation where flow complexities arising due to plant morphology were neglected [Nepf, 1999; Tanino and Nepf, 2008; Siniscalchi *et al*., 2011]. The response of the flow structure under emergent and submerged vegetation conditions were also highlighted. Nepf [1999] has developed a physically based model to link drag, turbulence, and diffusion within rigid emergent vegetation. This was followed by understanding the physics behind Kelvin-Helmholtz instability and the generation of coherent vortices in submerged aquatic vegetation [Ghisalberti and Nepf, 2002]. To study the effect of plant morphology on turbulence structure, Wilson *et al*. [2003] have conducted laboratory experiments on flexible vegetation with and without fronds. Many of the other studies were focused on vegetation arrangement, pattern [e.g., Nezu and Sanjou, 2008; Chen *et al*., 2011] and effects of vegetation density [e.g., Y. Li *et al*., 2014; Devi *et al*., 2016] on flow and turbulent structure. The effect of seepage on turbulent parameters has also been investigated, indicating no significant changes in flow profile characteristics [Devi and Kumar, 2015, 2016, 2016]. Although studies on natural vegetation were limited, there exists few works on sediment entrapment [Abt *et al*., 1994], flow resistance [Jarvela, 2002; Wilson, 2007], longitudinal mixing [Shucksmith *et al*., 2010] and turbulence measurements [Yagci *et al*., 2010]. Shucksmith *et al*. [2010] have conducted detailed laboratory experiments over natural vegetation at different time scales to study the impact of plant growth on turbulence structure and mixing processes. Researchers also contributed towards developing numerical models to determine mean flow and turbulence structure in vegetated channels [Lopez and Gracia, 1998, 2001; Dijikstra and Uittenbogaard, 2010; Larsen and Harvey,

2010; Nardin and Edmonds, 2014; Kim *et al*., 2015; Marjoribanks *et al*., 2015]. Other studies also focused on highlighting the importance of vegetation in coastal bays on ecosystem services and function [Orth *et al*., 2017]. For example, Temmerman *et al*. [2012] report the effect of removal of tidal marsh vegetation and Gurbisz *et al*. [2016, 2017] studies the interaction of submerged aquatic vegetation (SAV) on physical and biological feedbacks and their resilience towards extreme bay events. Additionally, modeling based approaches for the synergistic effect of vegetation communities [Nardin *et al*., 2018] and SAV for river mouth bar development [Lera *et al*., 2019] were reported.

Existing research has provided good process based understanding of flow-plant interactions in terms of turbulent structure associated with canopies. However, these studies are limited to particular vegetation type and, the influence of plant morphology, heterogeneity in their behavior has not been widely discussed, which is the prime focus in this paper. In natural river environments, vegetation can be observed as patches of reeds, grasses and heterogeneous plant forms [Figure 5.1; also refer to Nepf, 2008]. Considering the importance of vegetation for planform stability and ecological aspects [Gurnell, 2014], the present study attempts to understand the flow behavior in flexible grasses and patches of heterogeneous plant forms which are less focused. The objectives of this paper are, therefore: (a) to investigate the effect of heterogeneity in plant forms, and alignment on the flow and turbulent structure along the vegetated patch; and (b) how their behavior is different from existing studies of single plant type. For this objective, laboratory experiments were conducted over different vegetation layouts, and detailed flow measurements (such as velocity and turbulence parameters) were carried to describe the flow response to heterogeneous characteristics. All the experiments were conducted under submerged conditions where flow depth is greater than vegetation height.

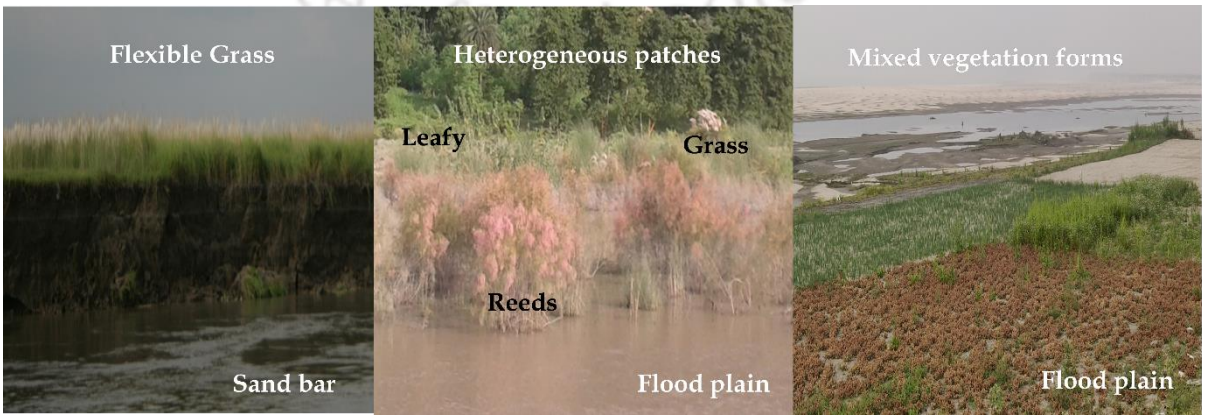

Figure 5.1 Vegetation forms in the Brahmaputra River, India

5.2 MATERIALS AND METHODS

5.2.1 Experimental Setup

All experiments were conducted at the Water Resources Engineering laboratory (Civil Engineering Department, IIT Guwahati) in a 20 m long, 1 m wide and 0.72 m deep glass walled flume filled with 0.2 m layer of river sand [Figure 5.2]. Three 10 HP pumps were used to drive and recirculate the flow between overhead tank, channel and the underground sump. A collecting chamber of 2.8 m long, 1.5 m wide and 1.5 m depth with wooden baffles and other roughness elements was placed at the upstream to diminish the turbulence and to straighten the incoming flow to the channel. Slope of the flume was fixed to 0.0015 throughout the experiments. The median sand diameter was D_{50}=0.5 mm, and the density was 2650 kg/m^3. The discharge was measured using a rectangular notch located at the tail end of the flume, and the digital point gauge was used to measure the flow depth.

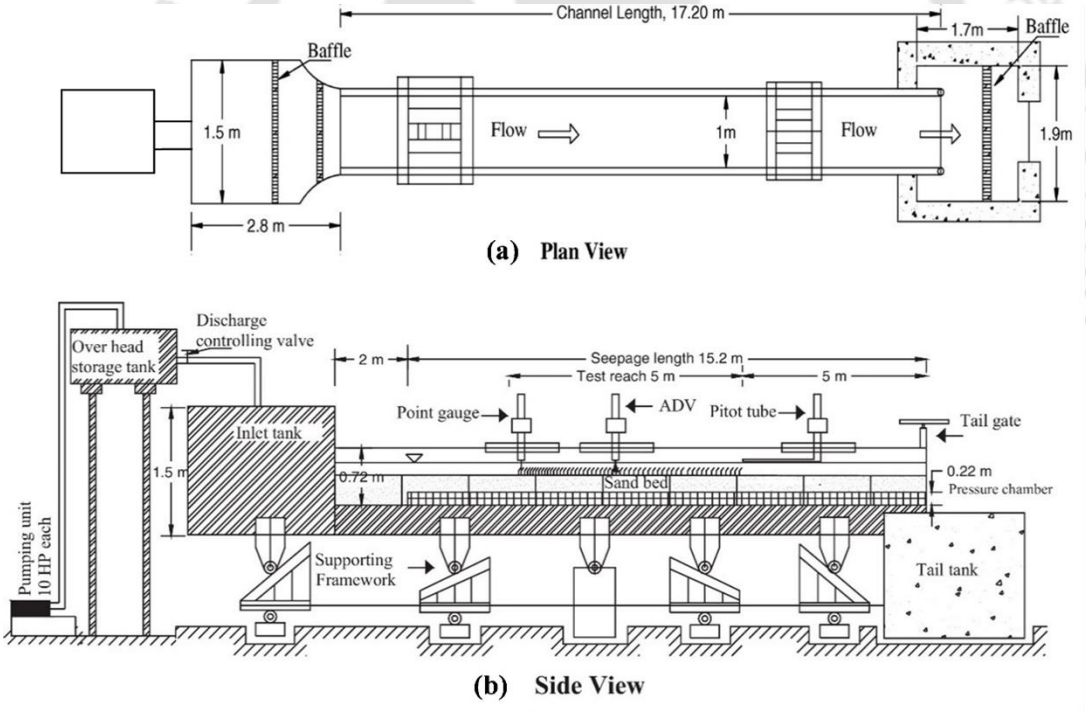

Figure 5.2 Experimental flume setup at IIT Guwahati: (a) plan view showing basic components and dimensions; (b) side view showing test section, vegetated bed and measuring equipments

Instantaneous velocity measurements were obtained with three-dimensional Acoustic Doppler Velocimeter (ADV), (4 probes, 10 MHz Vectrino ADV manufactured by Nortek) at a sampling frequency of 200 Hz [Yagci *et al*., 2010; Devi, 2016] with data

collection up to 5 min duration at each point. Accelerating threshold method was used to post-process the time series velocity data for removing the spikes [Goring and Nikora, 2002; Dey *et al.*, 2012; Devi, 2016]. To carry out the experiments, test section of 5 m length was chosen at the middle of the flume to minimize the effects of upstream entry and downstream exit. The test section starts at a distance of 60 times the flow depth from the flume entry where the flow is in fully developed condition [Sharma and Kumar, 2017]. Natural plants were planted in different configurations along the test section in the staggered pattern, and experiments were performed to analyze the turbulent characteristics.

5.2.2 Vegetation Types and Arrangement

Three different forms of natural vegetation *viz*. bladed, leafy, and cylindrical vegetation were used to bring out the heterogeneous characteristics in experiments. *Oryza sativa* (young rice plants) for bladed type, sprigs of *Duranta erecta* for leafy type and, the stems (without leaves) of *Sphagneticola trilobata* to represent rigid cylinders were used. These plants morphologically characterize the real species like *flexible grasses, leafy bushes, and reedy vegetation* along the riparian zones of the Brahmaputra River [Figure 5.1)]. Selected plants represent heterogeneity in terms of their form, swaying motion, and the drag effect. Bladed form was flexible to sway, leafy vegetation was semi-flexible with the stem being rigid and leaves flexible and, the cylindrical was rigid in nature. Additionally, the canopy porosity and projected area occupied by these plants also vary differently. Table 5.1 shows the physical characteristics of the plant forms used in the study. To carry out the experiments, four different vegetation layouts [Figure 5.3] were framed based on field observations [Figure 5.1] along the riparian zones of the Brahmaputra River, India. All the plants were placed in a staggered pattern along the test section with a density of 440 plants/m^2.

5.2.3 Flow Conditions and Measurement Locations

Experiments were conducted in submerged flow conditions in which flow depth is greater than the vegetation height. In the present work, considering the bed under no transport condition, the main channel depths were maintained lesser than the incipient motion depths [Devi *et al.*, 2016]. At incipient motion condition, the Shields parameter and grain Reynolds number were observed to be 0.028 and 7.41 for no-vegetation scenario with D_{50} =0.5 mm. The corresponding flow depth (H) and discharge (Q) were 14.2 cm and 0.0389 m^3/s. Table 5.2 shows the hydraulic conditions maintained in the channel for different

vegetation layouts. Flow measurements were carried at different locations along the channel to study the effect of heterogeneous characteristics of vegetation on flow and turbulent behavior. For experiments 1 and 2 measurement locations were positioned at upstream (P1), center (P3) and downstream (P5) of the vegetation patch, and in experiments 3 and 4, additional locations (P2 and P4) at the transition between the vegetation patches were also considered. Figure 5.3 shows the measurement locations (▲), numbered P1 to P5 located inside and outside of the vegetation zone along the channel. At each position in the vegetation zone, three to four plants were removed to provide a clear space for data collection. Instantaneous velocity components were measured with ADV along the flow depth at increments of 0.25-0.3 cm from the near bed. Thus, more than 20 measurement points at each vertical profile were obtained. The uncertainty in ADV data was also tested by collecting 15 pulses of 30000 samples, each within the test section of mixed heterogeneous vegetation layout [Deshpande and Kumar, 2015]. Table 5.3 shows uncertainty in time-averaged velocity components (U, V, W) and root-mean-square of fluctuating components (u', v', w') of sampled data.

Table 5.1: Summary of plant parameters

S. No.	Plant form	Plant parameter	Value
1		*Bladed vegetation*	
		Average plant height (h)	6 cm
		Average deflected height (h_d)	4 cm
		Average blade width	2 mm
		Approx. no. of blades in one plant	6
		Relative canopy porosity	Medium
		Projected area	7.2 cm^2
		Plant flexibility (h_d/h)	0.67
2		*Leafy vegetation*	
		Average plant height (h)	6 cm
		Average deflected height (h_d)	5.4cm
		Diameter of the stem	0.1 cm
		Approx. no. of leaves in each stem	9
		Average width of leaf	1.5cm
		Average length of leaf	2 cm
		Relative canopy porosity	Low
		Projected area	21.795 cm^2
		Plant flexibility (h_d/h)	0.90
3		*Cylindrical vegetation*	
		Average plant height (h)	6 cm
		Average deflected height (h_d)	5.8 cm
		Diameter of the stem	0.25 cm
		Relative canopy porosity	High
		Projected area	1.5 cm^2
		Plant flexibility (h_d/h)	0.97

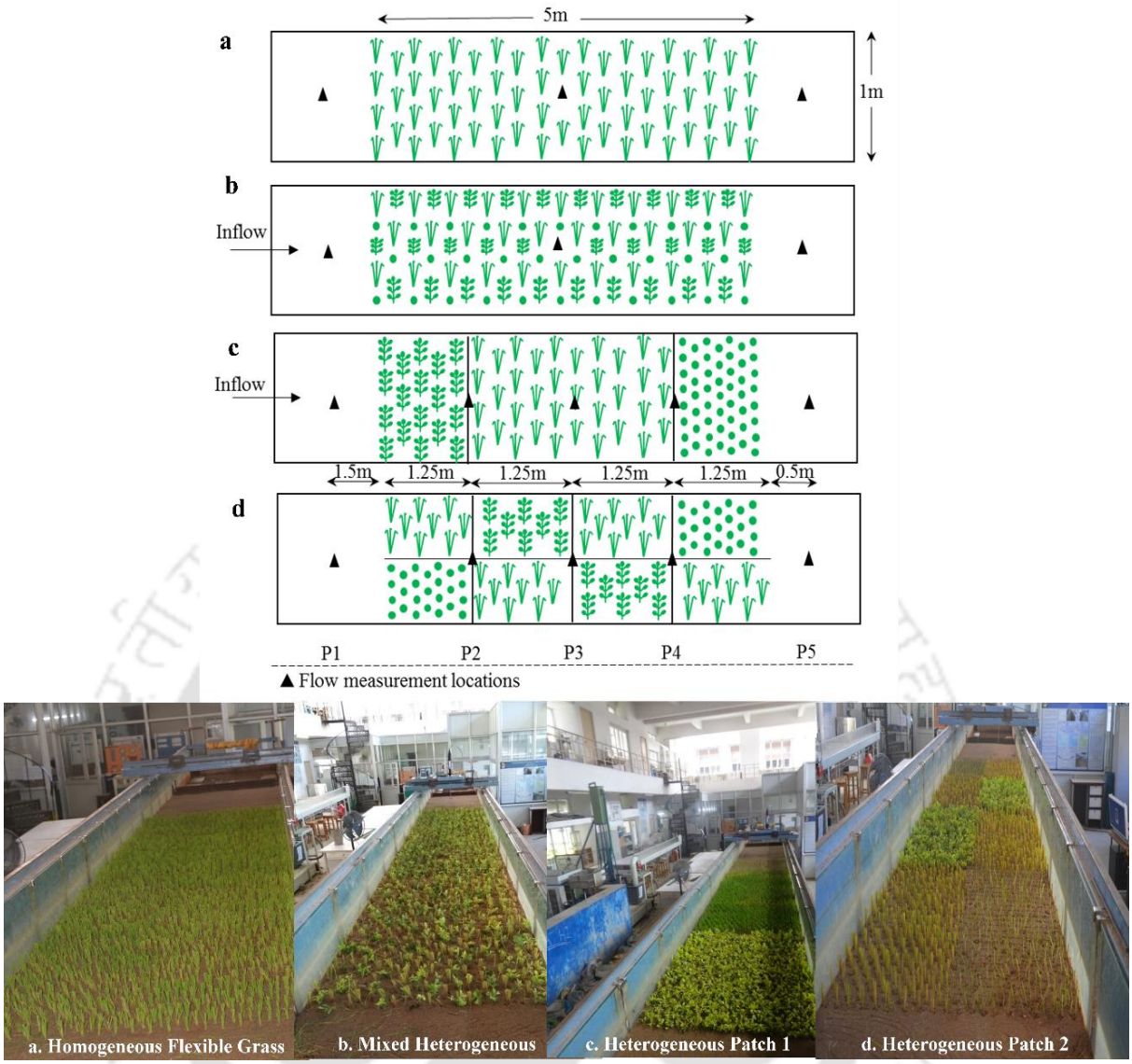

Figure 5.3 A schematic representation of vegetation patch layouts and measurement locations. No. of plants per sq. m remained same irrespective of plant form in all the experiments.

Table 5.2: Summary of the experiments

S. No.	Vegetation layout	Pattern	Flow Depth (m)	Fr	Re
1	Homogeneous bladed vegetation	Figure 5.3a	0.14	0.23	34705
2	Mixed heterogeneous vegetation	Figure 5.3b	0.14	0.224	33833
3	Heterogeneous patch 1	Figure 5.3c	0.117	0.229	27410
4	Heterogeneous patch 2	Figure 5.3d	0.118	0.214	25769

Table 5.3: Uncertainty in ADV data

Parameter	U	V	W	$(\overline{u'u'})^{0.5}$	$(\overline{v'v'})^{0.5}$	$(\overline{w'w'})^{0.5}$
Standard deviation (m/s)	$5.2*10^{-3}$	$8.6*10^{-4}$	$6.2*10^{-4}$	$1.37*10^{-3}$	$7.03*10^{-4}$	$3.62*10^{-4}$
% uncertainty	0.4	0.09	0.05	0.09	0.07	0.06

5.2.4 Flow Resistance

The type (flexible or rigid), form (plant morphology) and the layout of vegetation influences the Manning's n due to the difference in flow velocity and energy dissipation. In order to understand the heterogeneous effect on flow resistance, Manning's roughness coefficient was computed. Noarayanan *et al.* [2011] modified the general Manning's equation by writing the same equation for a vegetated and non-vegetated channel individually and, subtracted the later from former. Thus, the modified equation gives the resistance only due to the vegetation effect. The present work utilizes the Manning's equation given by Noarayanan *et al.* [2011], and the equation is shown below.

$$n=\left\{\left(\frac{1}{U_{o\,(veg+non)}}\right)*\left(R^{2/3}*S_{(veg+non)}^{1/2}\right)\right\}-\left\{\left(\frac{1}{U_{o\,(non)}}\right)*\left(R^{2/3}*S_{(non)}^{1/2}\right)\right\} \quad (5.1)$$

and, S : Energy slope = h_f/length of test section

$$h_{f\,(veg+non)}=\left\{\left(\frac{U_{o\,u(veg+non)}^2-U_{o\,d(veg+non)}^2}{2g}\right)+\left(H_{u(veg+non)}-H_{d(veg+non)}\right)\right\} \quad (5.2)$$

$$h_{f\,(non)}=\left\{\left(\frac{U_{o\,u(non)}^2-U_{o\,d(non)}^2}{2g}\right)+\left(H_{u(non)}-H_{d(non)}\right)\right\} \quad (5.3)$$

Where

n is Manning coefficient relative only to vegetation; $U_{o\,(veg+non)}$ and $U_{o\,(non)}$ is average velocity with (inside the whole patch) and without vegetation; R is hydraulic radius; $S_{veg+non}$ and S_{non} is the energy slope with and without vegetation; $U_{o\,u(veg+non)}$ and $U_{o\,u(non)}$ is upstream velocity measured with and without vegetation at position 1; $U_{o\,d(veg+non)}$ and $U_{o\,d(non)}$ is downstream velocity with and without vegetation at position 5; H_u and H_d are upstream and downstream flow depths at P1 and P5.

5.3 RESULTS

5.3.1 Homogeneous Flexible Grass vs. Mixed Heterogeneous Vegetation

Figure 5.4a shows vertical distribution of velocity measured inside (P3) and outside (P1 and P5) of vegetation zone in a flexible grass and mixed heterogeneous vegetated layout. At P1 *i.e.*, in upstream of the vegetation zone, the flow was fully developed and followed a logarithmic law. In the vegetated zone (flexible grass or mixed heterogeneous layout) *i.e.*, at P3, a clear distinction in shape of the velocity profile was observed. At this location, the velocity was highly reduced, and the profile no longer followed a logarithmic law. In flexible grass layout, velocity varied between 0.10 to 0.25 m/s in the canopy region and 0.25 to 0.32 m/s above the canopy and, in mixed heterogeneous layout the same varied between 0.08 to 0.21 m/s in canopy region and 0.21 to 0.31 m/s above the canopy. The additional mean velocity reduction of 10% was observed in mixed heterogeneous vegetation layout. The presence of other vegetation forms such as leafy and rigid cylindrical stems relatively offered more resistance to the flow than flexible grass vegetation alone. A similar type of velocity profiles was observed by Wilson *et al*. [2003] in flexible stipes with and without foliage. More characteristics of the plant form response to flow behavior is discussed in later sections. The effect of vegetation was observed at non-vegetated section (P5) where velocity profile is still reduced.

Profiles of the vertical Reynold stress (-u'w') and streamwise turbulence (u_{rms}) at P3 clearly differed for both the flexible grass and mixed heterogeneous vegetation layout. Within the lower canopy region (z/H= 0-0.25), the magnitude of $RS_{u'w'}$ was relatively greater for mixed heterogeneous. In the upper canopy region (z/H=0.25-0.5) and above the canopy (z/H≥0.5), vertical momentum exchange is higher for flexible grass than observed for mixed heterogeneous vegetation. This shows that, the presence of uneven canopy porosity and swaying motion of leafy forms can be the reason for higher turbulent stress in lower canopy region of mixed heterogeneous layout. Whereas in upper canopy region, highly flexible nature of grass forms increased the mixing activity between the vegetation and overflow region resulting in higher values of Reynolds stress [Wilson *et al*., 2003]. The position of peak $RS_{u'w'}$ for flexible grass is at z/H~ 0.45, and mixed heterogeneous is at z/H~0.54 against the canopy top of z/H~0.5. The local depression [see, Figure 5.4b] in peak $RS_{u'w'}$ of the flexible grass was noticed. However, this effect was not observed in mixed heterogeneous vegetation where the presence of additional drag at canopy top due to other

vegetation forms is more dominating. In addition, the peak $RS_{u'w'}$ value was pushed a little above the canopy top. Figure 5.4c shows the variability in streamwise turbulence along the patch. A relatively higher value of streamwise turbulence (at P3) is observed in flexible grass than mixed heterogeneous vegetation layout. The analysis of the results suggests that the presence of different vegetation forms as in mixed heterogeneous layout can be helpful for more reduction of flow velocity and vertical momentum exchange than flexible grass of same vegetation density and flow conditions.

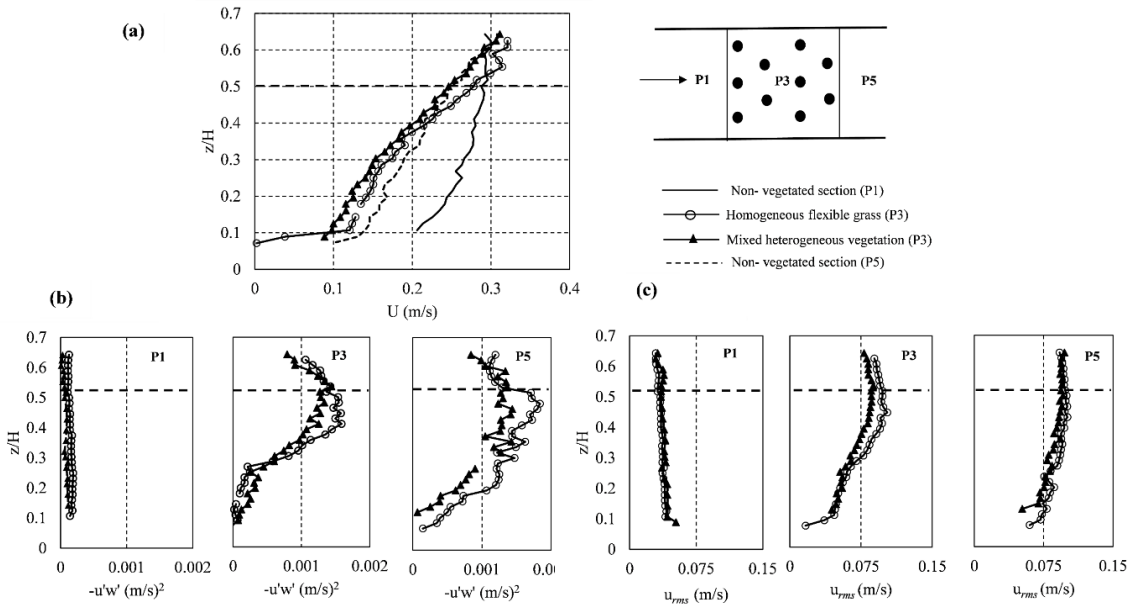

Figure 5.4 Vertical distribution of (a) stream wise velocity, (b) Vertical Reynold stress ($RS_{u'w'}$), (c) streamwise turbulence (u_{rms}) in homogeneous flexible grass and mixed heterogeneous vegetation

5.3.2 Flow Characteristics in Heterogeneous Patch 1

Velocity Profiles

In heterogeneous patch 1, patch type varies in longitudinal direction [Figure 5.3c]. Figure 5.5b shows flow velocity profiles measured along the heterogeneous patch 1 where greater deviation between the individual profiles was noticed with the passage of flow through leafy (dynamic), bladed (flexible grass) and cylindrical stem (rigid) patches. The velocity magnitude at different positions varied as P2<P4<P3<P5<P1. At P2, the flow velocity was greatly reduced and mostly uniform in lower canopy region due to higher resistance offered by the leafy patch. The average velocity was reduced by 55% at P2 and in lower canopy region, significant velocity reduction of 80% was observed. This reduction

results from complex and congested flow paths due to low flow permeability inside the staggered leafy patch. As the flow leaves highly resistant leafy patch (zone 1) and reaches P3 of flexible grass patch (zone 2), the increase in velocities was noticed. In the lower canopy region the velocity profile was showing accelerating trend ranging between 6 -15 cm/s. This high difference in velocity variation may be attributed from flexibility of bladed forms. Overall the depth-averaged velocity reduction of 25 % and, 50 % in the lower canopy region was observed at P3. As flow fully traverses zone 2 and reaches P4, it suddenly encounters rigid cylindrical stems. The presence of rigid cylindrical stems at this interface (P4), reduced the flow velocity again and, made velocity profile approximately constant in lower canopy region. The average velocity reduction of 38% over whole region and 60% in the lower canopy region was observed at P4. In the upper canopy region and above the canopy top, though the velocity profiles at P2, P3, and P4 were showing accelerating trend, there was a noticeable difference in their magnitude. The values followed similar order (P2<P4<P3) as reported for lower canopy region. Above the canopy, velocities in the vegetated zones were higher than the non-vegetated ones. This is because of flow obstruction inside the vegetation forms forcing the flow upward and increasing the velocities above the canopy [Chen *et al.*, 2011]. At P5, the velocity profile and its magnitude were gradually retaining logarithmic nature as the flow leaves the vegetation patch. A fully developed zone would be returned at further downstream of this location.

Reynolds Stresses

The effect of heterogeneous patch 1 layout on Reynold stress variability in vertical ($RS_{u'w'}$), lateral ($RS_{u'v'}$) and stream-wise ($RS_{v'w'}$) directions is shown in Figure 5.5c-e. In this section, firstly vertical direction of Reynold stress ($RS_{u'w'}$) is discussed, followed by other components. The shape of $RS_{u'w'}$ profiles exhibited a strong mixing activity (peak value) at and slightly above the canopy top (z/H=0.4) as reported by the other works [Wilson *et al.*, 2003; Devi, 2016]. However, the intensity of the peak value differed significantly as the flow traverses through leafy, grass, and cylindrical patches. The magnitude of peak $RS_{u'w'}$ values at P2, P3, and P4 varied as 14, 16 and 24 cm^2/s^2. In the lower canopy region (z/H: 0-0.2), the profiles were approximately uniform with values ranging between -0.5-1.8, 0.2-3.2 and 0.37-0.39 cm^2/s^2 at P2, P3, and P4 respectively. These values were significantly lesser than the near bed values of non-vegetated positions (P1 and P5). To better explain this variability, it is necessary to understand the influence of vegetation form on flow structure. At P2, significant reduction of Reynold stress in all

regions was observed, with almost negligible values in lower canopy region. The shift in peak value to slightly above the canopy top was also noticed. This is because the larger drag due to the presence of leaves (additional surface area) in zone 1 [refer to Figure 5.5a] alters the momentum transfer by inhibiting the vertical momentum exchange between the vegetated and the over flow region. Also, negative $RS_{u'w'}$ at near bed is due to negative velocity gradient ($\frac{\partial\langle U\rangle}{\partial\langle z\rangle}$<0) indicating upward momentum transfer [Siniscalchi *et al*., 2012]. The flow field in zone 2 is now through flexible grass patch. At P3, the values of $RS_{u'w'}$ were increased relative to P2. The grass vegetation is such that the plant form is relatively stiff at bottom part (as blades are closely spaced) than upper part (blades are spread). This feature is clearly depicted in Reynold stress profile as uniform $RS_{u'w'}$ in the bottom part and accelerating $RS_{u'w'}$ in the upper part. Unlike in homogeneous flexible grass layout (section 5.3.1), local depression in peak $RS_{u'w'}$ into canopy was not observed at P3. This may be explained by the presence of highly resistant leafy patch at the beginning absorbed the flow momentum, and thereby, reducing the translational speed (or weaker enough) of KH vortices to deflect the canopy although higher momentum exchange (relative to P2) is noticed. Moreover, the availability of sufficient length required for downstream progression of vortices is restricted in this zone [Ghisalberti and Nepf, 2002] due to confinement of grass patch between leafy and cylindrical patches. At P4, *i.e.*, the interface between flexible bladed and rigid cylindrical patch, a relatively distinct $RS_{u'w'}$ profile with greater shear interaction at the canopy top and lesser momentum exchange region into the canopy is observed. This may be mainly due to two reasons, one is, unlike leafy and bladed forms, rods have no additional surface area (like leaves or blades) to absorb the shear generated turbulence and, second is due to the rigidity of stems. The rigidity of the stems made $RS_{u'w'}$ profile uniform throughout the canopy zone.

The thickness of active momentum exchange (h_t) is defined as the distance from the canopy top to 10% decay of maximum Reynold stress into the canopy [Nepf and Vivoni, 2000]. In this layout, h_t clearly showed response to vegetation forms. The penetration ratio (h_t normalized by plant height) was higher for bladed form (0.65 at P3) followed by leafy (0.50 at P2) and rigid cylindrical stems (0.45 at P4). A simple conceptual sketch showing the mixing activity and penetration ratio at the canopy top is shown in Figure 5.5a. The other components of Reynold stress ($RS_{u'v'}$ and $RS_{v'w'}$) have not shown significant variation over the depth expect for $RS_{u'v'}$ at P2 and P3. Unlike $RS_{u'v'}$ values at P2 and P3, the uniform velocity distribution or least difference in velocities between the layers of canopy region at

P4 may be the reason for lower or unvarying values of lateral Reynold stress ($RS_{u'v'}$). This shows vegetation form and its swaying motion is controlling the non-homogeneous nature in RS profiles.

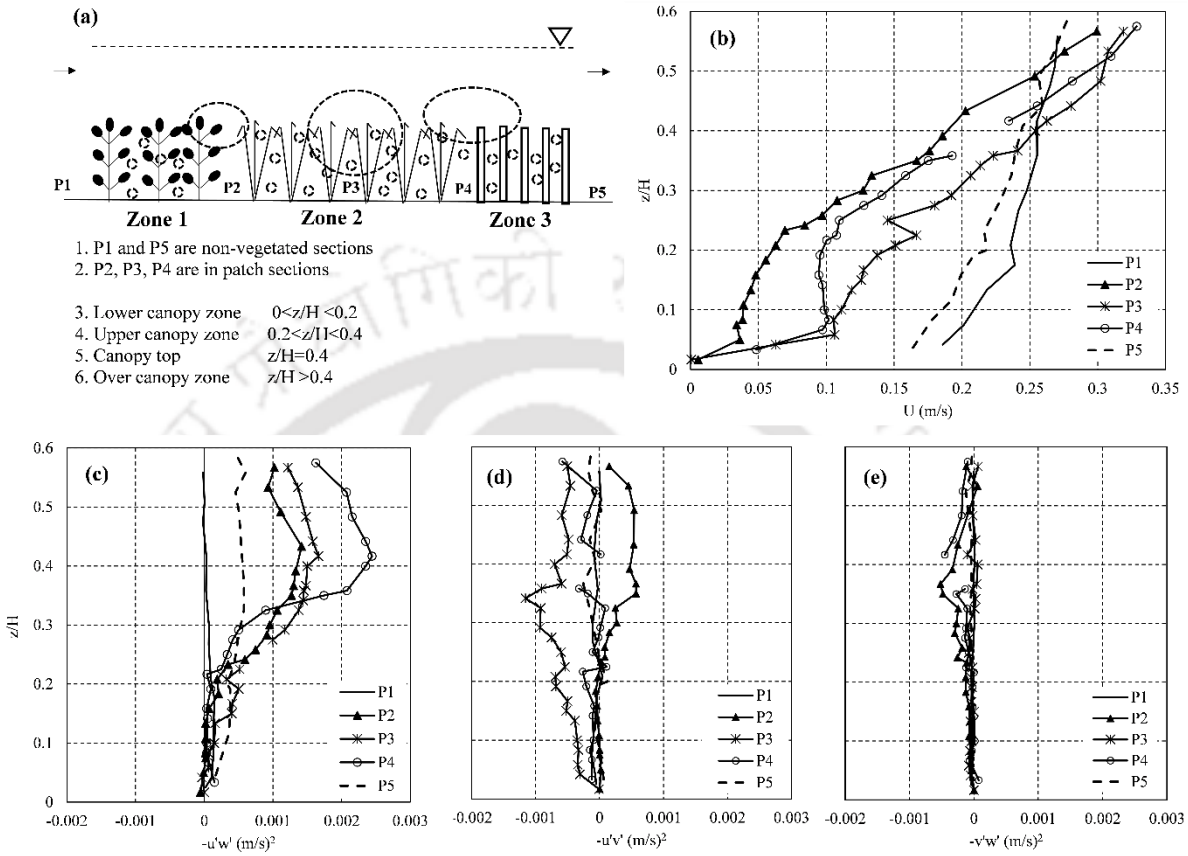

Figure 5.5 **a** Conceptual picture of mixing activity (represented by dotted ellipse) in side view; where, horizontal axis of ellipse represent intensity of mixing activity and portion of ellipse into the canopy zone represent thickness of active momentum exchange. Vertical distribution of **b**: stream wise velocity (U); Reynolds stress **c**: $RS_{u'w'}$, **d**: $RS_{u'v'}$, **e**: $RS_{v'w'}$ measured at different positions in Heterogeneous patch 1

5.3.3 Flow Characteristics in Heterogeneous Patch 2

In heterogeneous patch 2 layout, the vegetation patches are varied in both longitudinal and transverse direction [see Figure 5.3d or 5.6a]. There is a patch geometric dissimilarity on either side of the flume center line and, at junctions (P2, P3, P4) on all sides. Therefore, in this layout, the flow and turbulent structure are expected to be different from heterogeneous patch 1.

Velocity Profiles

Figure 5.6b shows flow velocity measured inside (P2, P3, P4) and outside (P1, P5) of heterogeneous patch 2 vegetated zone. In this layout, the mean velocity along the channel varied as, velocity at P1> P5> P2> P4> P3. At P1, the velocity profile strictly followed the logarithmic law and, at other positions, the flow through different alternative forms of vegetation patches significantly altered the profile characteristics. Also, the varying flow obstruction due to bladed, leafy and cylindrical forms along the vegetated zone affected the percentage of velocity reduction. To understand the flow behavior, depth-wise velocity profiles were segregated into three regions, *viz.* lower canopy (z/H: 0-0.2), upper canopy region (z/H:0.2-0.4) and above the canopy top (z/H≥0.4). The depth-averaged velocity reduction of 12 % at P2, 25% at P3 and 17% at P4 was noticed. Within the lower canopy region, more velocity reduction was observed at P3 (48%) followed by P4 (40%) and P2 (24%). This variability could be better explained as follows. In the beginning, the incoming flow enters through flexible grass and largely porous cylindrical patch (see zone 1 in Figure 5.6a) where the flow obstruction is sparse, and velocity was less reduced compared to the next zone covered with leafy-bladed patch (zone 2). And, the presence of highly resistant leafy forms and complex flow path due to the reversal of resistance at P3 (i.e., from zone 2 to zone 3 where leafy-bladed shifts to bladed-leafy) resulted in significant velocity reduction than observed at P2 and P4. At P4, two distinct characteristics in the velocity profile were noticed. One is, the lower canopy region experiences increase in velocity (relative to P3) and second, is greater velocities above the canopy top. The first is maybe due to enhanced flow speed generated due to the sudden shift in canopy porosity from low (zone 3: bladed-leafy) to high (zone 4: cylindrical-bladed) and also, variability in flow resistance. The latter is possible due to rigid cylindrical stems at P4 interface pushing the flow above the canopy. The presence of rigid cylindrical forms at P4 also caused uniform vertical velocity profile in the lower canopy region. In upper canopy region and above the canopy, velocity profiles were found to be accelerating and mostly similar at P2, P3, and P4. The effect of vegetation starts to disappear gradually as the flow leaving the patch showed a tendency to follow the logarithmic profile at P5.

Reynolds Stresses

Figure 5.6c-e shows the Reynold stress profiles in vertical ($RS_{u'w'}$), lateral ($RS_{u'v'}$) and stream-wise ($RS_{v'w'}$) directions measured along the heterogeneous patch 2 layout. It can be observed that as the flow traverses through the patch, heterogeneous characteristics

in vegetation significantly altered the shape of Reynold stress profiles at various locations. Generally, vegetation reduces the near bed turbulence and shifts the position of the maximum Reynolds stress away from the bed and thereby, the bed is protected. In this layout, there was a noticeable difference in depth-wise variability of $RS_{u'w'}$ in vegetated and non-vegetated sections and, the effect of patch alignment is clearly observed. The shape of the RS profiles was distorted. At z/H= 0 to 0.2, the absolute $RS_{u'w'}$ values ranged from 0.80-1.32, 1.20-7.60, 0.73-3.62 cm^2/s^2 at P2, P3 and P4 and 1.02-1.2, 2.2-5.1 cm^2/s^2 at P1 and P5. In lower canopy region, vegetation has shown a significant effect on $RS_{u'w'}$ by reducing its near bed value and showing nearly uniform profiles (P2 and P4). This effect is in-turn different at P3 where negative near bed $RS_{u'w'}$ was observed and then showing a rising trend in its profile. In the upper canopy region, all the $RS_{u'w'}$ profiles in the vegetated section were on a rising trend with increasing order of variability as P2, P3, and P4. These profile shapes can show a clear variability in vertical momentum exchange activity. At P2, though the $RS_{u'w'}$ profile followed a general trend, the amount of mixing activity occurred at canopy top (or in upper canopy region) was comparatively less than P3 and P4. Also, above the canopy top ($z/H \geq 0.4$), the $RS_{u'w'}$ profile was fairly uniform. This is probably due to diminished turbulence at section A-A' [see Figure 5.6a] where the flow through bladed vegetation suddenly encounters highly resistant leafy patch (very low canopy porosity). But, this observation must be further investigated with detailed lateral measurements.

At the canopy top, the discontinuity in vegetation elements induces large scale vertical mixing and generally results in maximum values of $RS_{u'w'}$. In heterogeneous patch 2, the peak $RS_{u'w'}$ values were not located as expected, which is explained as follows. At positions P3 and P4, though the $RS_{u'w'}$ profiles were similar to other reported works, the location of the peak value differed. At P3, the peak was nearly at canopy top, and in P4 there was a shift in peak value to over canopy region. The inhibition of vertical momentum exchange at canopy top of P4 is may be due to, one, drag discontinuity at the interface, two, the sudden encounter of flow with rigid cylindrical stems and three, resistance variability. The velocity profiles at P4 also showed forcible pushing of the flow to over canopy region. Local regions of negative $RS_{u'w}$ was also noticed in lower canopy region of P4 though $\frac{\partial \langle U \rangle}{\partial \langle z \rangle}$ >0; indicating the transfer of turbulent energy to mean flow. In over canopy zone, the values of the $RS_{u'w'}$ were found to decreasing with increment in flow depth. In this layout, the higher thickness of active momentum exchange (40 % higher than heterogeneous patch

1) was observed at all locations. A simple conceptual sketch showing the mixing activity and penetration ratio at the canopy top is shown in Figure 5.6a.

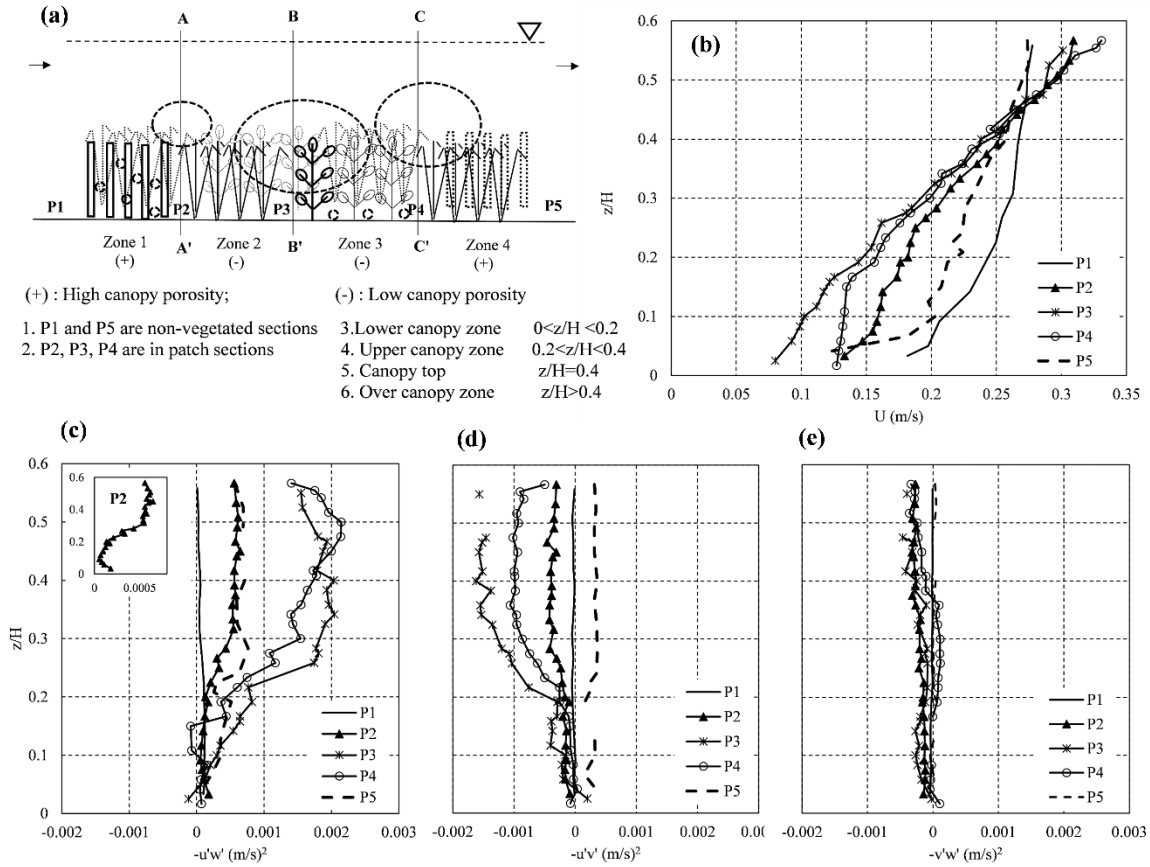

Figure 5.6 (a) Conceptual picture of mixing activity (represented by dotted ellipse) in side view; where, horizontal axis of ellipse represent intensity of mixing activity and portion of ellipse into the canopy zone represent thickness of active momentum exchange. Vertical distribution of **b**: stream wise velocity (U); Reynolds stress **c**: $RS_{u'w'}$, **d**: $RS_{u'v'}$, **e**: $RS_{v'w'}$ measured at different positions in Heterogeneous patch 2

Figure 5.6d and 5.6e show the variability of Reynold stress in lateral ($RS_{u'v'}$) and stream-wise ($RS_{v'w'}$) directions. It can be seen that absolute values of $RS_{u'v'}$ in lower canopy region were equally varied as $RS_{u'w'}$ and, especially at P2 the magnitude is relatively higher. Moreover, the shape of $RS_{u'v'}$ profiles in upper and above the canopy regions showed similar variation as $RS_{u'w'}$ with opposite sign and lesser magnitude. The increase in $RS_{u'v'}$ value indicates an increase in lateral momentum exchange, which is higher at P3, followed by P4. The position of peak $RS_{u'v'}$ and rising nature of profiles in the upper canopy zone is mostly similar to $RS_{u'w'}$ at P3 and P4. The plan view at section P3 shows the reversal of patch forms (resistance), allowing changes in flow pattern and interaction behavior.

Velasco *et al.* [2003] highlight the development of pressure gradients in the form of turbulent wakes generating lateral diffusion of momentum. This anisotropic behavior in flow structure clearly shows stream-wise and cross-stream geometric dissimilarity in vegetation patch forms, and their alignment has considerable influence on turbulence measurements. Also, it may be expected that, at measurement locations, interaction among flow structure due to multiple vegetation patches creates a zone of influence. Within this zone, the turbulent structure can be of varying intensity and depends on vegetation type and alignment. Hence, the turbulent flow structure may be heterogeneous throughout the patch and, could be investigated further with more detailed lateral measurements.

5.4 VARIABILITY IN ROUGHNESS COEFFICIENT

In our experiments, though the vegetation density (No. of plants per m^2) remained same, plant form, canopy porosity, and patch alignment has shown a significant effect on flow structure. The response of the flow to varying vegetation and its characteristics certainly influences the flow resistance, which is computed here in terms of Manning's roughness coefficient.

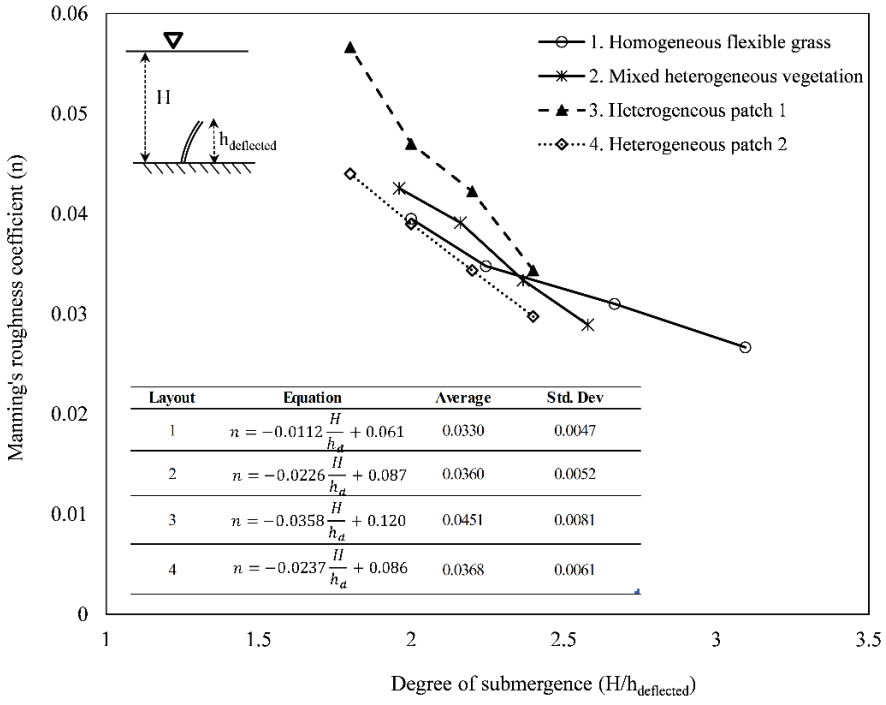

Figure 5.7 Variation of Manning's roughness coefficient with degree of submergence

Figure 5.7 shows the Manning's n variability computed by using Eqns. 1 to 3 of section 5.2.4 [Y. Li *et al.*, 2014; Y. Li *et al.*, 2015; also refer to Errico *et al.*, 2018] for

different degree of submergence. It is observed that Manning's *n* tends to follow similar trend for all the vegetation layouts. In the case of heterogeneous layouts, Manning's *n* is considerably higher and varied with vegetation patch alignment. With an increase in plant deflected height, the similar flow conditions in homogeneous flexible grass resulted in lower roughness value due to higher submergence depth. While comparing homogeneous flexible grass and mixed heterogeneous layouts, an increase in average resistance of 9% is noticed due to the addition of leafy and rigid cylindrical forms to only flexible forms. For heterogeneous patch layouts, patch 1 offered 25 % higher average resistance than patch 2. The presence of highly resistant leafy and rigid stem patches at the beginning and end increased the velocity reduction significantly. Although Manning's *n* is higher for lower discharges, it can be observed that the alignment of vegetation patches significantly increases the flow resistance.

5.5 DISCUSSIONS

This section discusses changes in flow structure due to heterogeneity in plant forms and their alignment. The depth-wise velocity profile in the vegetated channels can be roughly divided into flow through the canopy zone and the over-canopy zone [Klopstra *et al*., 1997]. Previous studies further divided the canopy zone into lower and upper canopy zones depending on the nature of the velocity profiles [Huai *et al*., 2009a; Chen *et al*., 2011]. In the present study, the flow through different vegetation patches altered the division of velocity profiles due to physical characteristics of the plant form. For example, the velocity profiles in leafy and rigid cylindrical vegetation can be clearly divided based on its shape. In the lower canopy zone, velocity is constant and, upper canopy zone velocity profile shows accelerating trend due to shear layer interaction. While the bladed form has no such distinction due to flexibility of the vegetation causing velocity profile accelerating throughout the canopy zone. A similar phenomenon was reported by Wilson *et al*. [2003]. Earlier works have reported that the velocity profile over the canopy zone follows the logarithmic law [Jarvela, 2005; Chen *et al*., 2011; Y. Li *et al*., 2014]. This observation could not be seen in the present study as the experiments were conducted in shallow submerged flow condition (Flow depth/plant height<5; refer to Nepf, 2012). The results showed that the effect of plant form and alignment of the plant patch is significant in controlling the velocity reduction. The presence of mixed vegetation forms [Figure 5.3b vs. 5.3a] and/or highly resistant leafy patch at the beginning [Figure 5.3c vs. 5.3d] is favoring for increased velocity reduction. When the patch type varies in both the directions [Figure

5.3d], the difference between the velocities along the patch in upper and over-canopy zones is insignificant.

In flexible submerged canopies, under few conditions, there is a possibility for the canopy-scale or K-H vortices to overcome the plant rigidity causing monami effect [Nepf 2010; Ghisalberti and Nepf, 2002]. The intensity of the progressive waving and, local depression in the canopy increases the turbulent exchange or flux towards the bed, causing bed erosion. In our study, unlike in flexible grass vegetation [Figure 5.3a], there is no local depression of turbulence flux in mixed heterogeneous layout [Figure 5.3b]. In addition, the peak turbulent flux shifted to higher value, and more velocity reduction is also noticed. A common observation to the previous studies was that inclusion of high resistant vegetation forms like leafy, rigid cylindrical stems could help in restricting or prevention of turbulent flux penetration towards the bed. Next, the alignment of vegetation as patches, varying its form in longitudinal [Figure 5.3c] or in both directions [Figure 5.3d] has also shown interesting flow behavior. These observations mostly differed with existing studies which focused on working with single vegetation type like cylindrical form or strips [Tempest *et al*., 2015]. In heterogeneous patch 1 [Figure 5.3c], the highly flexible bladed patch is confined between highly resistant leafy and rigid cylindrical patches. Leafy and cylindrical patches favored zones of lower velocities and turbulent stresses which favor bed protection or sediment depositions. Whereas, inside the flexible bladed patch relatively higher mixing activity is observed, favoring zones of increased turbulence levels. In heterogeneous patch 2, when patch alignment is varied in both directions, the cross-stream patch dissimilarity induced additional changes to turbulence and significantly changed the flow structure. Moreover, the shape of flow profiles (for example, Reynold stress) is distorted in nature. To better explain this difference, Figure 5.8 is plotted showing comparative analysis between heterogeneous patch 1 and patch 2. Table 5.4 shows the percentage increase in turbulence structure of other locations in patch 1 and 2 with respect to section P2 in patch 1. A high degree of momentum exchange activity ($RS_{u'w'}$ and $RS_{u'v'}$) and turbulence (u_{rms}, w_{rms}, TKE) is observed in heterogeneous patch 2. This is further supplemented with a higher increase in vertical turbulence intensity levels (w_{rms}), which is a measure of vortex rotation. The overall layouts provide spatial heterogeneity in flow velocity and turbulence field, which is important for creating ecological habitat. For example, guppies (*Poecilia reticulata*) have shown to prefer staying in varying levels of velocity and turbulence zone for maintaining their life cycle and health [Trinci *et al*., 2017]. Other studies have reported

that few aquatic species favor zones of high turbulence intensity [Trinci *et al*., 2017], moderate velocities and low TKE [Hockley *et al*., 2014] showing the importance of heterogeneous flow conditions in rivers.

Table 5.4: Comparison of turbulence intensities and turbulent kinetic energy (TKE) in the lower canopy zone (z/H ~0.10)

	Patch type	**P2**	**P3**	**P4**
u_{rms}	Heterogeneous patch 1	*	32%	27%
	Heterogeneous patch 2	21%	79%	73%
w_{rms}	Heterogeneous patch 1	*	38%	30%
	Heterogeneous patch 2	18%	125%	89%
TKE	Heterogeneous patch 1	*	88%	69%
	Heterogeneous patch 2	40%	250%	179%

* refers to reference point relative to which percentages are expressed

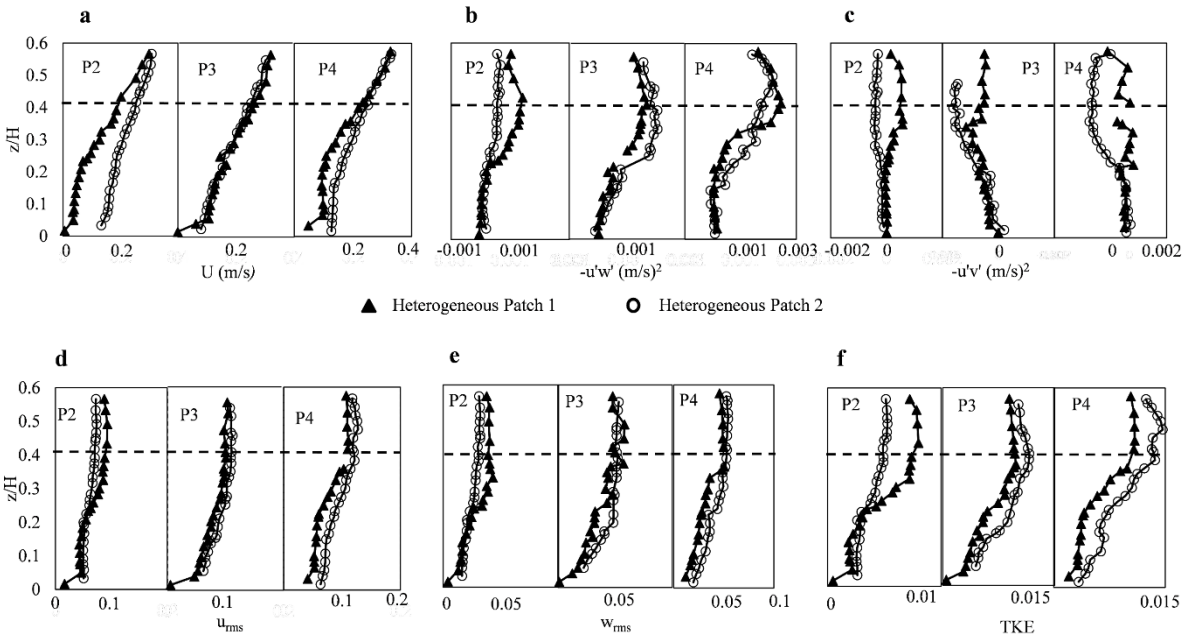

Figure 5.8 Comparative flow structure in Heterogeneous Patch 1 vs. Heterogeneous Patch 2. Where (a): Primary velocity; (b), (c) is Reynold stress in vertical and span-wise directions; (d), (e) is turbulence intensity in u, w directions; (f) is turbulent kinetic energy.

The plant swaying motion and K-H vortices due to flow instability at the canopy top interacts and transfer the momentum flux by forming an active momentum exchange region (h_t) along the vegetated channel [Ghisalberti and Nepf, 2005; Wang *et al*., 2009]. In the presence of single vegetation type, this thickness h_t is observed to be gradually increasing for flexible grass [Chen *et al*., 2011] or uniform for flexible leafy vegetation [Y.

Li *et al*., 2014] along the channel. The present work observes non-uniform variability in thickness h_t depending on the plant forms and patch alignment. With patch type varying in both the direction [Figure 5.3d], a further increase in thickness h_t is noticed. These observations are conceptually represented in Figure 5.9. Manning's roughness coefficient computed for different flow conditions and patch alignment describes the patch type variability effect in changing the flow resistance. This information can be helpful in incorporating appropriate Manning's value in the river and ecological modeling [Wu *et al*., 1999, Y. Li *et al*., 2014]. The study also reveals that horizontal and vertical distributions of plant form, patch alignment have a significant effect in controlling flow and turbulent structure and, roughness induced to the flow.

Finally, it can be said that spatial heterogeneity in flow structure due to heterogeneous vegetation layouts can be helpful for habitat life, biodiversity and also promote sedimentation zones. Unlike flexible grass vegetation, heterogeneous vegetation patches can be capable of providing both sedimentation zones and high mixing activity zones in one vegetated bed. This observation can be further strengthened with more experiments considering a different combination of heterogeneous patch layouts and, eventually helpful for implementing in river restoration schemes.

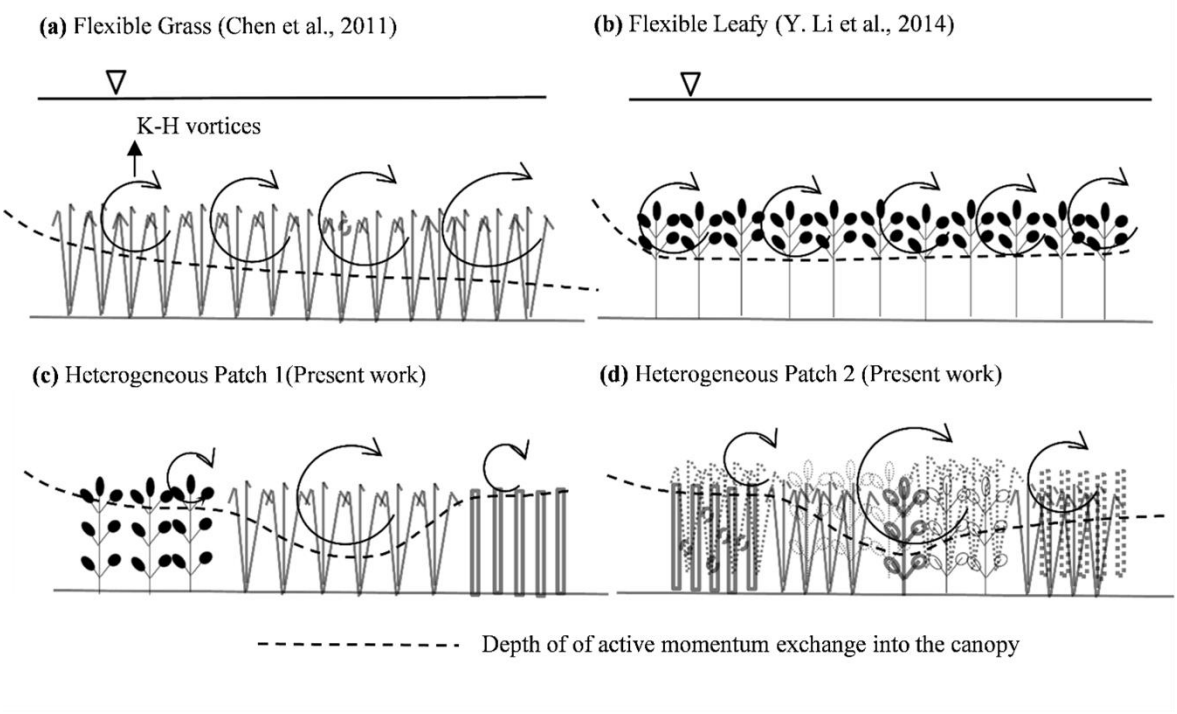

Figure 5.9 Comparison of momentum exchange zone variability in different layouts

5.6 CHAPTER SUMMARY

In the present paper, an analysis of laboratory experiments conducted to investigate the effect of submerged heterogeneous vegetation patches on flow structure is discussed. For this purpose, three natural plant forms (grass, leafy and cylindrical) arranged in four different layouts [Figure 5.3], namely homogeneous flexible grass, mixed heterogeneous patch, heterogeneous patch 1 and patch 2 were studied. The results of the study provided insights in understanding the effect of heterogeneous characteristics such as plant morphology, canopy porosity and patch alignment on flow behavior.

The major observations in the study lead to the following conclusions. First, in a mixed heterogeneous patch, the additional drag due to the presence of other vegetation forms like leafy and cylindrical stems results in 10% increased velocity reduction than homogeneous flexible grass alone. In addition, there was no local depression in peak Reynold stress (at z/H ~ 0.54) into the canopy as observed for flexible grass vegetation (at z/H~0.45). Second, in heterogeneous patch 1 and patch 2, different zones of increased and diminished turbulence levels, varying velocities were observed along the vegetated section. Plant form and the canopy porosity has significant control on altering the position and intensity of the vertical momentum exchange at the canopy top and also, thickness of the active momentum exchange. For example, in the leafy patch (of heterogeneous patch 1), the amount of mixing activity was 50% lesser than other vegetation forms. Third, other than plant form and canopy porosity, patch alignment has also controlled the flow structure by inducing additional turbulence to the flow. In heterogeneous patch 2, the flow instability aroused due to both longitudinal and cross-stream variability of patch forms resulted in increase in turbulence parameters to more than 100% than heterogeneous patch 1. The response of Manning's *n* was highly affected by plant form and patch alignment for different flow conditions.

This work can be further extended to study with different layouts of heterogeneous patches under varying flow conditions. To investigate further, detailed measurements in longitudinal and traverse directions will, however, be helpful for better understanding and justifying the processes in the flow field. With further improvement in knowledge, heterogeneous vegetation patches can be designed for riparian management practices in improving the ecological behavior and sediment deposition zones.

6

MORPHOLOGICAL RESPONSE OF A VEGETATED SAND BAR

The Brahmaputra River exhibits complex hydrodynamic and morphological characteristics with different levels of interdependent processes occurring simultaneously. On the other hand, vegetation improves the river ecological condition and helps for the planform stability. The riparian zones of the Brahmaputra River are also covered with vegetation patches and this makes important to study vegetation influence on river morphology. This chapter addresses following question through numerical modeling.

- How is the capability of mathematical models to predict the morphological changes in the Brahmaputra River?
- How is the morphological response of a braided loop in the Brahmaputra River, where the sand bar is vegetated? How do braided loop characteristics change with different percentages of vegetation cover?

6.1 INTRODUCTION

Braided rivers exhibit complex and dynamic channel network due to high stream power and associated morphological processes; such as erosion, deposition and channel migration [Bridge, 1993a; Ferguson, 1993; Klaassen *et al.*, 1993]. They produce unstable morphological features over the river corridor in response to fluctuating flow and sediment supply [Smith, 1977; Ashworth *et al.*, 2000; Piegay *et al.*, 2009; Zolezzi *et al.*, 2009]. In the recent decades, riparian vegetation has become an important implication for

management of the river corridors for improving the planform stability and ecological functioning [Wilson *et al.*, 2003; Nepf and Ghisalberti, 2008; Bertoldi *et al.*, 2011]. Many of the previous studies report the positive feedback from vegetation in controlling the braiding intensity and dynamics of braided river network. For example, a laboratory study by Gran and Paola [2001] shows vegetation cover reduced the number of active channels and migration rate of braided river network. With the addition of vegetation to a sidebar Rominger *et al.* [2010] observed reduction in longitudinal velocity over the bar and increased sediment deposition. Tal and Paola [2010] through laboratory experiments observed a shift of multi-thread network to single thread stable channel due to vegetation over the braided network. A similar study by Van dijk *et al.* [2013] observes channel deepening, stable banks with tighter bends with the increase in vegetation densities. Bertoldi *et al.* [2015] investigated the combined effect of vegetation and wood dispersal on braided morphology subjected to cycles of flooding. Their study reports, riparian vegetation increased channel stability, reduced braiding intensity, and lateral erosion.

The Brahmaputra River exhibit complex morphological characteristics due to wider braided belt width, high flow and sediment variability, and erodible banks [Karmaker *et al.*, 2017]. Moreover, sand bars are highly dynamic and migrate over a short-period of time. Large scale bank erosion annually affects the millions of people along the river course. In order to mitigate the river bank erosion, land spurs, permeable structures like bamboo bandalling and concrete porcupines, bank revetments and geo synthetic based training measures are in practice [Wiebe, 2006; B. Board, 2012]. However, the effect of river training works are local measures and their performance is highly uncertain to river flow characteristics, and site dependent. Moreover, the river training measures are observed to be short-term protection measures due to dynamic morphological changes. The Brahmaputra River riparian zones are covered with different vegetation elements such as long and flexible grasses over the sand bars, and heterogeneous vegetation patches are observed in the flood-plain zones. Previous studies report the importance of vegetation cover for river stability and natural means of long-term training the river [Tal and Paola, 2007]. This makes important to understand the link between vegetation response and morphological changes. In the present objective, an attempt has been made to understand the river response to vegetation using two-dimensional morphological model. The aims is therefore: (a) to investigate the capability of mathematical model in predicting the morphological changes of the Brahmaputra River; and (b) to study the morphological

response of a braided loop subjected to different percentages of braided cover. For this objective, a two-dimensional hydrodynamic and morphological model CCHE2D was set up with river bathymetry and simulated for different cases of vegetation cover. The morphological changes are then analyzed and compared with no vegetation case to observe the changes resulted due to vegetation cover.

6.2 STUDY AREA

River reach of the Brahmaputra River at Ganeshpahar is considered for the study. The reach is nearly 16 km long, and 4 km wide at this location and, the study area is about 100 km downstream of Tezpur and 30 km upstream of Guwahati. The Brahmaputra river at Ganeshpahar is very dynamic which experiences frequent change in its morphology *i.e.*, change in dimensions of the sand bars, shifting of the main channel, new bifurcations and formation of new tertiary channels are commonly observed [Figure 6.2]. In addition, the frequent shifting of channels allows two rocks *viz.* one stone outcrop on the northern side and another hill rock on the southern side [Figure 6.1] protruding into the river and creates navigational problems by generating high turbulence and forming severe bends. The south bank of the river at Ganeshpahar is protected by hills, whereas the north bank is unprotected sediment deposits. The river exhibits severe braiding pattern in the upstream of Ganeshpahar and follows several tortuous paths. The satellite imagery, along with the morphological issues observed in the study area is shown in Figure 6.1 and Figure 6.2.

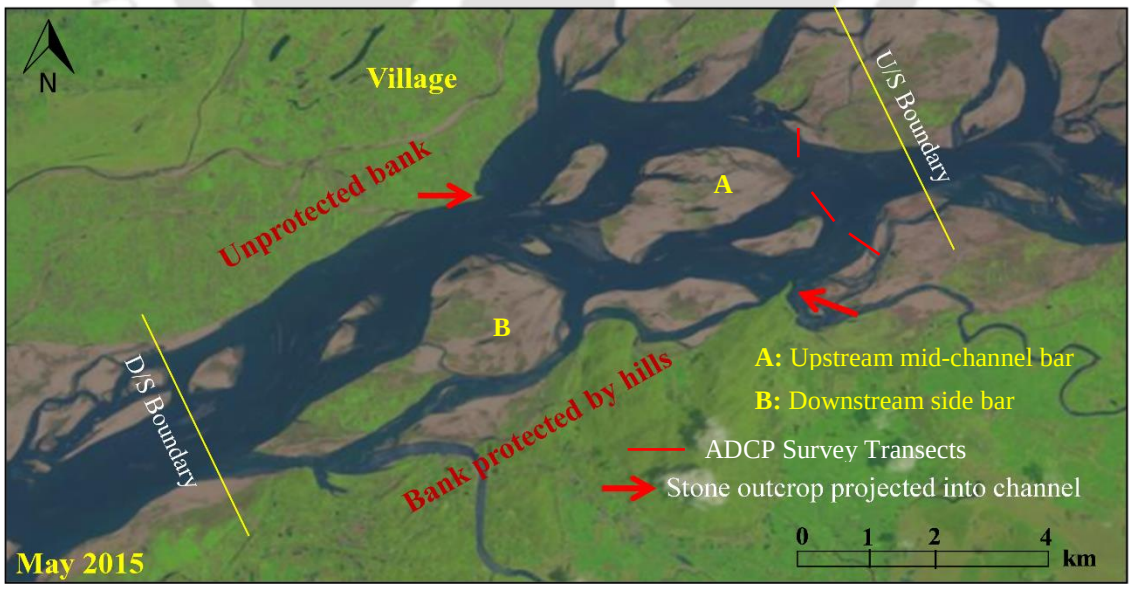

Figure 6.1 Satellite imagery of the Brahmaputra River at Ganeshpahar, showing details of the study area and morphological condition in May 2015.

Figure 6.2 Morphological changes at Ganeshpahar from 2013 to 2015; (a) 1 is main channel in 2013; (b) 2 is main channel in 2015

6.3 SURVEY PARTICULARS AND DATA COLLECTION

6.3.1 Hydrographic Survey

Detailed river survey for the Brahmaputra River reach at Ganeshpahar was conducted in low flow season (February 2015) and bank full condition (September 2015). The low flow season survey includes collection of river bed and bank samples and, water samples for laboratory analysis of suspended sediment concentration. The bank full survey includes collection of (a) bank to bank bathymetry survey using GPS integrated multi-frequency echo sounder; (b) velocity profile data using four beam, 614.4 kHz Workhorse Rio Grande acoustic Doppler current profiler (ADCP); (c) water samples at bank erosion zones, turbulence locations for sediment concentration analysis. All the surveying equipment were mounted on a moving survey vessel and operated by helmsman for respective data collection. Satellite imagery analysis, historical bathymetry and surveyors experience clearly show the morphology of the river at Ganeshpahar highly changes with time. Therefore, bank to bank cross-sectional survey was conducted at 400 m interval and 200 m interval at critical bifurcation locations. Thus, a total of 50 cross-sections were collected with 20 m horizontal interval. The analysis of bathymetry data indicates primary channel is towards the northern bank and secondary channel is on the southern side. This indicates shift in primary channel from 2013 to 2015 and, major flow is diverted towards the northern side. In this channel, the maximum depths in the order of 15 to 20 m were recorded and, in secondary channel the maximum depth recorded was 10 m. Although higher depths were recorded, ADCP data reveals 50% of the channel is in stagnation zone (<0.4 m/s) and may indicate partial closure in the next season by large scale deposition. Furthermore, bathymetry data/satellite map reveals the growth of tertiary channel over the sand bar. This may become active in the next season when the deposition in the secondary

channel is allowed. The bed and bank material sample analysis revealed D_{50} was 0.18 mm and 0.21 mm. The longitudinal bed slope was very gentle with a slope of 1 in 8000.

6.3.2 Hydrological and Sediment Data

The hydrological data used in the study comprises of daily discharge, river stage and sediment concentration data obtained from IWAI Pandu, modeling and empirical relations. The study area, Ganeshpahar, is located at 30 km upstream of Guwahati and 100 km downstream of Tezpur gauging stations. At Ganeshpahar, there is no gauging and discharge site and, also no major tributary contribution till Guwahati. As a result, the daily discharge data available at Guwahati was used for modeling of Ganeshpahar and, corresponding river stage hydrograph was generated from one-dimensional model. More details of the modeling are discussed in the next sections. For the sediment concentration variability, Yang [1973] sediment transport function was used following the suggestion from Karmaker *et al.* [2010] for the middle Brahmaputra. This function evaluates the total sediment concentration in which suspended load and bed load fraction were segregated as 85% and 15% fraction [Karmaker *et al.*, 2010].

6.4 NUMERICAL MODELING.

6.4.1 Two Dimensional Hydrodynamic and Morphological Modeling

In this study two-dimensional (2D) hydrodynamic and morphological model CCHE2D (Mesh Generator and GUI) was used for studying the morphological changes. CCHE2D is a finite element based depth-integrated 2D model designed for performing steady, unsteady flows, sediment transport and morphological variations along the river reach. In this model, two zero equation models, namely parabolic and mixing length models and, two-equation k-€ turbulence closure model are available for calculating eddy viscosity. The model takes into account the effect of secondary flow on the sediment motion in the curved channel and bed load motion due to transverse slope while simulating the morphological changes. CCHE2D handles dry nodes formed due to varying discharges and changing plan form by treating with the moving boundary conditions. For setting up CCHE2D, input data such as detailed river cross-sections topography of flood plain, river bed and bank soil samples information, hydrological data are required. The technical details of the CCHE2D model are discussed in Appendix C.

6.4.2 One-Dimensional Modeling

HEC-RAS is developed by the Hydrologic Engineering Centre for the U.S. Army Corps of Engineers. HEC-RAS allows the user to perform one dimensional steady, unsteady flow analysis, movable sediment transport and water quality analysis. It is designed to perform one-dimensional hydraulic calculations for a combined network of natural and man-made channels. It numerically solves the Saint-Venant equations for a complex river network. The equations represent mass and momentum conservations at the control volume, which is the basic unit of flow analysis. HEC-RAS was set up for the study area with the 20 cross-sections extracted from topographic database. The chainage interval between cross-sections varies from 0.6 to 1 km. The daily discharge variations in the river and longitudinal slope were used as upstream and downstream boundary conditions. The unsteady flow simulations were performed to obtain stage hydrograph for the input discharge hydrograph. Figure 6.3 shows the 1D HEC-RAS setup with input discharge hydrograph and simulated stage hydrograph.

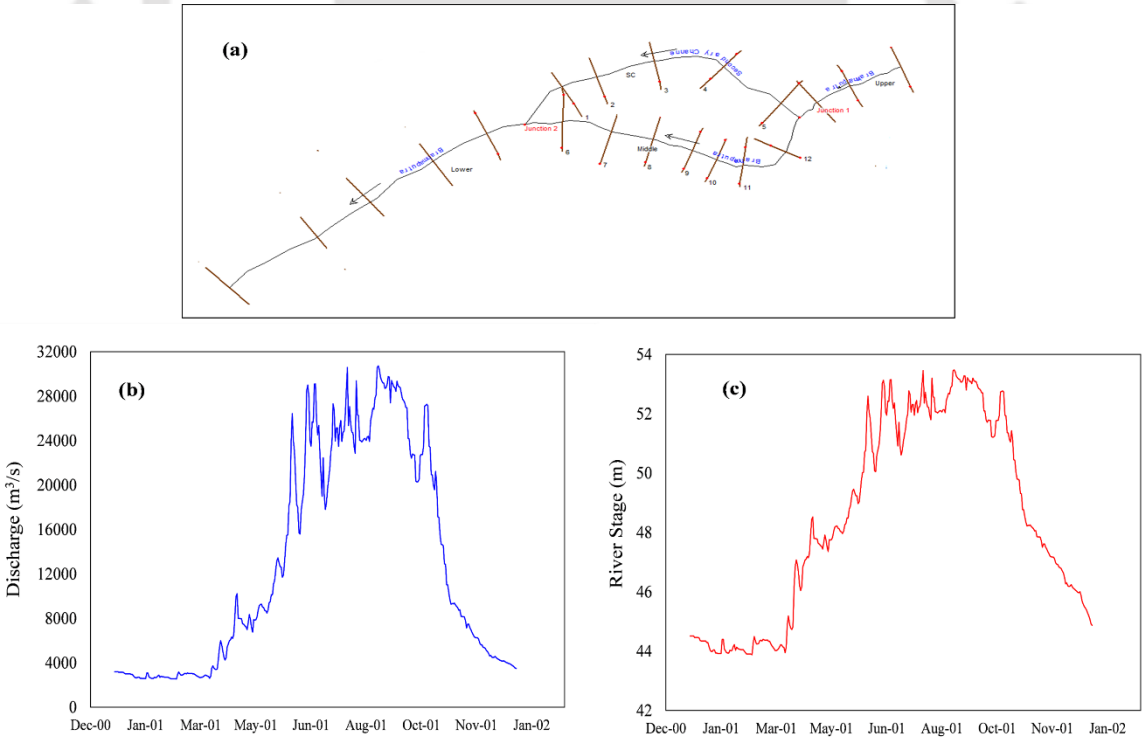

Figure 6.3 (a) HEC-RAS model setup for generation of (c) river stage for a given (b) discharge hydrograph

6.4.3 Methodology

Hydrographic survey of Ganeshpahar location conducted by IWAI Guwahati in September 2015 is used as a topographic database. The computational mesh (20*300) for the area having a length of 16 km and an average width of 4.0 km was generated [Figure 6.4] for the topographic data using CCHE2D mesh generator. At the channel bifurcation and confluence zones, the finer grid was generated than other parts of the mesh. The topography data is triangularly interpolated to get the bed level elevations at all mesh nodes and geometry file is created. For further analysis like the setting of flow initial and boundary conditions, sediment parameter requirements and to run simulations, CCHE2D GUI was used. The annual discharge hydrograph ranging from 2500 to 30,000 cumecs is given as upstream boundary condition and corresponding stage hydrograph as downstream boundary condition. The initial upstream and downstream water surface elevation is set based on water levels obtained from HEC-RAS. Values between upstream and downstream are interpolated perpendicular to the flow direction. Sediment parameters such as mean size (D_{50}=0.018 mm), sediment class, porosity (0.63), sediment transport mode and boundary conditions are given. The hydrodynamic and morphological simulations are carried out for 1 year period and the different cases of vegetation cover are studied individually.

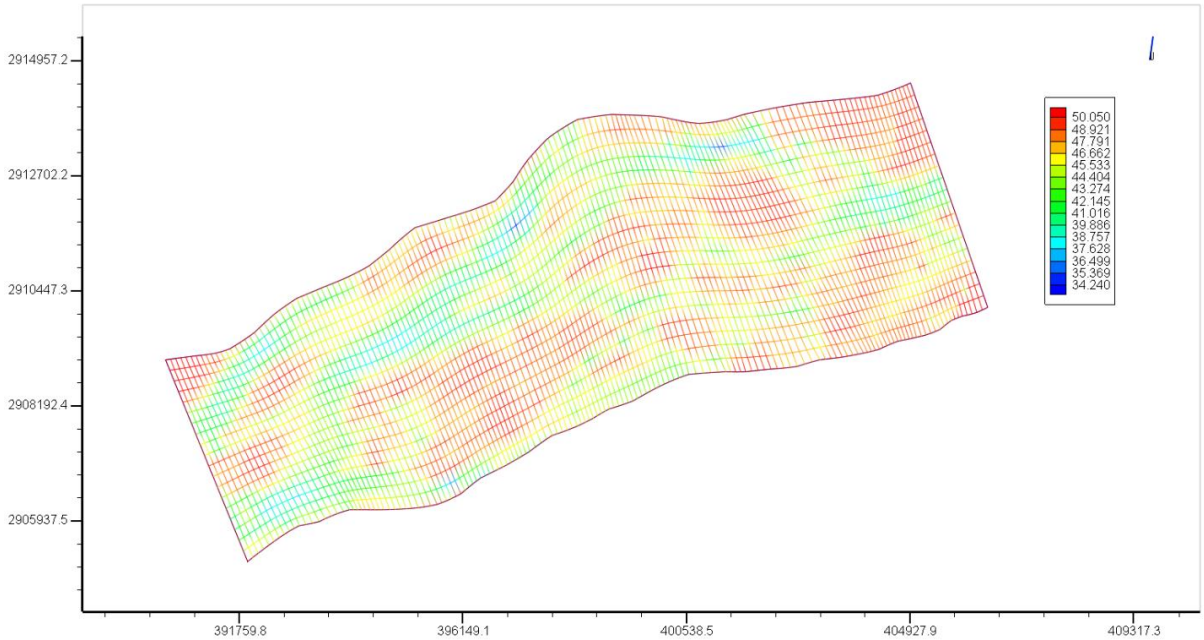

Figure 6.4 Interpolated river bathymetry collected during the high flow period

6.5 SELECTION OF MANNING'S ROUGHNESS FOR VEGETATION

The present objective aims to study the effect of vegetation cover over a sand bar on the morphological changes in and around a braided loop. To simulate these changes, the effects of vegetation is incorporated in the model through additional resistance to the flow and, Manning's roughness coefficient is used to represent the vegetation roughness. SCS [1954] developed the graphical methods for different types of vegetation resistance as a function of hydraulic radius and velocity of the flow. The chart includes Manning's roughness coefficient for type A: very high resistance; type B: high; type C: moderate; type D: low and type E: very low resistance values for various kinds of grass. For the case of Brahmaputra River, one of the common type of vegetation observed on the sand-bars or flood-plains is grass forms. In low flow period, the sand bars and vegetation is exposed and, no flow vegetation interaction is seen. Within the monsoon period, it is expected that the vegetation responds to the changes in the river stage by varying its physical characteristics. For example, in rising and falling river stage, the vegetation is emergent and offers more resistance to the flow, while in high flow period, the vegetation is submerged and relatively offers less resistance. This changes in vegetation resistance may influence the sediment deposition pattern over the sand bars and also, flow characteristics in braided channels. Although sand bar is fully vegetated, high energy river flow, fluctuating flow stage and location of the vegetated sand-bar over the braided corridor may strongly affect the resistance offered by the vegetation. Considering the river characteristics, moderate flow resistance by the vegetation cover is assumed for selecting the Manning's roughness value at different flow conditions. CCHE model is simulated for one monsoon season and, hydraulic parameters (velocity V, hydraulic radius R) over the un-vegetated sand bar are obtained during rising, high flow and falling river stage period. To obtain the initial Manning's (n) roughness value, VR is segregated for three flow stages (rising, high and falling), averaged and compared with n-VR curve for moderate vegetation resistance. In the next step, this trial *n* is used in model for VR computation and for n estimation. This is continued and, at the end of the third trial, final selection of the n was confirmed where difference in VR was very less. Figure 6.5 shows the variation of VR (product of velocity and hydraulic radius) averaged over the sand bar at different river stages, while Table 6.1 shows the obtained Manning's value for different flow stages. These values are used in morphological modeling to study the effect of vegetation roughness on morphological changes.

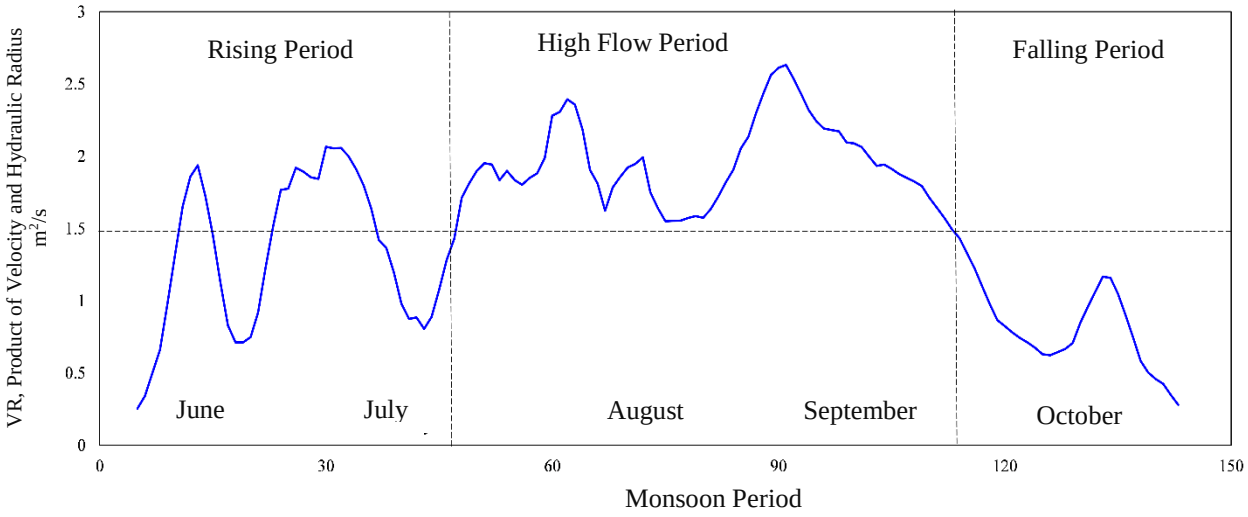

Figure 6.5 Variability in VR in rising, high flow and falling monsoon period over the sand bar

Table 6.1: Details of the zones in study area

S. No.	Season	Manning's n
1	Rising Period	0.035
2	High Flow Period	0.030
3	Falling Period	0.037

6.6 RESULTS AND DISCUSSION

6.6.1 Hydrodynamic Validation

CCHE2D model was set up with the required input data without incorporating any vegetation roughness and initially simulated for a steady discharge of 14,000 m^3/s for three days period. This is done to smoothen the abrupt fluctuations in the initial bathymetry aroused during data collection and bed interpolation. Furthermore, to evaluate the model performance simulations were carried for steady, bank full discharge of 20,000 m^3/s obtained during ADCP survey. ADCP survey conducted at three selective transects *i.e.,* entrance of primary, secondary and tertiary channels [Figure 6.1] was used for the analysis.

The model calibration was tested with grid adjustment, time step and turbulence model and results were compared with observed ADCP data (flow depths and velocity) at

respective locations as shown in Table 6.2 and Figure 6.6. The model simulated results show that predicted depth and velocity are reasonably in a good agreement with observed data, with a deviation of 15-25% in average depth and velocity prediction. The predicted values were in close to the observed range, but, the maximum values were relatively more deviated. Although there was a deviation in predicted values, the velocities across the cross-section [Figure 6.6] were close to the observed trend with lower velocities in stagnation zones and higher velocities in main channel flow zones. The difference in flow parameters in simulated and observed velocities can be due to different reasons: (a) limitation of computational nodes to maximum 12000 due to beta version; (b) limitation to capture complex river bathymetry, macro-turbulence interactions and influence of upstream morphological changes. However, the study by Papanocolaou *et al.* [2011] reports errors of 25 to 35% are normally acceptable in simulated flow parameters due to uncertainties in both observed and simulated values.

6.6.2 Morphological Validation

CCHE2D predicts the change in bed elevations occurred due to scouring and deposition of the river bed, movement of suspended and bed load etc. To understand the performance of the model in predicting the morphological changes, a comparison analysis was carried out between observed and simulated planform changes. In this study, the initial bathymetry data were collected in August 2015. As the bathymetry data was not available for the next season for observing the bed level changes, morphological validation was carried by comparing the one year simulated planform and corresponding satellite imagery. Figure 6.7 shows the simulated planform of the study reach and the satellite imagery map. It is observed that major channel changes such as flow directions, locations of primary and secondary channels, bifurcations and confluences were well predicted but local scale in-channel depositions and consequent channel division could not be predicted. One point to highlight this change was, no bank erosion phenomenon in the model. In the Brahmaputra River, bank erosion is an important process controlling local scale, abrupt in-channel deposition patterns due to changes in flow structure. This local changes subsequently alter the upstream and downstream flow structure and morphological changes. Therefore, this may be one reason for not accurate prediction in local scale morphological features. However, the model results performed fairly well in predicting the thalweg, large scale morphological features which may be sufficient for the present analysis.

Table 6.2: Comparison of Observed and Simulated flow parameters in different channels

S. No.	Location	Water depth (m)		Avg. water depth (m)		Velocity range (m/s)		Avg. Velocity (m/s)	
		Obs.	Sim.	Obs.	Sim.	Obs.	Sim.	Obs.	Sim.
1	*Primary	2.7-15.2	2.1-13	9	7	0.24-2.02	0.6-1.51	1.7	1.4
2	*Secondary	2.4-9.5	3.3-8	6	5	0.03-1.6	0.3-1.47	0.98	1.02
3	*Tertiary	4.8-5.1	4.1-6.3	4.5	5	1.04-1.85	1.1-1.38	1.25	1.26

Note: * cross-sections at primary, secondary and tertiary channel

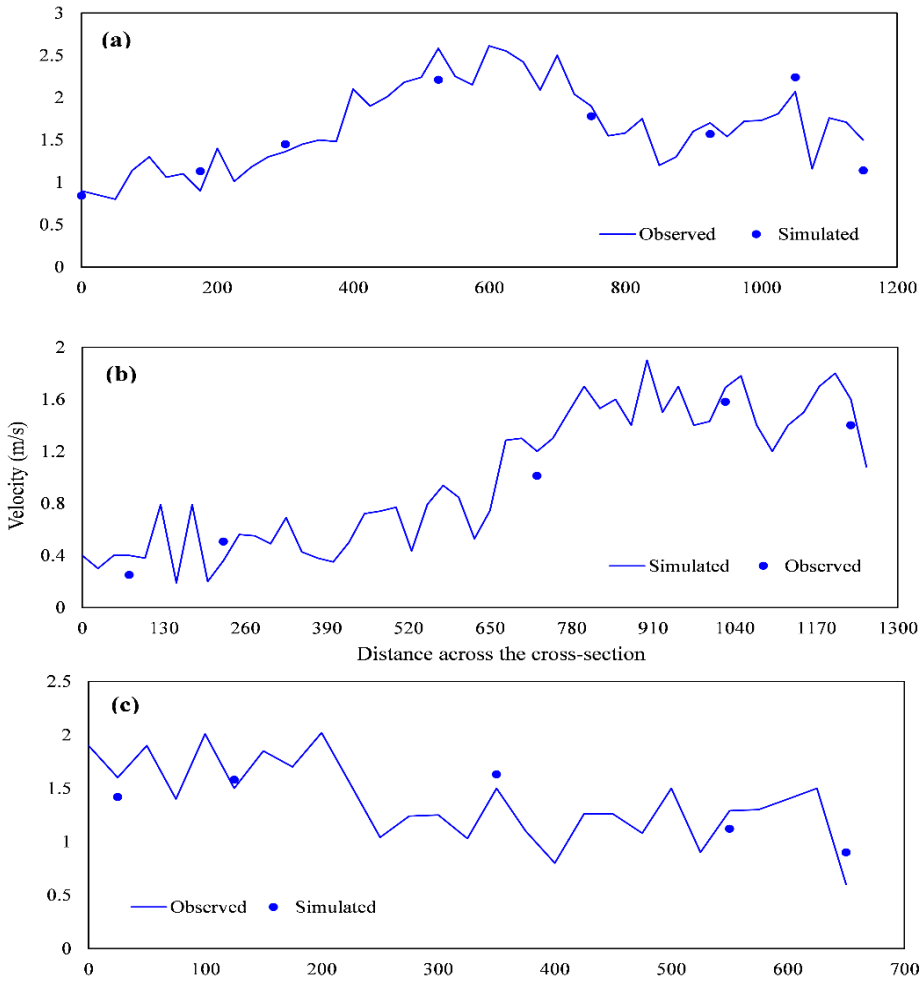

Figure 6.6 Comparison of observed and simulated data at (a) primary channel; (b) secondary channel and (c) tertiary channel

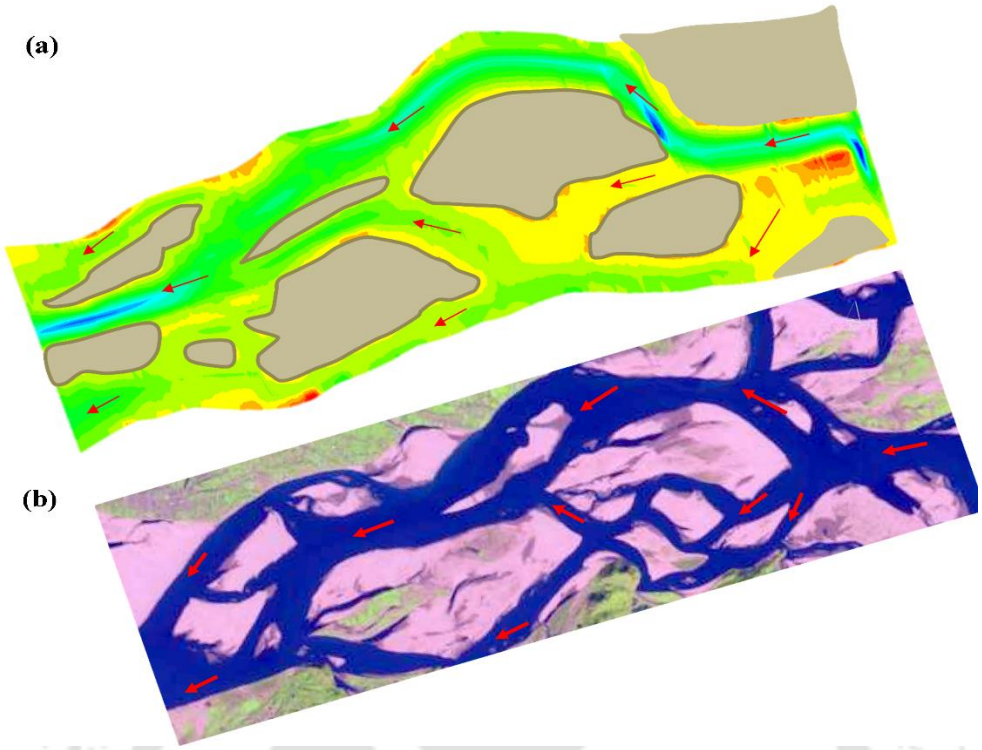

Figure 6.7 Comparison of (a) simulated planform and (b) satellite imagery planform

6.6.3 Vegetation Cover Induced Planform Morphological Changes

Bathymetry conditions prevailed in September 2015 of the Brahmaputra River reach were considered for morphological changes for various vegetation cover layouts. To investigate the vegetation cover induced morphological changes, the following three cases were studied.

- Case 1: Full vegetation cover over the mid-channel bar surrounded by the primary and secondary channels;
- Case 2: Half vegetation cover over the mid-channel bar surrounded by the primary and secondary channels;
- Case 3: Full vegetation cover over downstream bar

Vegetation cover was introduced in the model by increasing the Manning's roughness coefficient value over the sand bar. To consider the changes in flow stage on vegetation roughness, the Manning's coefficient was changed in rising, high flow and falling monsoon stage. For each case, the hydrodynamic and morphological simulations were carried for one year period and results were analyzed. The results

include changes in planform morphology, channel bed elevation, and discharge distribution in braided channels and braiding parameters.

Case 1: Full Vegetation Cover over the Mid-Channel Bar

In this case, vegetation cover roughness is introduced over the mid-channel sand bar [A in Figure 6.1] surrounded by primary channel on the right side and secondary channel on the left side. The dimensions of the sand bar are 4 km in length and 3 km in width. The bathymetry map reveals growth of an elongated bar inside the secondary channel. The model predicted morphological changes due to natural conditions is shown in Figure 6.7a, and full vegetation cover is shown in Figure 6.8. It can be observed that in natural conditions, the sand bar in secondary channel is laterally growing, and divided the secondary channel into two tertiary channels on either side. This phenomenon is not observed in the presence of vegetation cover. Morphological changes analysis showed that vegetation roughness increased the flow resistance and promoted the sediment deposition over the sand bar. Moreover, the lateral expansion of the bar growth is also noticed. This lateral expansion blocked the bifurcation in the secondary channel resulted from bar growth, and contributed towards the development of secondary channel.

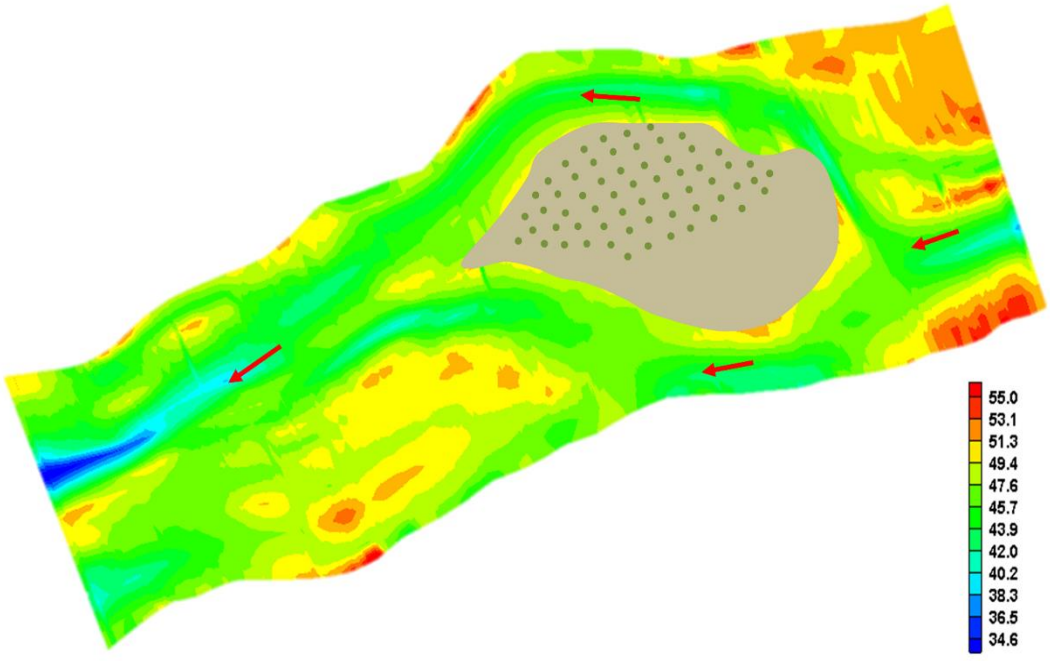

Figure 6.8 Simulated morphological changes for full vegetation cover on upstream sand bar

Case 2: Half Vegetation Cover over the Mid-Channel Bar

In case 2, half-vegetation cover *i.e.*, 50% of the vegetation roughness cover introduced over the mid-channel bar [A in Figure 6.1] was simulated [Figure 6.9]. Planform map shows morphological changes were similar to as observed in full vegetation cover. However, the dimensions of the bar growth and braided channels are different from full vegetation cover. In both case 1 and case 2, the lateral bar growth is close to 0.5 km, and the length of bar developed remained different. In half vegetation cover, the length of the bar closely remained similar to the initial condition while in full cover the bar length is increased by 0. 3 km. Planform view also suggests the difference in channel development of left and right braided channels with full vegetation cover more developed. Discussion on changes in channel elevation and other morphological parameters is presented in the next section.

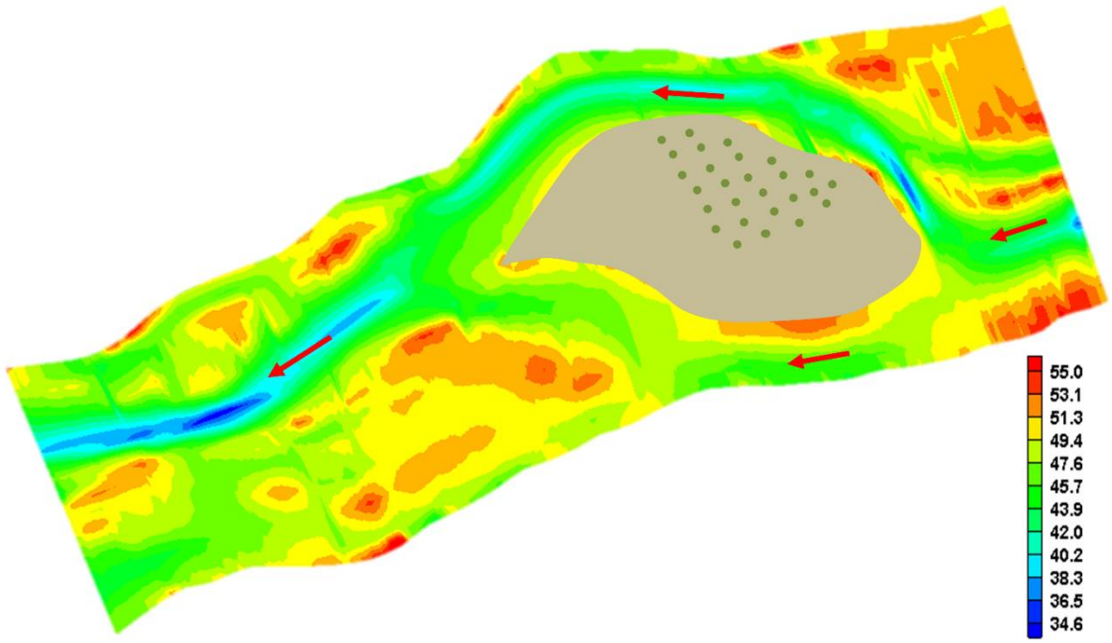

Figure 6.9 Simulated morphological changes for half vegetation cover on upstream sand bar

Case 3: Full Vegetation Cover over the Downstream Sand Bar

In the first two cases, the vegetation cover is on the upstream mid-channel bar and, in this case, vegetation cover is on the downstream bar [B in Figure 6.1]. Here, initial bar dimensions include 5.5 km in length and, 2 km in width with an elongated shape. Planform

morphological analysis showed that, compared with natural conditions [Figure 6.7a], the development of left anabranch surrounding the downstream bar in terms of channel configuration and deepening is clearly visible in vegetated case [Figure 6.10]. It can be noticed that the deepening of the channel is close to 2 m and consistent throughout the channel [Figure 6.11]. This deepening allows more discharge to the left anabranch than in natural conditions. It can also be observed that no vegetation cover or roughness on the upstream bar [A in Figure 6.1] allowed the growth of bar in the secondary channel and divided into two tertiary channels on either side. In this case, vegetation cover has not shown influence on downstream bar dimensions *i.e.*, lateral and longitudinal bar growth were not observed. As the major flow diversion is towards the right anabranch and the bar position is away from the main channel flow, there is no development of anabranch pattern or bar dimension changes over the downstream bar in both natural conditions and vegetated case.

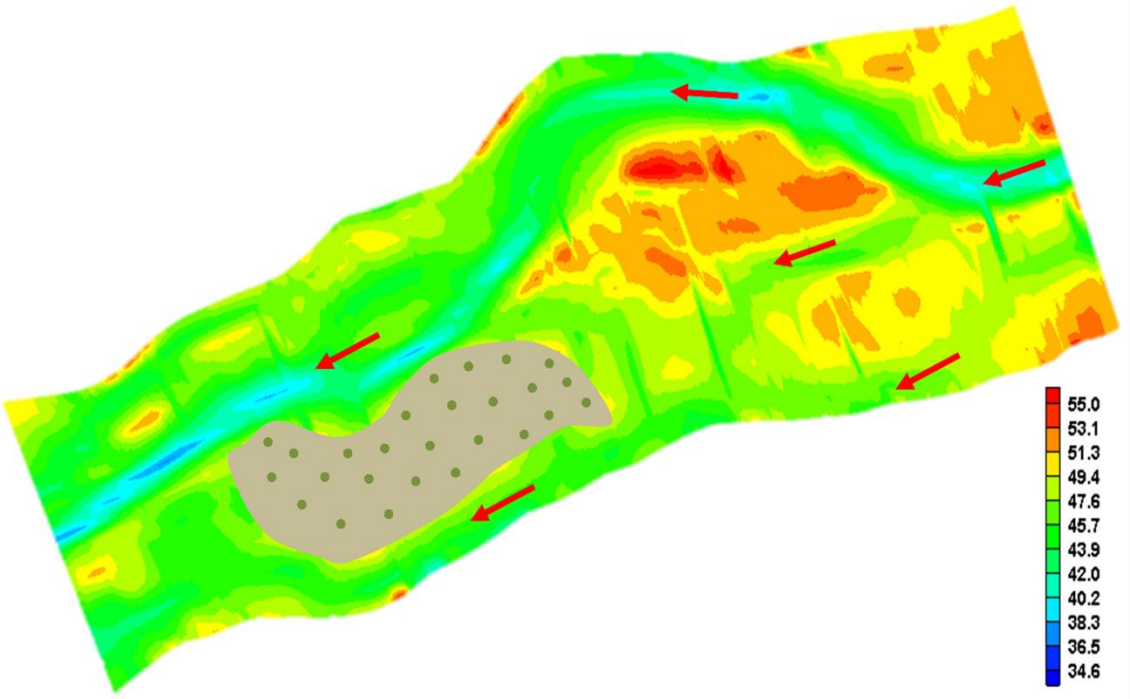

Figure 6.10 Simulated morphological changes for full vegetation cover on downstream sand bar

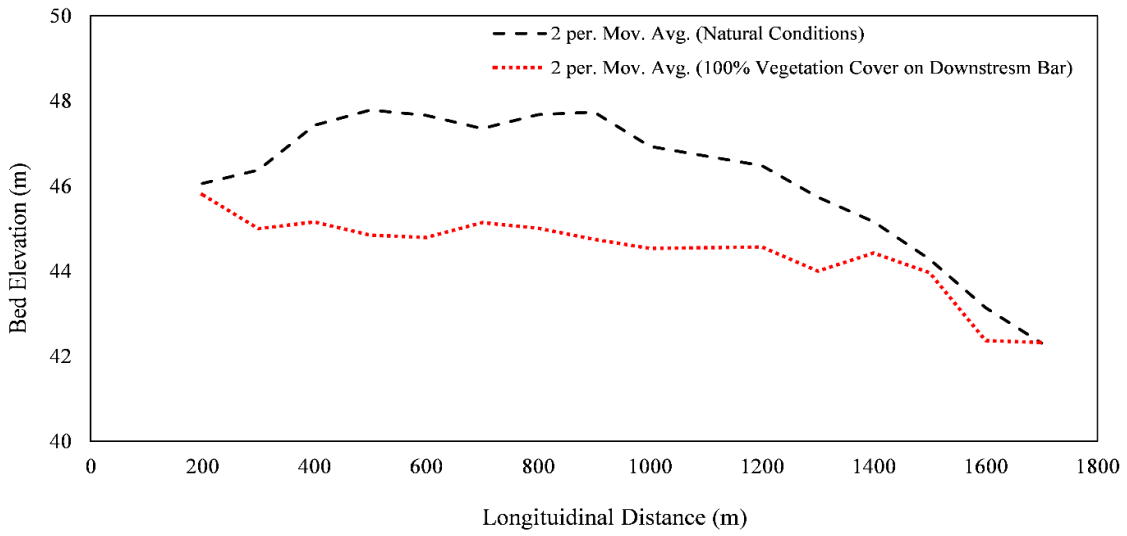

Figure 6.11 Comparison of channel bed elevation in downstream secondary channel for natural and vegetation cover conditions

6.6.4 Channel Development, Discharge Distribution and Braiding Parameters

Two types of vegetation cover (100% and 50% cover) were studied for the upstream mid-channel bar surrounded by the primary channel and secondary channel. In natural conditions, one primary channel and division of secondary channel into two tertiary channels were observed. For the vegetated case, one primary channel and one secondary channel was noticed. It is clear that the lateral growth of vegetated mid-channel bar resulted in arresting channel fragmentation of secondary channel and thus, allowing more flow towards the secondary channel. This allows the secondary channel development and affects the discharge distribution between primary and secondary channels. Figure 6.12 shows the channel bed elevation in primary and secondary channels for natural, 100% vegetation cover, and 50% vegetation cover conditions. This shows in natural conditions primary channel is deeper and secondary channel (divided into two tertiary channel) is shallower due to channel fragmentation. With the increase in vegetation cover, development of secondary channel is observed to be significant, which resulted in more deepening. This is probably due to increased flow diversion resulting from resistance over the sand bar. Also, it is noted that flow towards the secondary channel takes a less curved path and development of in-channel deposition at the mouth of primary channel together with

vegetation roughness may also be another reason contributed for the development of secondary channel.

Table 6.3 shows the discharge distribution in the channels at different seasons in natural, 100%, 50% vegetation cover. It is observed that for natural conditions primary channel carries 70% of the discharge and other 30% is shared between tertiary channels. In low flow season, 85% to primary channel and 15% to other channels. The newly formed tertiary channel over the sandbar carries lesser discharge as compared to the existing channel. In the low flow season (discharge less than 2,500 m^3/s), this channel is observed to be dried up and remains as a trace. With the vegetation cover, the development of the secondary channel results in more discharge flow into the channel. Furthermore, the increase of vegetation cover from 50% to 100% favored equal sharing of discharge between the channels.

In the above sections, it is discussed that the presence of vegetation roughness alters the planform morphology of the river due to changes in flow distribution pattern, sediment accretion over the sand bars. To evaluate the changes in planform morphology, indicators such as braiding intensity and thalweg sinuosity were computed and presented in Table 6.4. For the initial bathymetry conditions, the braiding intensity is high, and thalweg sinuosity is low, which is due to multiple channel fragmentations along the river reach. This is closely similar for the natural conditions simulated with no vegetation cover over the sand bar. With the presence of vegetation cover, the decrease in value of braiding intensity and increase in thalweg sinuosity is noticed. This may be due to (a) vegetation resistance arresting the channel anabranching over the sand bars; (b) flow resistance over the sand bar resulting in more flow diversion into the channels and channel development through erosion of in-channel depositions.

Table 6.3 Discharge distribution in channels at different conditions

S. No	Case 1: Natural Conditions			Full Cover		Half Cover	
	Primary Channel	Tertiary Channel 1	Tertiary Channel 2	Primary Channel	Secondary Channel	Primary Channel	Secondary Channel
A	73%	10%	17%	54%	46%	60%	40%
B	83%	2%	15%	51%	49%	67%	33%
C	85%	0	15%	53%	47%	67%	33%

A: Monsoon Season (12,500 m^3/s); B: Low Season 1 (5,000 m^3/s); C: Low Season 2 (3,000 m^3/s)

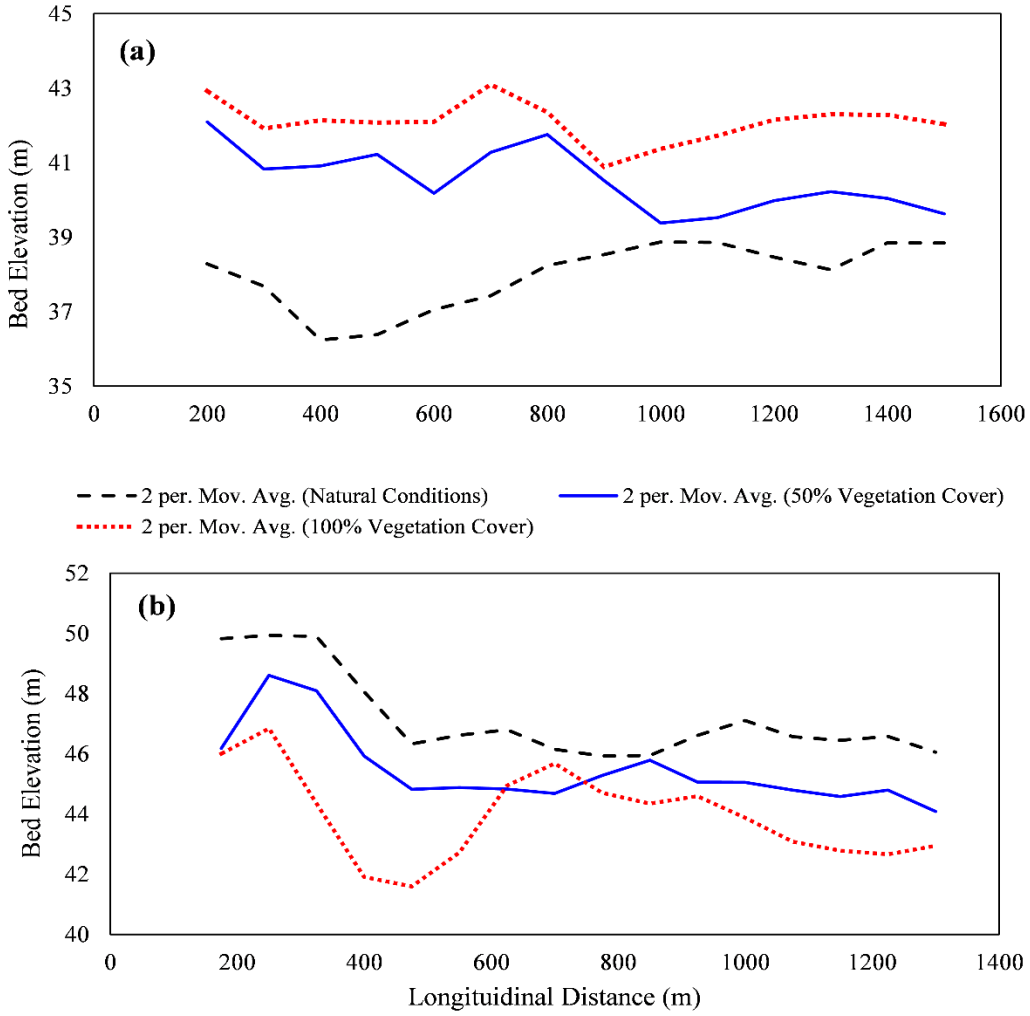

Figure 6.12 Comparison of channel bed elevation in primary and secondary channel for natural, full vegetation cover and half vegetation cover conditions

Table 6.4 Variability in braiding parameters in study area for different conditions

S. No.	Condition	Braiding Intensity	Thalweg Sinuosity
1	Initial Bathymetry	2.7	1.06
2	Natural Conditions	2.4	1.08
3	Full Vegetation Cover	1.64	1.12
4	Half Vegetation Cover	1.66	1.1
5	Downstream Bar, Full Vegetation Cover	1.70	1.1

6.7 CHAPTER SUMMARY

In the present objective, a two-dimensional hydrodynamic and morphological model CCHE2D was simulated to investigate the morphological response of a braided loop subjected to different percentages of a vegetative cover. Vegetation is incorporated in the model as an additional roughness to the flow by varying Manning's roughness coefficient value. The results of the study provided insights in understanding the link between vegetation roughness and braided planform dynamics. The results of the study lead to following observations.

1. Vegetation roughness over the sand bar reduced the flow velocity and increased the sand bar stability. This resulted in arresting the formation of tertiary channels or anabranches over the sand bar.
2. Vegetation roughness increased the flow diversion towards the secondary channels, and helped in channel development and maintaining higher depths. This process is observed to accelerate with increase in percentage of vegetation cover.
3. The presence of vegetation cover decreased the braiding intensity and increased the thalweg sinuosity. This values remain unaffected with percentages of vegetation cover.
4. Vegetation cover improved the discharge sharing between the braided channels. With increase in vegetation cover over the sand bar, discharge sharing of close to 50% between the braided channels is noticeD. This sharing remained closely similar in different seasons.

Thus, the vegetation cover is observed to decrease the planform dynamics. To investigate further, the response of vegetation cover at different locations along the braided river network can be studied. With further improvement in knowledge, vegetation can be tested in field for observing the planform stability and sediment deposition zones.

7

SUMMARY AND FUTURE SCOPE

7.1 SUMMARY

The present research aims to understand the hydrodynamics and morphodynamics of the Brahmaputra River, a large sand bed braided river system. The river is characterized by different levels of micro and macro scale processes generating complex morphological adjustments. This study attempted to investigate river morphological behavior and mechanics by analyzing the hierarchical processes such as energy and morphological adjustments, flow structure-morphology interactions and flow-vegetation interaction mechanisms. For this work, the middle Brahmaputra River reach between Tezpur to Guwahati was considered as a study area. This reach comprises of different zones of flow and morphological variability due to changes in braided belt width and, suits best for studying the river behavior. The following sub-sections are the brief summary of the work done and observations made in the present research.

7.1.1 Entropy Based Morphological Analysis

This objective utilized the concept of intensity entropy to assess the annual variability associated with the distribution of sandbars over the braided planform of the Brahmaputra River. Two indices namely intensity disorder index (*IDI*) and planform disorder index (*PDI*) relating to the variability in sandbars distribution were computed. Indices provided understanding of the time-dependent adjustment of sandbars in the Brahmaputra River. The results of the study lead to the following observations. First, the annual variability in

sandbars arrangement for a braided reach tends to be decreasing. The contribution of medium to large sized bars is increasing with time resulting in less deviation from a uniform sandbar arrangement. For individual zones within the reach, the variability also decreased with time. The changing variability in peak flood magnitudes and the relaxed effect of 1950 Assam earthquake may have caused this change in sandbars adjustments. Second, for the Brahmaputra River, monsoonal stream power is found to be better related to the annual planform disorder index than the peak flood stream power. As the river usually experiences average 9 flood waves of different durations annually, the peak flood alone may not be responsible for planform change. Third, two distinctive trends in stream power variability are found; when decreasing, stream power is well correlated with the planform disorder index. When increasing, adjustments in other morphological parameters such as thalweg shift, bank erosion are dominant rather than sand bar changes. The study presented a new approach to represent planform disorder of a braided river system in terms of sandbars adjustments. The entropy theory can be further explored to study its applications in detail in geomorphic studies.

7.1.2 Flow Structure and Morphological Changes in Hierarchical Channels

In this objective a detailed investigation of flow structure and short-term morphological changes at hierarchical channels with varying width-to-depth ratios in the middle Brahmaputra River, India was carried. Measurements of flow, suspended sediment transport combined with satellite imagery-based analysis are carried to understand the morphological response of a large sand bed braided river. The results of the study lead to the following conclusions.

1. Morphological variables tend to adjust in response to seasonal variability in energy dissipation. In the low flow season, thalweg sinuosity is observed to be dominant with magnitude ~25% higher than monsoon, while sand bars count increased from ~100 in low flow season to ~400 in monsoon season. Neither of the variables dominates in peak flooding period showing the contribution of other morphological parameters to energy dissipation.
2. The cross-section morphology of large channels with high width-to-depth ratios is observed as multi-thread with velocity core position depending on channel geometry. Planform curvature in these channels is significant in generating secondary helical cells overcoming the effect of bedforms.

3. In channels with width-to-depth ratio <100, the cross-section is a single thread with maximum velocity core at mid-section. The generation of secondary helical cells at meander and confluence sections are similar to those observed in other smaller rivers.
4. Short-term morphological changes are very prominent in the Brahmaputra River. The influence of upstream morphological changes coupled with local flow structure favored a significant change in planform and cross-section morphology. Further, at channels of w/d < 100, the order of upstream changes is much higher to influence the cross-section morphology irrespective of flow structure.
5. Higher concentrations of suspended sediment are noticed at specific locations influenced by local flow features such as the angle of attack, helical cells, and active sediment transport zones. Other sections are closely prone to lower sediment concentration ranging between 100 to 400 mg/L.

7.1.3 Flow Characteristics in Heterogeneous Vegetation Patches

This objective presents an analysis of laboratory experiments conducted to investigate the effect of submerged heterogeneous vegetation patches on flow structure. For this purpose three natural plant forms (grass, leafy and cylindrical) arranged in four different layouts, namely homogeneous flexible grass, mixed heterogeneous patch, heterogeneous patch 1 and patch 2 are studied. The results of the study provided insights in understanding the effect of heterogeneous characteristics such as plant morphology, canopy porosity and patch alignment on flow behavior.

The major observations in the study lead to the following conclusions. First, in the mixed heterogeneous patch, the additional drag due to the presence of other vegetation forms like leafy and cylindrical stems results in 10% increased velocity reduction than homogeneous flexible grass alone. In addition, there was no local depression in peak Reynold stress (at z/H ~ 0.54) into the canopy as observed for flexible grass vegetation (at z/H~0.45). Second, in heterogeneous patch 1 and patch 2, different zones of increased and diminished turbulence levels, varying velocities were observed along the vegetated section. Plant form and the canopy porosity has significant control on altering the position and intensity of the vertical momentum exchange at the canopy top and also, thickness of the active momentum exchange. For example, in the leafy patch (of heterogeneous patch 1), the amount of mixing activity was 50% lesser than other vegetation forms. Third, other

than plant form and canopy porosity, patch alignment has also controlled the flow structure by inducing additional turbulence to the flow. In heterogeneous patch 2, the flow instability aroused due to both longitudinal and cross-stream variability of patch forms resulted in increase of turbulence parameters to more than 100% than heterogeneous patch 1. The response of Manning's n was highly affected by plant form and patch alignment for different flow conditions.

7.1.4 Morphological Response of Vegetated Braided Loop

This objective utilizes a two-dimensional hydrodynamic and morphological model CCHE2D to investigate the morphological response of a braided loop subjected to different percentages of a vegetative cover. Vegetation is incorporated in the model as an additional roughness to the flow by varying Manning's roughness coefficient value. The results of the study provided insights in understanding the link between vegetation roughness and braided planform dynamics. The results of the study lead to following observations

1. Vegetation roughness over the sand bar reduced the flow velocity and increased the sand bar stability. This resulted in arresting the formation of tertiary channels or anabranches over the sand bar.
2. Vegetation roughness increased the flow diversion towards the secondary channels, and helped in channel development and maintaining higher flow depths. This process is observed to accelerate with increase in percentage of vegetation cover.
3. The presence of vegetation cover decreased the braiding intensity and increased the thalweg sinuosity. This values remain unaffected with percentages of vegetation cover.
4. Vegetation cover improved the discharge sharing between the braided channels. With increase in vegetation cover over the sand bar, discharge sharing of close to 50% between the braided channels is noticed. This sharing remained closely similar in different seasons.

7.2 FUTURE SCOPE

The present research has provided better insights to understand the hydrodynamic and morphological condition of the Brahmaputra River. However, there are many other important aspects to be looked in detail for process-form based understanding of this river. The present work can be extended further with prime focus to following aspects

- Entropy based morphological analysis can be extended to upper and lower Brahmaputra River reaches to investigate the morphological condition of the river.
- Analysing the ADCP survey data at river bifurcations of varying discharge, width-to-depth ratios can improve our understanding on channel bifurcation development.
- Detailed ADCP river survey across highly active morphological reach can help to relook and/or modify the specific energy and width-to-depth relation established for lower Brahmaputra River.
- Parametric study on heterogeneous vegetation patches with detailed lateral and longitudinal measurements can help to justify more detailed mechanism of turbulence generation due to plant patch heterogeneity.
- Interlinking of flow-vegetation-turbulence interactions to fish behaviour can be helpful for management of ecological zones of the Brahmaputra River.

APPENDIX A

PUBLICATIONS

A.1 PUBLISHED

Chembolu, V., & Dutta, S. (2018). An entropy based morphological variability assessment of a large braided river. *Earth Surface Processes and Landforms*, *43*(14), 2889-2896.

A.2 MINOR REVISION

Chembolu, V., Kakati, R., & Dutta, S. (2019). A laboratory investigation of flow characteristics in natural heterogeneous vegetation patches under submerged conditions. *Advances in Water Resources*.

A.3 UNDER REVIEW

Chembolu, V., & Dutta, S. Influence of high energy macro-turbulent structures on navigational hazards in the Brahmaputra River. *National Academy of Science Letters.*

Chembolu, V., Akkimi, A., & Dutta, S. Bathymetry methods- A review. *Geomorphological Techniques*.

Chembolu, V., & Dutta, S. Flow structure and associated morphological changes in hierarchical channels of a large braided river. *Journal of Geomorphology*

A.4 UNDER PREPARATION

Chembolu, V., & Dutta, S. Morphological response of a braided loop subjected to different percentages of vegetation cover.

A.5 CONFERENCES

Chembolu, V., & Dutta, S. (2015). Entropy and energy dissipation of a braided river system. 12th International Conference on Vibrational Problems, Indian Institute of Technology Guwahati, 14-17 Dec., 2015.

Chembolu, V., & Dutta, S. (2017). Hydrodynamic and morphological understanding of the Brahmaputra River, India: Challenges and Experiences. 13th International Conference on Vibrational Problems, Indian Institute of Technology Guwahati, 29 Nov.-2 Dec., 2017.

Chembolu, V., & Dutta, S. (2019). Flow structure in natural heterogeneous vegetation patches. Research Conclave, 2019, Indian Institute of Technology Guwahati, 14-17 Mar., 2019.

APPENDIX B

ONE DIMENSIONAL MODELING

B.1 HEC-RIVER ANALYSIS SYSTEM

HEC-RAS is a one dimensional hydrodynamic and morphological model allows user to perform one dimensional steady, unsteady flow analysis, movable sediment transport and water quality analysis. This section discusses the mathematical equations used in performing steady and unsteady flow calculations in HEC-RAS.

B.1.1 Steady Flow Analysis

Energy equation is used in HEC-RAS for computing the water surface profiles from one cross section to another. The equation is

$$Z_2+Y_2+\alpha V_2^2/2g=Z_1+Y_1+\alpha V_1^2/2g+h_L$$

Z_1, Z_2 = elevation of main channel inverts

Y_1, Y_2 = depth of water at cross sections

V_1, V_2 = average velocities

h_L= energy head loss and α_1 α_2 = weighted velocity coefficients

B.1.2 Unsteady Flow Analysis

In HEC-RAS, unsteady flow equations are expressed in terms of set of partial differential equations to solve the water flow in the open channel govern by gravity. The governing equations i.e. continuity equation and momentum equations are listed below.

$$\frac{\partial A}{\partial t}+\frac{\partial Q}{\partial x}+q_l = 0$$

$$\frac{\partial Q}{\partial t}+\frac{\partial QV}{\partial x}+gA\left(\frac{\partial Z}{\partial x}+S_f\right)=0$$

Where,

A is total flow area

q_l is lateral flow per unit length

S_f is friction slope

These equations are approximated using implicit finite difference scheme and are solved with necessary boundary conditions. Flow hydrograph is provided as upstream boundary condition and stage hydrograph, normal depth or rating curve can be provided as downstream boundary conditions.

The details on working with HEC-RAS is discussed in detail on http://www.hec.usace.army.mil/software/hec-ras.

APPENDIX C

TWO DIMENSIONAL MODELING

C.1 CCHE2D HYDRODYNAMIC AND MORPHOLOGICAL MODEL

CCHE 2D is a finite element based depth integrated two dimensional hydrodynamic and morphological model used for steady and unsteady flow and sediment transport simulations developed at National Centre for Computational Hydro science and Engineering. CCHE2D numerical model consists of two parts. CCHE 2D Mesh Generator for generating computational mesh and CCHE2D GUI for setting of flow and sediment requirements and to run simulations. In this appendix the governing equations for flow and sediment transport analysis are discussed.

C.1.1 Governing Equations

Hydrodynamic Model

The two dimensional depth integrated continuity and momentum equations used in the model are

Continuity equation

$$\frac{\partial Z}{\partial t}+\frac{\partial (uh)}{\partial x}+\frac{\partial (vh)}{\partial y}=0$$

Momentum equation

$$\frac{\partial u}{\partial t}+u\frac{\partial u}{\partial x}+v\frac{\partial u}{\partial y}=-g\frac{\partial Z}{\partial x}+\frac{1}{h}\left(\frac{\partial \tau_{xx}}{\partial x}+\frac{\partial \tau_{xy}}{\partial y}\right)-\frac{\tau_{bx}}{\rho h}+f_{cor}v$$

$$\frac{\partial v}{\partial t}+u\frac{\partial v}{\partial x}+v\frac{\partial v}{\partial y}=-g\frac{\partial Z}{\partial y}+\frac{1}{h}\left(\frac{\partial \tau_{yx}}{\partial x}+\frac{\partial \tau_{yy}}{\partial y}\right)-\frac{\tau_{bx}}{\rho h}+f_{cor}u$$

Where

u, v are depth integrated velocities along x and y directions

Z is water surface elevation

g is acceleration due to gravity

h is local water depth

f_{cor} is coriolis parameter

$\tau_{xx},\tau_{xy},\tau_{yx},\tau_{yy}$ are depth integrated Reynolds stresses.

τ_{bx},τ_{by} are shear stresses acting on bed.

Morphological Model

Three approaches are adopted in CCHE 2D for sediment transport modeling. They are total load as bed load, total load as suspended load, total load as bed load plus sediment load.

Bed load type model

The bed load type model is used to simulate bed load only or bed material load without considering the diffusion of suspended load. The governing equation of bed load transport is

$$\frac{\partial(\propto_{bx} q_{bk})}{\partial x}+\frac{\partial(\propto_{by} q_{bk})}{\partial y}+\frac{1}{L_b}\left(q_{bk}-q_{b*k}\right)=0$$

Where $\propto_{bx}, \propto_{by}$ are direction-cosines of bed load transport and q_{bk}, q_{b*k} are the actual transport rate and transport capacity of k_{th} size class of bed load

The bed deformation is determined by

$$(1-p^{I})\frac{\partial(z_{bk})}{\partial t}=\frac{1}{L_b}\left(q_{bk}-q_{b*k}\right)$$

Where L_b is the adaptation length for bed load and p^I is the porosity of bed material

Suspended load type model

The governing convection diffusion equation of bed material load transport is

$$\frac{\partial(hC_{tk})}{\partial t}+\frac{\partial(UhC_{tk})}{\partial x}+\frac{\partial(VhC_{tk})}{\partial y}=\frac{\partial}{\partial x}\left(\epsilon_s h\frac{\partial C_{tk}}{\partial x}\right)+\frac{\partial}{\partial y}\left(\epsilon_s h\frac{\partial C_{tk}}{\partial y}\right)+\alpha\omega_{sk}(C_{tk}-C_{t*k})$$

Where h is flow depth

U and V are depth averaged flow velocities

ω_{sk} is settling velocity

ϵ_s is eddy diffusivity of sediment.

The bed deformation can be determined by sediment continuity equation.

Bed load plus Suspended load type model

The bed load and suspended load are calculated separately, so more information can be provided in this approach. In this method bed material load formulas cannot be used unlike in approaches 1 and 2.

The details on working with CCHE 2D can be found in http://www.ncche.olemiss.edu/

REFERENCES

- Abt S, Clary W, Thornton C. 1994. Sediment deposition and entrapment in vegetated streambeds. Journal of Irrigation Drainage Engineering. 120(6), 1098-1111.
- Akhtar MP, Sharma N, Ojha, CSP. 2011. Braiding process and bank erosion in the Brahmaputra River. International Journal of Sediment Research 26(4): 431-444.
- Alam JB, Uddin M, Ahmed JU, Cacovean H, Rahman H M, Banik BK, Yesmin N. 2007. Study of morphological change of river old Brahmaputra and its social impacts by remote sensing. Geographia Technica 2: 1-11.
- Ashmore PE. 1991. How do gravel-bed rivers braid?. Canadian journal of earth sciences, 28(3), 326-341.
- Ashmore P. 2013. Morphology and dynamics of braided rivers. 289-312.
- Ashworth PJ, Best JL, Roden JE, Bristow CS, Klaassen GJ. 2000. Morphological evolution and dynamics of a large, sand braid-bar, Jamuna River, Bangladesh. Sedimentology 47(3): 533-555.
- Ashworth PJ, Lewin J. 2012. How do big rivers come to be different?. Earth-Science Reviews 114(1-2): 84-107.
- Bagnold RA. 1966. An approach to the sediment transport problem from general physics. US government printing office.
- Baki ABM, Gan TY. 2012. Riverbank migration and island dynamics of the braided Jamuna River of the Ganges–Brahmaputra basin using multi-temporal Landsat images. Quaternary International 263: 148-161.
- Bandyopadhyay S, Sinha S, Jana NC, Ghosh D. 2014. Entropy application to evaluate the stability of landscape in Kunur River Basin, West Bengal, India. Current Science: 1842-1853.
- Barker DM, Lawler DM, Knight DW, Morris DG, Davies HN, Stewart EJ. 2009. Longitudinal distributions of river flood power: the combined automated flood, elevation and stream power (CAFES) methodology. Earth Surface Processes and Landforms 34(2): 280-290.
- Baptist M. 2003. A flume experiment on sediment transport with flexible, submerged vegetation. In: Proceeedings of the International workshop on riparian forest vegetated channels: hydraulic, morphological and ecological aspects. Trento, Italy.
- Bawa N, Jain V, Shekhar S, Kumar N, Jyani V. 2014. Controls on morphological variability and role of stream power distribution pattern, Yamuna River, western India. Geomorphology 227: 60-72.
- Bennett S, Simon A. 2004. Riparian vegetation and fluvial geomorphology (Vol. 8). American Geophysical Union.

- Bennett S, Pirim T, Barkdoll B. 2002. Using simulated emergent vegetation to alter stream flow direction within a straight experimental channel. Geomorphology, 44(1-2), 115-126.
- Bertoldi, W., & Tubino, M. (2007). River bifurcations: Experimental observations on equilibrium configurations. Water Resources Research, 43(10).
- Bertoldi W, Zanoni L, Tubino M. 2009. Planform dynamics of braided streams. Earth Surface Processes and Landforms, 34(4), 547-557.
- Bertoldi W, Drake N, Gurnell A. 2011. Interactions between river flows and colonizing vegetation on a braided river: exploring spatial and temporal dynamics in riparian vegetation cover using satellite data. Earth Surface Processes and Landforms, 36(11), 1474-1486.
- Bertoldi W, Welber M, Gurnell AM, Mao L, Comiti F, Tal M. 2015. Physical modelling of the combined effect of vegetation and wood on river morphology. Geomorphology, 246, 178-187.
- Best JL. 1988. Sediment transport and bed morphology at river channel confluences. Sedimentology, 35(3), 481-498.
- Best JL, Roy AG. 1991. Mixing-layer distortion at the confluence of channels of different depth. Nature, 350(6317), 411.
- Best JL, Ashworth PJ, Bristow CS, Roden J. 2003. Three-dimensional sedimentary architecture of a large, mid-channel sand braid bar, Jamuna River, Bangladesh. Journal of Sedimentary Research, 73(4), 516-530.
- Best JL, Ashworth PJ, Sarker MH, Roden JE. 2007. The Brahmaputra-Jamuna River, Bangladesh. Large rivers: geomorphology and management, 395-430.
- Bhakal L, Dubey B, Sarma AK. 2005. Estimation of bank erosion in the river Brahmaputra near Agyathuri by using geographic information system. Journal of the Indian Society of Remote Sensing, 33(1), 81-84.
- Bhattacharjya BK, Bhaumik U, Sharma AP. 2017. Fish habitat and fisheries of Brahmaputra River in Assam, India. Aquatic Ecosystem Health and Management, 20(1-2), 102-115.
- Biron P, Roy A, Best JL, Boyer CJ. 1993. Bed morphology and sedimentology at the confluence of unequal depth channels. Geomorphology, 8(2-3), 115-129.
- Bizzi S, Lerner DN. 2012. Characterizing physical habitats in rivers using map-derived drivers of fluvial geomorphic processes. Geomorphology 169: 64-73.
- Bizzi S, Lerner DN. 2015. The use of stream power as an indicator of channel sensitivity to erosion and deposition processes. River research and applications 31(1): 16-27.
- Board B. 2012. Protection of Majuli Island from Floods and erosion. Guwahati, May.
- Bolla Pittaluga M, Repetto R, Tubino M. 2003. Channel bifurcation in braided rivers: Equilibrium configurations and stability. Water Resources Research, 39(3).
- Bornette G, Puijalon S. 2011. Response of aquatic plants to abiotic factors: a review. Aquatic Sciences, 73(1), 1-14.
- Brachet C, Magnier J, Valensuela D, Petit K, Fribourg B, Bernex N, Tarlock D. 2015. The handbook for management and restoration of aquatic ecosystems in river and lake basin.
- Bradbrook KF, Lane SN, Richards KS, Biron PM, Roy AG. 2001. Role of bed discordance at asymmetrical river confluences. Journal of Hydraulic Engineering, 127(5), 351-368.

- Bridge JS. 1993. The interaction between channel geometry, water flow, sediment transport and deposition in braided rivers. Geological Society, London, Special Publications 75(1): 13-71.
- Bristow CS, Best JL. 1993. Braided rivers: perspectives and problems. Geological Society, London, Special Publications 75(1): 1-11.
- Brunner GW. 1995. HEC-RAS River Analysis System. Hydraulic User's Manual. Version 1.0. Hydrologic Engineering Center Davis CA.
- Brunsell NA. 2010. A multiscale information theory approach to assess spatial–temporal variability of daily precipitation. Journal of Hydrology 385(1): 165-172.
- Coulthard TJ, Wiel, MJVD. 2006. A cellular model of river meandering. Earth Surface Processes and Landforms: The Journal of the British Geomorphological Research Group, 31(1), 123-132.
- Charlton R. 2007. Fundamentals of fluvial geomorphology. Chapter 9: Pg.159. Routledge.
- Chembolu V, Dutta S. 2018. An entropy based morphological variability assessment of a large braided river. Earth Surface Processes and Landforms, 43(14), 2889-2896.
- Chembolu V, Pradhan C, Dutta S. 2016. Mathematical Modeling Studies for Brahmani Delta Network from Talcher to Mangalgadi for Development of Inland Water Transport in the Proposed National Waterway-5, Odisha. Inland Waterway Authority of India.
- Chen C. 1976. Flow resistance in broad shallow grassed channels. Journal of Hydraulic Division, 102(3), 307-322.
- Chen S, Kuo Y, Li Y. 2011. Flow characteristics within different configurations of submerged flexible vegetation. Journal of Hydrology, 398(1-2), 124-134.
- Chen YC, Wei C, Yeh HC. 2008. Rainfall network design using kriging and entropy. Hydrological Processes 22(3): 340.
- Claps P, Fiorentino M, Oliveto G. 1996. Informational entropy of fractal river networks. Journal of Hydrology 187(1-2): 145-156.
- Claude N, Rodrigues S, Bustillo V, Bréhéret JG, Tassi P, Jugé P. 2014. Interactions between flow structure and morphodynamic of bars in a channel expansion/contraction, Loire River, France. Water Resources Research, 50(4), 2850-2873.
- Coleman JM. 1969. Brahmaputra River: channel processes and sedimentation. Sedimentary Geology 3(2-3), 129-239.
- Costa JE, O'Connor JE. 1995. Geomorphically effective floods. Natural and anthropogenic influences in fluvial geomorphology 45-56.
- Curran J, Hession W. 2013. Vegetative impacts on hydraulics and sediment processes across the fluvial system. Journal of Hydrology, 505, 364-376.
- Davoren A, Mosley MP. 1986. Observations of bedload movement, bar development and sediment supply in the braided Ohau River. Earth Surface Processes and Landforms, 11(6), 643-652.
- Deines KL. 1999. Backscatter estimation using broadband acoustic Doppler current profilers. In Proceedings of the IEEE Sixth Working Conference on Current Measurement (Cat. No. 99CH36331) (pp. 249-253). IEEE.
- Deshpande V, Kumar B. 2016. Turbulent flow structures in alluvial channels with curved cross-sections under conditions of downward seepage. Earth Surface Processes and Landforms, 41(8), 1073-1087.
- Devi, T. (2016). Hydrodynamics of vegetative channel with downward seepage (Doctoral dissertation).

- Devi T, Kumar B. 2015. Turbulent flow statistics of vegetative channel with seepage. Journal of Applied Geophysics 123, 267-276.
- Devi T, Kumar B. 2016. Channel hydrodynamics of submerged, flexible vegetation with seepage. Journal of Hydraulic Engineering, 142(11).
- Devi T, Kumar B. 2016. Experimentation on submerged flow over flexible vegetation patches with downward seepage. Ecological Engineering, 91, 158-168.
- Devi T, Daga R, Mahto S, Kumar B. 2016. Drag and Turbulent Characteristics of Mobile Bed Channel with Mixed Vegetation Densities under Downward Seepage. Journal of Fluids Engineering, 138(7).
- Dijkstra J, RE, U. 2010. Modeling the interaction between flow and highly flexible aquatic vegetation. Water Resources Research, 46, W12547.
- Dosskey M, Vidon P, Gurwick N, Allan C, Duval T, Lowrance R. 2010. The role of riparian vegetation in protecting and improving chemical water quality in streams. JAWRA Journal of the American Water Resources Association, 46(2), 261-277.
- Dhar ON, Nandargi S. 2000. A study of floods in the Brahmaputra basin in India. International Journal of Climatology, 20(7), 771-781.
- Dubey AK. 2016. Dynamics of braided river morphology using advanced geo-spatial technology and modeling techniques. PhD Thesis. Indian Institute of Technology Guwahati.
- Errico A, Pasquino V, Maxwald M, Chirico G, Solari L, Preti F. 2018. The effect of flexible vegetation on flow in drainage channels: Estimation of roughness coefficients at the real scale. Ecological Engineering, 120, 411-421.
- Federici B, Paola C. 2003. Dynamics of channel bifurcations in noncohesive sediments. Water Resources Research, 39(6).
- Ferguson RI. 1993. Understanding braiding processes in gravel-bed rivers: progress and unsolved problems. Geological Society, London, Special Publications 75(1): 73-87.
- Ferguson RI, Ashmore PE, Ashworth PJ, Paola C, Prestegaard KL. 1992. Measurements in a braided river chute and lobe: 1. Flow pattern, sediment transport, and channel change. Water Resources Research, 28(7), 1877-1886.
- Fiorentino M, Claps P, Singh VP. 1993. An entropy-based morphological analysis of river basin networks. Water Resources Research 29(4): 1215-1224.
- Follett EM, Nepf HM. 2012. Sediment patterns near a model patch of reedy emergent vegetation. Geomorphology, 179, 141-151.
- Ghisalberti M, Nepf H. 2002. Mixing layers and coherent structures in vegetated aquatic flows. Journal of Geophysics Research, Oceans, 107(C2).
- Gilfellon GB, Sarma, JN, Gohain K. 2003. Channel and bed morphology of a part of the Brahmaputra River in Assam. Journal Geological Society of India 62(2): 227-236.
- Gilvear DJ 1993. River management and conservation issues on formerly braided river systems; the case of the River Tay, Scotland. Geological Society, London, Special Publications 75(1): 231-240.
- Goring D, Nikora V. 2002. Despiking Acoustic Doppler Velocimeter Data. Journal of Hydraulic Engineering, 128(1), 117-126.

- Goswami DC. 1985. Brahmaputra River, Assam, India: Physiography, basin denudation, and channel aggradation. Water Resources Research 21(7): 959-978.
- Gran K, Paola C. 2001. Riparian vegetation controls on braided stream dynamics. Water Resources Research, 37(12), 3275-3283.
- Guo-bin XU, Ted YC. 2012. Analysis of river bed changes based on the theories of minimum entropy production dissipative structure and chaos [J]. Journal of Hydraulic Engineering, 8: 011.
- Guo-bin X, Lina Z. 2013. Analysis of fluvial process based on information entropy. Journal of Tianjin University 4: 011.
- Gurbisz C, Kemp WM, Sanford LP, Orth RJ. 2016. Mechanisms of Storm-Related Loss and Resilience in a Large Submersed Plant Bed. Estuaries and Coasts.
- Gurbisz C, Kemp WM, Cornwell JC, Sanford LP, Owens MS, Hinkle DC. 2017. Interactive Effects of Physical and Biogeochemical Feedback Processes in a Large Submersed Plant Bed. Estuaries and Coasts, 40(6), 1626–1641.
- Gurnell A. 2014. Plants as river system engineers. Earth Surfaces Processes and Landforms, 39(1), 4-25.
- Graf WL. 1981. Channel instability in a braided, sand bed river. Water Resources Research, 17(4), 1087-1094.
- Gran K, Paola C. 2001. Riparian vegetation controls on braided stream dynamics. Water Resources Research, 37(12), 3275-3283.
- Hackney CR, Darby SE, Parsons DR, Leyland J, Aalto R, Nicholas AP, Best, JL. 2018. The influence of flow discharge variations on the morphodynamics of a diffluence–confluence unit on a large river. Earth Surface Processes and Landforms, 43(2), 349-362.
- Harms JC, Fahnestock RK. 1965. Primary sedimentary structures and their hydrodynamic interpretation. Soc. Econ. Paleontol. Mineral., Spec. Publ., 12, 84-115.
- Hockley FA. Wilson CAME, Brew A, Cable J. 2014. Fish responses to flow velocity and turbulence in relation to size, sex and parasite load. Journal of Royal Society International, 11(91), 20130814.
- Huai X, Zeng YH, Xu ZG, Yang ZH. 2009a. Three-layer model for vertical velocity distribution in open channel flow with submerged rigid vegetation. Advances in Water Resources. 32(4), 487-492.
- Jain V, Preston N, Fryirs K, Brierley G. 2006. Comparative assessment of three approaches for deriving stream power plots along long profiles in the upper Hunter River catchment, New South Wales, Australia. Geomorphology 74(1): 297-317.
- Järvelä J. 2002. Flow resistance of flexible and stiff vegetation: a flume study with natural plants. Journal of Hydrology, 269(1-2), 44-54.
- Järvelä J. 2005. Effect of submerged flexible vegetation on flow structure and resistance. Journal of hydrology, 307(1-4), 233-241.
- Jordanova A, James C. 2003. Experimental study of bed load transport through emergent vegetation. Journal of Hydraulic Engineering, 129(6), 474-478.
- Kale VS. 2008. A half-a-century record of annual energy expenditure and geomorphic effectiveness of the monsoon-fed Narmada River, central India. Catena 75(2): 154-163.
- Karmaker T, Dutta S. 2010. Generation of synthetic seasonal hydrographs for a large river basin. Journal of hydrology 381(3): 287-296.

- Karmaker T, Dutta S. 2011. Erodibility of fine soil from the composite river bank of Brahmaputra in India. Hydrological Processes 25(1): 104-111.
- Karmaker T, Dutta S. 2013. Modeling seepage erosion and bank retreat in a composite river bank. Journal of hydrology 476: 178-187.
- Karmaker T, Dutta S. 2015. Stochastic erosion of composite banks in alluvial river bends. Hydrological processes 29(6): 1324-1339.
- Karmaker T, Medhi H, Dutta S. 2017. Study of channel instability in the braided Brahmaputra river using satellite imagery. Current Science (00113891), 112(7).
- Karmaker T, Ramprasad Y, Dutta S. 2010. Sediment transport in an active erodible channel bend of Brahmaputra river. Sadhana, 35(6), 693.
- Khan NI, Islam A. 2003. Quantification of erosion patterns in the Brahmaputra–Jamuna River using geographical information system and remote sensing techniques. Hydrological Processes 17(5): 959-966.
- Kim HS, Kimura I, Shimizu Y. 2015. Bed morphological changes around a finite patch of vegetation. Earth Surface Processes and Landforms, 40(3), 375-388.
- Kim H, Nabi M, Kimura I, Shimizu Y. 2015. Computational modeling of flow and morphodynamics through rigid-emergent vegetation. Advances in Water Resources, 84, 64-86.
- King A, Tinoco R, Cowen E. 2012. A k–ε turbulence model based on the scales of vertical shear and stem wakes valid for emergent and submerged vegetated flows. Journal of Fluid Mechanics, 701, 1-39.
- Klopstra D, Barneveld HJ, Van Noortwijk JM, Van Velzen EH. 1996. Analytical model for hydraulic roughness of submerged vegetation. The 27th Congress of the International Association for Hydraulic Research: Proceedings of Theme A, Managing Water: Coping with Scarcity and Abundance. ASCE New York, pp.775-780
- Klaassen GJ, Mosselman E, Bruhl H. 1993. On the prediction of planform changes of braided sand-bed rivers.
- Klaassen GJ, Mosselman E, Bruhl H. 1993. On the prediction of planform changes of braided sand-bed rivers. In Advances in Hydro-Science and Engineering, Wang SSY (ed). Publication of the University of Mississippi: University, MS; 134–146
- Kondolf G, Podolak K, Grantham T. 2013. Restoring Mediterranean Climate Rivers. Hydrobiologia, 719(1), 527–545.
- Kothyari U, Hashimoto H, Hayashi K. 2009. Effect of tall vegetation on sediment transport by channel flows. Journal of Hydraulic Research, 47(6), 700-710.
- Kouwen N. 1992. Modern approach to design of grassed channels. Journal of Irrigation Drainage Engineering, 118(5), 733-743.
- Lahiri SK, Sinha R. 2014. Morphotectonic evolution of the Majuli Island in the Brahmaputra valley of Assam, India inferred from geomorphic and geophysical analysis. Geomorphology 227: 101-111.
- Lane SN, Bradbrook KF, Richards KS, Biron PM, Roy AG. 2000. Secondary circulation cells in river channel confluences: measurement artefacts or coherent flow structures?. Hydrological Processes, 14(11-12), 2047-2071.
- Leopold LB, Wolman MG. 1957. River channel patterns: braided, meandering, and straight. US Government Printing Office.
- Leopold LB, Langbein WB. 1962. The concept of entropy in landscape evolution.

- Lera S, Nardin W, Sanford L, Palinkas C, Guercio R. 2019. The impact of submersed aquatic vegetation on the development of river mouth bars. Earth Surface Processes and Landforms, 44(7).
- LG L. JW H. 2010. How vegetation and sediment transport feedbacks drive landscape change in the everglades and wetlands worldwide. The American Naturalis.
- Li Y, Wang Y, Anim D, Tang C, Du W, Ni L, Acharya K. 2014. Flow characteristics in different densities of submerged flexible vegetation from an open-channel flume study of artificial plants. Geomorphology, 204, 314-324.
- Liu D, Diplas P, Fairbanks J, Hodges C. 2008. An experimental study of flow through rigid vegetation. Journal of Geophysical Research: Earth Surface, 113(F4).
- Lick W. 2008. Sediment and contaminant transport in surface waters. CRC press.
- Liu C, Nepf H. 2016. Sediment deposition within and around a finite patch of model vegetation over a range of channel velocity. Water Resources Research, 52(1), 600-612.
- Liu B, Chen X, Lian Y, Wu L. 2013. Entropy-based assessment and zoning of rainfall distribution. Journal of Hydrology 490: 32-40.
- Liu C, Nepf H. 2016. Sediment deposition within and around a finite patch of model vegetation over a range of channel velocity. Water Resources Research, 52(1), 600-612.
- López F, García M. 1998. Open-channel flow through simulated vegetation: Suspended sediment transport modeling. Water Resources Research, 34(9), 2341-2352.
- López, F, García M. 2001. Mean flow and turbulence structure of open-channel flow through non-emergent vegetation. Journal of Hydraulic Engineering, 127(5), 392-402.
- Magilligan FJ, Buraas EM, Renshaw CE. 2015. The efficacy of stream power and flow duration on geomorphic responses to catastrophic flooding. Geomorphology 228: 175-188.
- Maruyama T, Kawachi T, Singh VP. 2005. Entropy-based assessment and clustering of potential water resources availability. Journal of Hydrology 309(1): 104-113.
- Marjoribanks T, Hardy R, Lane S, Parsons R. 2014. High-resolution numerical modelling of flow-vegetation interactions. Journal of Hydraulic Research, 52 (6), 775-793.
- Matthes GH. 1947. Macro-turbulence in natural stream flow, Eos Trans. AGU, 28, 255-262.
- McLelland SJ, Ashworth PJ, Best JL. 1996. The Origin and Downstream Development of Coherent Flow. Coherent flow structures in open channels, 459.
- Mirauda D, De Vincenzo A, Pannone M. 2017. Statistical characterization of flow field structure in evolving braided gravel beds. Spatial Statistics.
- Mishra AK, Özger M, Singh VP. 2009. An entropy-based investigation into the variability of precipitation. Journal of Hydrology 370(1): 139-154.
- Mosley MP. 1976. An experimental study of channel confluences. The journal of geology, 84(5), 535-562.
- Mosselman E, Huisink M, Koomen E, Seijmonsbergen AC. 1995. Morphological changes in a large braided sand-bed river.
- Mosselman E. 1995. Morphological changes in a large braided sand-bed river. River geomorphology.
- Mueller DS. 2018. Assessment of acoustic Doppler current profiler heading errors on water velocity and discharge measurements. Flow Measurement and Instrumentation, 64, 224-233.

- Mueller DS, Wagner CR, Rehmel MS, Oberg KA, Rainville F. 2009. Measuring discharge with acoustic Doppler current profilers from a moving boat (p. 72). Reston, Virginia (EUA): US Department of the Interior, US Geological Survey.

- Murray AB, Paola C. 2003. Modelling the effect of vegetation on channel pattern in bedload rivers. Earth Surface Processes and Landforms: The Journal of the British Geomorphological Research Group, 28(2), 131-143.

- Nardin W, Larsen L, Fagherazzi S, Wiberg P. 2018. Tradeoffs among hydrodynamics, sediment fluxes and vegetation community in the Virginia Coast Reserve, USA. Estuarine, Coastal and Shelf Science, 210, 98-108.

- Nepf H. 1999. Drag, turbulence, and diffusion in flow through emergent vegetation. Water Resources Research, 35(2), 479-489.

- Nepf H. 2012. Flow and transport in regions with aquatic vegetation. Annual Review of Fluid Mechanics, 44, 123-142.

- Nepf H, Ghisalberti M. 2008. Flow and transport in channels with submerged vegetation. Acta Geophysica, 56(3), 753-777.

- Nepf H, Vivoni E. 2000. Flow structure in depth-limited, vegetated flow. Journal of Geophysical. Research: Oceans, 105(C12), 28547-28557.

- Nezu I, Sanjou M. 2008. Turbulence structure and coherent motion in vegetated canopy open-channel flows. Journal of Hydro-environment Research, 2(2), 62-90.

- Noarayanan L, Murali K, Sundar V. 2012. Manning's 'n' co-efficient for flexible emergent vegetation in tandem configuration. Journal of Hydro-Environment Research, 6(1), 51-62.

- Nicholas AP. 2003. Investigation of spatially distributed braided river flows using a two-dimensional hydraulic model. Earth Surface Processes and Landforms: The Journal of the British Geomorphological Research Group, 28(6), 655-674.

- Nicholas AP, Thomas R, Quine TA. 2006. Cellular modelling of braided river form and process. In Smith S, GH, Best, J, Bristow, Petts C, GE (Eds.) Braided Rivers, Blackwell: 136-150.

- Nicholas AP, Ashworth PJ, Sambrook Smith GH, Sandbach SD. 2013. Numerical simulation of bar and island morphodynamics in anabranching megarivers. Journal of Geophysical Research: Earth Surface, 118(4): 2019-2044.

- Nield JM. 2006. Equilibrium morphological modelling in coastal and river environments: the development and application of self-organization and entropy-based techniques (Doctoral dissertation).

- Ortiz AC, Ashton A, Nepf H. 2013. Mean and turbulent velocity fields near rigid and flexible plants and the implications for deposition. Journal of Geophysical Research: Earth Surface, 118(4), 2585-2599.

- Orth RJ, Dennison WC, Lefcheck JS, Gurbisz C. 2014. Optimum vegetation height and density for inorganic sedimentation in deltaic marshes. Nature Geoscience.

- Orth RJ, Dennison WC, Lefcheck JS, Gurbisz C. 2017. Submersed aquatic vegetation in chesapeake bay: Sentinel species in a changing world. Bio Science, 698-712.

- Öztürk M, Work P. 2016. Acoustic doppler velocimeter backscatter for quantification of suspended sediment concentration in South San Francisco Bay. Coastal Engineering Proceedings, 1(35), 34.

- Paola C. 1996. Incoherent structure: turbulence as a metaphor for stream braiding. Coherent flow structures in open channels 65: 705-723.

- Paola C. 2001. Modelling stream braiding over a range of scales. In Gravel Bed Rivers V, Mosley MP (ed.). New Zealand Hydrological Society: New Zealand; 11–46.
- Paola C, Tal M. 2007. Dynamic single-thread channels maintained by the interaction of flow and vegetation. Geology, 35(4), 347-350.
- Parker G. 1976. On the cause and characteristic scales of meandering and braiding in rivers. Journal of fluid mechanics, 76(3), 457-480.
- Perucca E, Camporeale C, Ridolfi L. 2009. Estimation of the dispersion coefficient in rivers with riparian vegetation. Advances in Water Resources, 32(1), 78-87.
- Parsons DR, Best JL, Lane SN, Orfeo O, Hardy RJ, Kostaschuk R. 2007. Form roughness and the absence of secondary flow in a large confluence–diffluence, Rio Paraná, Argentina. Earth Surface Processes and Landforms: The Journal of the British Geomorphological Research Group, 32(1), 155-162.
- Piégay H, Grant G, Nakamura F, Trustrum N. 2009. Braided river management: from assessment of river behaviour to improved sustainable development. Braided Rivers: Process, Deposits, Ecology and Management, Sambrook Smith GH, Best, JL, Bristow, CS, & Petts, GE (Eds), 257-276.
- Piegay H, Alber A, Slater L, Bourdin L. 2009. Census and typology of braided rivers in the French Alps. Aquatic Sciences, 71(3), 371.
- Pitchford J, Strager M, Riley A, Lin L, Anderson J. 2015. Modelling streambank erosion potential using maximum entropy in a central Appalachian watershed. Proceedings of the International Association of Hydrological Sciences 367: 122.
- Pizarro A, Samela C, Fiorentino M, Link O, Manfreda S. 2017. BRISENT: An entropy based model for bridge-pier scour estimation under complex hydraulic scenarios. Water 9(11): 889.
- Richardson WR, Thorne CR. 1998. Secondary currents around braid bar in Brahmaputra River, Bangladesh. Journal of hydraulic engineering, 124(3), 325-328.
- Richardson, WR, Thorne CR. 2001. Multiple thread flow and channel bifurcation in a braided river: Brahmaputra–Jamuna River, Bangladesh. Geomorphology, 38(3-4), 185-196.
- Repetto R. 2000. Unit processes in braided rivers. PhD thesis, University of Genova, Genova.
- Rhoads BL, Sukhodolov AN. 2001. Field investigation of three-dimensional flow structure at stream confluences: 1. Thermal mixing and time-averaged velocities. Water Resources Research, 37(9), 2393-2410.
- Riley JD, Rhoads BL. 2012. Flow structure and channel morphology at a natural confluent meander bend. Geomorphology, 163, 84-98.
- Ree W. 1958. Retardation coefficients for row crops in diversion terraces.
- Rominger JT, Lightbody AF, Nepf HM. 2010. Effects of added vegetation on sand bar stability and stream hydrodynamics. Journal of Hydraulic Engineering, 136(12), 994-1002.
- Saikia L, Mahanta C, Borah SB. 2018. A novel approach to calculate braiding of a large alluvial river. CURRENT SCIENCE, 115(6), 1179-1185.
- Salas HD, Poveda G. 2015. Scaling of entropy and multi-scaling of the time generalized q-entropy in rainfall and stream flows. Physica A: Statistical Mechanics and its Applications, 423: 11-26.
- Sarker MH, Thorne CR. 2009. Morphological response of the Brahmaputra–Padma–Lower Meghna river system to the Assam earthquake of 1950. Braided Rivers: Process, Deposits, Ecology and Management (Special Publication 36 of the IAS) 21: 289.

- Sarker MH, Thorne CR, Aktar MN, Ferdous MR. 2014. Morpho-dynamics of the Brahmaputra–Jamuna River, Bangladesh. Geomorphology 215: 45-59.
- Sarma JN. 2005. Fluvial process and morphology of the Brahmaputra River in Assam, India. Geomorphology 70(3): 226-256.
- Sarma, JN, Phukan MK. 2006. Bank erosion and bankline migration of the Brahmaputra River in Assam during the twentieth century. Journal Geological Society of India 68(6): 1023.
- Sassi MG, Hoitink AJF, Vermeulen B. 2012. Impact of sound attenuation by suspended sediment on ADCP backscatter calibrations. Water Resources Research, 48(9).
- Schuurman F, Marra WA, Kleinhans MG. 2013. Physics-based modeling of large braided sand-bed rivers: Bar pattern formation, dynamics, and sensitivity. Journal of geophysical research: Earth Surface, 118(4), 2509-2527.
- SCS. 1954. Handbook of channel design for soil and water conservation Soil Conservation Service SCS-TP-61, USDA, Washington, DC (1954)
- Sharma A, Kumar B. 2017. Boundary layer development over non-uniform sand rough bed channel. ISH Journal of Hydraulic Engineering, 1-8.
- Shucksmith J, Boxall J, Guymer I. 2010. Effects of emergent and submerged natural vegetation on longitudinal mixing in open channel flow. Water Resources Research, 46(4).
- Simon A. 1992. Energy, time, and channel evolution in catastrophically disturbed fluvial systems. Geomorphology, 5(3-5), 345-372.
- Szupiany RN, Amsler ML, Parsons DR, Best JL. 2009. Morphology, flow structure, and suspended bed sediment transport at two large braid-bar confluences. Water Resources Research, 45(5).
- Szupiany RN, Amsler ML, Hernandez J, Parsons DR, Best JL, Fornari E, Trento A. 2012. Flow fields, bed shear stresses, and suspended bed sediment dynamics in bifurcations of a large river. Water Resources Research, 48(11).
- Shannon CE. 1948. A mathematical theory of communication. Bell. System Tech. J. 27: 379-423, 623-656
- Sharpe RG, James CS. 2006. Deposition of sediment from suspension in emergent vegetation. Water Sa, 32(2), 211-218.
- Shi Y, Jiang B, Nepf HM. 2016. Influence of particle size and density, and channel velocity on the deposition patterns around a circular patch of model emergent vegetation. Water Resources Research, 52(2), 1044-1055.
- Singh VP. 1997. The use of entropy in hydrology and water resources. Hydrological processes 11(6): 587-626.
- Singh V, Sharma N, Ojha CSP. 2004. The Brahmaputra basin water resources (Vol. 47). Springer Science & Business Media.
- Smith ND. 1971. Transverse bars and braiding in the lower Platte River, Nebraska. Geological Society of America Bulletin, 82(12), 3407-3420.
- Smith ND. 1977. Some comments on terminology for bars in shallow rivers, in Miall, A. D., ed., Fluvial Sedimentology: Can. Soe. Pet. Geol. Mere. 5, p. 85-88.
- Tal M, Paola C. 2010. Effects of vegetation on channel morphodynamics: results and insights from laboratory experiments. Earth Surface Processes and Landforms, 35(9), 1014-1028.

- Tanino Y, Nepf HM. 2008. Laboratory Investigation of Mean Drag in a Random Array of Rigid, Emergent Cylinders. Journal of Hydraulic Engineering, 134(1).
- Takagi T, Oguchi T, Matsumoto J, Grossman MJ, Sarker MH, Matin MA. 2007. Channel braiding and stability of the Brahmaputra River, Bangladesh, since 1967: GIS and remote sensing analyses. Geomorphology 85(3): 294-305.
- Tejedor A, Longjas A, Edmonds DA, Zaliapin I, Georgiou TT, Rinaldo A, Foufoula-Georgiou E. 2017. Entropy and optimality in river deltas. Proceedings of the National Academy of Sciences 201708404.
- Teledyne RD Instruments (TRDI). 2009. WinRiver II User's Guide, version 2.06, Poway, CA.
- Temmerman S, Moonen P, Schoelynck J, Govers G, Bouma TJ. 2012. Impact of vegetation die-off on spatial flow patterns over a tidal marsh. Geophysical Research Letters, 39(3).
- Tempest JA, Möller I, Spencer T. 2015. A review of plant-flow interactions on salt marshes: the importance of vegetation structure and plant mechanical characteristics. Wiley Interdisciplinary Review, Water, 2(6), 669-681.
- Teuling AJ, Van Andel SJ, Troch PA, Hoitink, AJ. 2006. Entropy and river meander planform. In International Conference on Fluvial Hydraulics-River Flow 2006.
- Thomas R, Nicholas AP. 2002. Simulation of braided river flow using a new cellular routing scheme. Geomorphology, 43(3-4), 179-195.
- Thorne CR, Russell AP, Alam MK. 1993. Planform pattern and channel evolution of the Brahmaputra River, Bangladesh. Geological Society, London, Special Publications 75(1): 257-276.
- Topping DJ, Wright SA, Melis TS, Rubin DM. 2007. High-resolution measurements of suspended-sediment concentration and grain size in the Colorado River in Grand Canyon using a multi-frequency acoustic system. In Proceedings of the 10th International Symposium on River Sedimentation (Vol. 3, No. 470, p. 19). Moscow: World Association for Sediment and Erosion Research.
- Trinci G, Harvey GL, Henshaw AJ, Bertoldi W, Hölker F. 2017. Life in turbulent flows: interactions between hydrodynamics and aquatic organisms in rivers. Wiley Interdisciplinary Review, Water, 4(3), e1213.
- Valdiya KS. 1999. Why does river Brahmaputra remain untamed?. Current Science 76(10): 1301-1305.
- Van Dijk WM, Teske R, Van de Lageweg WI, Kleinhans MG. 2013. Effects of vegetation distribution on experimental river channel dynamics. Water Resources Research, 49(11), 7558-7574.
- Vargas-Luna A, Crosato A, Anders N, Hoitink A, Keesstra S, Uijttewaal W. 2018. Morphodynamics effects of riparian vegetation growth after stream restoration. Earth Surface Processes and Landforms
- Velasco D, Bateman A, Redondo JM, DeMedina V. 2003. An Open Channel Flow Experimental and Theoretical Study of Resistance and Turbulent Characterization over Flexible Vegetated Linings. Flow, Turbulence and Combustion, 70(1–4), 69–88.
- Velasco D, Bateman A, Medina V. 2008. A new integrated, hydro-mechanical model applied to flexible vegetation in riverbeds. Journal of Hydraulic Research, 46(5), 579-597.
- Venditti JG, Church M, Attard ME, Haught D. 2016. Use of ADCPs for suspended sediment transport monitoring: An empirical approach. Water Resources Research, 52(4), 2715-2736
- Vercruysse K, Grabowski RC, Rickson RJ. 2017. Suspended sediment transport dynamics in rivers: multi-scale drivers of temporal variation. Earth-Science Reviews, 166, 38-52.
- Wang C, Yu JY, Wang PF, Guo PC. 2009. Flow structure of partly vegetated open-channel flows with eelgrass. Journal of Hydrodynamics, 21(3), 301-307.

- Wiebe H. 2006. River Flooding and Erosion in North East India: Exploratory Consideration of Key Issues. Northwest Hydraulic Consultants (NHC), Alberta, Canada.

- Wilson C. 2007. Flow resistance models for flexible submerged vegetation. Journal of Hydrology, 342(3-4), 213-222.

- Wilson C, Stoesser T, Bates P, Pinzen A. 2003. Open channel flow through different forms of submerged flexible vegetation. Journal of Hydraulic Engineering, 129(11), 847-853.

- Wu F, Shen H, Chou Y. 1999. Variation of roughness coefficients for unsubmerged and submerged vegetation. Journal Hydraulic Engineering, 125(9), 934-942.

- Wright SA, Topping DJ, Williams CA. 2010. Discriminating silt-and-clay from suspended-sand in rivers using side-looking acoustic profilers. In Joint Federal Interagency Conference 2010: Hydrology and sedimentation for a changing future: existing and emerging issues.

- Yalin MS. 1992. River Mechanics. Pergamon Press.

- Yagci O, Tschiesche U, Kabdasli M. 2010. The role of different forms of natural riparian vegetation on turbulence and kinetic energy characteristics. Advances in Water Resources, 33(5), 601-614.

- Zolezzi G, Bertoldi W, Tubino M, Smith GHS, Best JL, Bristow CS, Petts GE. 2006. Morphological analysis and prediction of river bifurcations. Braided rivers: process, deposits, ecology and management, 36, 233-256.

- Zolezzi G, Bertoldi W, Tubino M. 2009. Morphological analysis and prediction of river bifurcations. In Braided rivers: Processes, Deposits, Ecology and Management. Blackwell Publishing Ltd Oxford, UK. 233-256.

- Zong L, Nepf HM. 2009. Flow and deposition in and around a finite patch of vegetation. Geomorphology, 116, 363-372.